(2)

STUDIES ON THE MASS TRANSFER THROUGH PERFLUORINATED CATION EXCHANGE MEMBRANES AND THEIR ELECTROCHEMICAL APPLICATIONS

KATSUMI KATAKURA

1995

Preface

The present study has been carried out under the direction of Professor Zen-ichiro Takehara at Department of Industrial Chemistry, Faculty of Engineering, Kyoto University (1993- Division of Energy and Hydrocarbon Chemistry, Graduate School of Engineering, Kyoto University).

The object of this study is to investigate the mass transfer behavior of hydrophobic materials through perfluorinated cation exchange membranes and through porous metal electrode bound on the polymer electrolyte membranes.

The author is greatly indebted to Professors Zen-ichirou Takehara and Zempachi Ogumi for their valuable suggestions and supervision throughout the work. The author also would like to express his thanks to Professor Seiichi Nishimoto for his helpful comments and discussions.

Grateful acknowledgment is also given to Professor emeritus Tadao Ishikawa at Nara National College of Technology for giving chance to studying this work.

The author also would like to express their thanks to Professors Ikuichiro Izumi, Tadashi Umehara and the other professors in Department of Chemical Engineering, Nara National College of Technology, for their kind encouragement. The author is also grateful to Drs. Takeshi Yao, Yoshiro Tomida, Kiyoshi Kanamura, Yoshiharu Uchimoto, Kenji Kikuchi, James T. Hinatsu, and Minoru Inaba for their support and encouragement. Many thanks also are due to all the members of the Profes-

sor Takehara's and the Professor Ogumi's laboratories, Kyoto University, for their kind encouragement and constant interest in accomplishing this work.

Finally, the author would like to thank his wife for her hearty encouragement.

Katsumi Katakura

Contents

Introduction and General Summary

Introduction and General Summary

Background of the work

Mass transfer through ion exchange membrane

Organic polymer membranes containing ionic groups such as sulfonate, calboxylate, and ammonium groups show an ion perm-selective behavior[1,2], and they are called ion-exchange membranes. Hydrocarbon type cation/anion-exchange membranes and perfluorinated cation-exchange membranes are now commercially available. Main subject of hydrocarbon type ion exchange membranes is their use in electro dialysis. In contrast to hydrocarbon type ion exchange membranes, perfluorinated cation exchange membranes can be applied for not only a diaphragm in electro dialysis but also diaphragm in brine cells and in the other electolyzers[3], and electro organic syntheses[4], because the membranes have stability against oxidizing and reducing reagents, various solvents, acid or base, and high temperature (ca. 100 ℃)[5,6]. The chemical stability of the perfluorinated ion exchange membranes also enable us to bind a metal electrode on the membrane surfaces[7–10]. When ion exchange membrane used for these purposes, the membranes composites called the SPE® composite electrode. The SPE® composite electrode can be utilized for solid polymer electrolyte membrane fuel cells (PEMFCs)[7–10], and electro organic syntheses[4,11–24].

Fundamental properties of the ion exchange membrane such as a transference number of perm-selective ions, ionic conductivity, membrane

potential, and so on are governed by mass transfer mechanism of ions through the membrane[2].

Theoretical treatment of mass transfer mechanism of ions through the ion exchange membrane is based on Nernst-Plank equation[25] or on irreversible thermodynamics[26]. In practical usage of the ion exchange membrane, properties of ion exchange membranes such as ion exchange selectivity and swelling properties have been corelated to degree of polymer cross-linking, exchange group contents, and others. Some of the results reported for hydrocarbon type ion exchange membranes are summarized as follows[2]:

Although concentration of ion exchange groups of a membrane increases with increasing ion exchange capacity of the membrane, Donnan exclusion of co-ions is dominated by concentration of ion exchange groups other than an ion exchange capacity of the membrane. Water uptake of cation exchange membrane increases with increasing pKa of anionic exchange group and with decreasing a degree of cross-linking of the membrane. Decreasing water uptake of the membrane results in the decreasing the ionic conductivity and increasing the concentration of ionic group of the ion exchange membrane.

Applying DC current also affects the mass transfer behavior of ions but their effects have not been well acomplished[27].

Applications of the perfluorinated cation exchange membranes

In applications of perfluorinated cation-exchange membranes, use of the membranes are classified into following two groups.

1. Application as diaphragm in electrolyzer. In this application, a cation-exchange membrane separates two electrolyte solution phases, namely anolyte and catholyte. The arrangement for this application is schemcatically described in Fig. 1 (a). In this case, the membrane acts merely as a cation perm-selective diaphragm and cations permeate through the membrane under electrochemical potential gradient[3,25].

2. Application as solid polymer electrolyte membrane. In this application, a porous electrode is directly bound on the surface of cation exchange membrane. A porous electrode/polymer electrolyte interface offers an active site for electrochemical reactions and the arrangements of (b), (c) of Fig. 1. are available for use in fuel cells[7–10], and the other electrochemical applications. For example, the new type of electroorganic synthesis (SPE electroorganic synthesis) have been reported by Ogumi et al.[4,11–24].

Applications of perfluorinated cation exchange membranes in the latter case are of interest. When the membrane is applied as diaphragm in brine cell using the cell arrangement shown in Fig. 1 (c), electrochemical reactions occurred at the both side of the polymer electrolyte membrane composite electrode surfaces. Chlorine and hydrogen are produced at the anode and cathode, respectively. Since the thickness of the membrane is thin, the produced gases easily permeate through the ion exchange membrane and reach to the opposite compartments. This mixing of the gases is not favorable to the system and one of the most important role of the diaphragm in these applications is to prevent the reactants/products from mixing one another. Therefore, much attention has been so far focused on the permeation behavior of neutral species like ionic species[28–33].

Mass transfer through the perfluorinated cation exchange membranes and the structure of the membranes

Perfluorinated ion-exchange membrane is consisted of perfluoro-backbone and anionic groups are fixed to the backbone. Chemical structures of typical perfluorinated cation-exchange membranes containing sul-

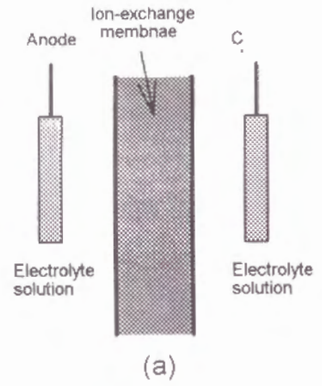

(a)

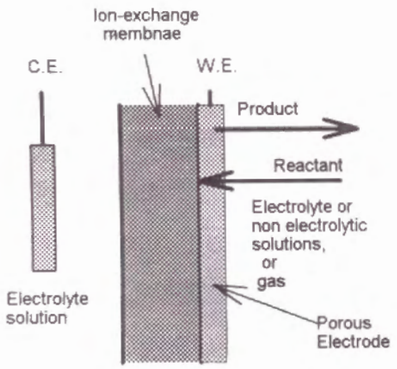

(b)

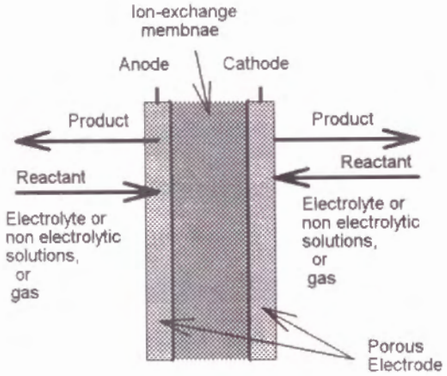

(c)

Figure 1 Arrangements of a cation-exchange membrane in electrochemical applications.

fonate groups (Nafion®, available from E.I. Dupont de Nemours and Company) and containing carboxylate groups (Flemion®, available from ASAHI Glass Co.) are shown in Fig. 2 (a) and (b), respectively[3]. PTFE-like perfluoro-backbone of the membranes results in high chemical and thermal stability of the membranes. Previously Matsui et al. had been attempted to prepare a perfluorinated anion exchange membrane[34], but stability of the membrane was lower than that of cation exchange membranes.

As shown in Table 1, the dependencies of fundamental properties of the ion exchange membranes on fixed anionic groups are similar to those of hydrocarbon type ones. For example, pKa value of sulfonate group is smaller than that of carboxylate group and water uptake (mol sorbed water per mol exchange site) of Nafion is higher than that of Flemion[6]. Higher water uptake for Nafion than for Flemion leads to smaller ionic conductivity and higher cation perm selectivity for Flemion than for Nafion.

Table 1 Electrochemical properties of perfluorinated cation exchange membrane.

	Sulfonate (Nafion)	Carboxylate	ref.
pKa	< 1	1.9	(35)
t^+ in 4 M NaOH	0.8	0.95	(35)
t^+ in 12 M NaOH	0.6	0.9	
mol sorbed water per mol exchange site. (for Na^+ form)	11.9	9.5	(36)

On the other hand, swelling properties for perfluorinated cation

(a) Chemical strucure of Nafion

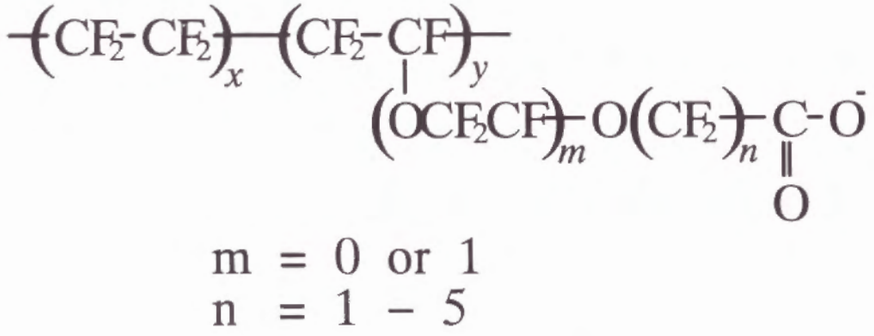

(b) Chemical strucure of Flemion

Figure 2 Chemical structure of Nafion and Flemion.

exchange membranes are quite different from those for hydrocarbon type ones. For example, Yeo reported[37] that, two distinct swelling envelopes were observed for Nafion and he concluded that Nafion has dual cohesive energy.

Much attention have been so far focused on mechanical[38], structural[39–45], permeation[28–33,46–51] properties, and cation-exchange selectivity[52–54] of Nafion type perfluorinated cation-exchange membranes. Nafion has a microscopically phase separated structure consisted of ionic clusters and hydrophobic backbone, and the polymer is not cross-linking.[39–45] The ionic clusters are linked by narrow channels one another[45]. Yeager *et al.*[29] and Ogumi *et al.*[32] proposed that there exist an interfacial region between hydrophobic polymer backbone and hydrophilic ionic clusters as is shown in Fig. 3. This morphological structure of Nafion type perfluorinated cation exchange membranes is different from that of conventional hydrocarbon type ones. Hydrophobic species including organic cations interact with the hydrophobic region (both the perfluoro-backbone (A) and the interface region (B), which are located between perfluoro-backbone (A) and ionic clusters (C)) of the polymer and hydrophilic species interact with hydrophilic region (ionic clusters (C)) of the membrane. Mass transfer behaviors of ions and neutral species through the membranes are influenced by these peculiarly structure.

Inaba et al. applied these microscopically phase separated structure of Nafion to electrochemical organic synthesis using SPE® composite elecrode[23,24]. In the case of electroorganic syntheses using SPE® composite electrode, DC current is applied to the electrodes. Application of DC current also affects the mass transfer behavior of hydrophobic species through the membranes.

Ogumi et al. reported that[32,33], hydrogen and oxygen permeate through interfacial region between hydrophobic fluorocarbon and hy-

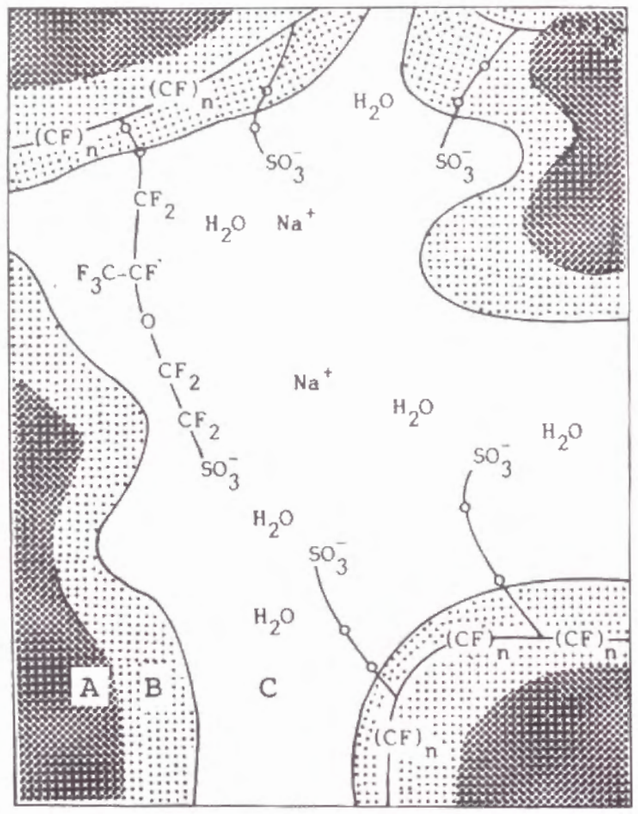

Figure 3 Schematic model of micro structure of Nafion type perfluorinated cation-exchange resin.
(A) : Hydrophobic polymer backbone region.
(B) : Interfacial region.
(C) : Hydrophilic ionic clusters region.

drophilic ionic clusters of the perfluorinated cation-exchange membrane, because concentration and diffusion coefficient of these gases in the membrane are quite different from those in water and they are close to those in perfluorinated organic solvents. Permeation phenomena of hydrophobic species through the perfluorinated cation exchanging membrane show interesting problem.

In application to fuel cell systems[7–10], H_2-O_2 solid polymer electrolyte membrane fuel cells (PEMFC) operating at low temperature (up to 100 ℃), many workers have been attempted to reduce the platinum loadings of catalyst layer in PEMFC[55–58]. However, criterion for designing of the catalyst layer in PEMFC has not been accomplished. In the polymer electrolyte membrane composite electrode, metal particle should be deposited in hydrophilic ionic cluster regions of the membrane. Microscopically phase separation structure of the perfluorinated cation exchange membrane and hydrophobic interaction between the membrane and hydrophobic species strongly affect the mass transfer behavior through the membrane. In this composite electrode, electrochemically active hydrophobic species such as oxygen and hydrogen may react at the composite electrode easily, because the composite electrode is expected to provide a suitable gas diffusion electrode.

Mass transfer of cationic and neutral species through the membranes should also be influenced by difference of anionic group fixed in the membrane. Studies of a perfluorinated carboxylate cation exchange membrane have recently been reported[59–61]. X-ray analysis results indicate that the membrane is consisted of ion clusters as well as Nafion[59,61]. In perfluorinated cation exchange membranes, it is expected that the difference in water uptake affect not only an ionic conductivity and cation transference number of the membranes but also properties of the ionic clusters.

Outline of the work

As descried in the above, the difference in water uptake of the ion exchange membranes affects the mass transfer behaviors through the membranes, which difference is strongly influenced by degree of cross-linking of the polymer, pKa of the fixed anionic groups, and co-existing cations. In application of the perfluorinated cation exchange membranes to PEMFC and electroorganic synthesis, mass transfer of hydrophobic species such as hydrogen, oxygen, and organo cationic species are important subjects to be clarified. The purpose of the present study is to understand the hydrophobic/hydrophilic interaction between ion exchange membrane and the materials to be permeated, and their effect of mass transfer behavior through the membrane.

In part I, mass transfer behavior of hydrophobic species through the perfluorinated cation exchange membrane was investigated from the viewpoint of the water uptake and pKa of the membranes. Influence of application of DC current across the perfluorinated cation exchange membrane on the permeation behavior of hydrophobic species through the membrane was also investigated. Oxygen and aniline were chosen for this purpose because of their electrochemical importance.

In chapter 1, dependency of the permeation behavior of oxygen through a perfluorinated cation exchange membrane on fixed anionic groups in the membrane was discussed. Solubility and diffusion coefficients of oxygen in the perfluorinated carboxylate cation exchange membrane (Flemion) of different counter-ions and different equivalent weights (EW = 700 and 800) were measured and were compared to those in Nafion. Solubility decreased with increasing water content of the membranes. The diffusion coefficient in 700 EW membranes increased with increasing water content, while that in 800 EW membranes decreased slightly. On the basis of these results, the diffusion path of oxygen through

the membranes was discussed in terms of morphology of perfluorinated ion-exchange membranes.

In chapter 2, the permeation behavior of aniline through Nafion 117, perfluorinated sulfonate cation-exchange membrane, was investigated from the viewpoint of water uptake of the membrane. The partition coefficient of anilinium cation to Nafion, k, was found to be 1.04 $\times 10^3$ and that of neutral aniline to Nafion, k_n, was 2. The selectivity coefficient for anilinium cation over proton, K_H^{AN}, was 69. These results indicated that anilinium cation has affinity to Nafion. The water content of anilinium form Nafion was 10.7 moles of H_2O per mole of SO_3^-. The apparent diffusion coefficient of aniline, D_{app}, through Nafions in different cationic form were measured. The diffusion coefficient linearly increased with increasing water contents in Nafion. On the other hand, the apparent diffusion flux of neutral aniline was high owing to the dissociation of anilinium cations within the membrane.

In chapter 3, transport phenomena of aniline through a perfluorinated sulfonate cation-exchange membrane, Nafion 117, in different water uptake were investigated under passage of DC current. Water uptake is controlled by ionic form of the membranes. In every form of the membranes, increase in transport number of anilinium cation was observed in the current density ranging from 0.3 to 1.3 mA cm^{-2}. The transport number of the anilinium cation in the Cs^+ form was larger than that expected from the concentration and diffusion coefficient of the anilinium cation in Cs^+ form Nafion. These transport phenomena of aniline may be attributable to a structural change of Nafion or a decrease in hydrophobic interaction between the anilinium cation and Nafion caused by the passage of DC current.

In part II, mass transfer phenomena through a composite electrode copmposed of the porous metal electrode layer directly bound on Nafion (SPE® composite electrode) and their utilization to electrochemical ap-

plications were investigated.

In chapter 4, hydrogen oxidation reaction on anode in polymer electrolyte membrane fuel cells (PEMFC) was chosen as a model reaction for understanding a mass transfer mechanism around the polymer electrolyte composite electrode. Although hydrogen is less soluble in the perfluoro-backbone of Nafion than oxygen, hydrogen oxidation reaction proceeds rapidly at platinum electrode. A platinum microelectrode was inserted into a perfluorinated sulfonate acid resin particle, Nafion® NR50, under hydrogen atmosphere and hydrogen oxidation current was measured at different insertion depths. The current dependencies on the insertion depth were calculated by mathematical calculation using cylindrical diffusion model and was compared to the experimental results. The results indicated that hydrogen oxidation reaction on anode in PEMFC proceeded under diffusion limiting conditions of the reactant gas through the polymer electrolyte layer.

As discussed in chapter 4, polymer electrolyte membrane composite electrodes serve as a high performance gas diffusion electrode for hydrophobic gas such as hydrogen. Even if the porous electrode is covered with gas permeable polymer film, the gas should penetrate the film and reach the active site for electrochemical reaction. In chapter 5, a new type amperometric oxygen sensor operating at room temperature was constructed using Nafion composite electrode and oxygen permeable polymer film which tightly bound on the electrode surface. Oxygen was chosen instead of hydrogen, because oxygen detection is of practical interest. For oxygen partial pressure ranging from 0 to 1 atm, oxygen reduction reaction at the composite electrode proceeds under the conditions of diffusion limiting of oxygen through the polymer film. From the discussion of fundamental properties of the new type oxygen sensor, furthermore, the sensor offers a new method for gas permeability coefficient measurement through polymer films.

In chapter 6, the attention was focused to miniaturization of the new type oxygen sensor composed of tightly stacked membrane/electrode/electrolyte. Nafion® NR50 was chosen for this purpose. A porous platinum cathode was directly deposited on Nafion NR50, and perfluoro-polymer layer was directly bound on the cathode using plasma polymerization. Plasma polymerization is well known as a method for covering a thin polymer film on a substrate. Decreasing the thickness of OTL membrane enhanced response time and sensitivity of the sensor. Dissolved oxygen content in water was determined by the new sensor and found that the signal current of the sensor linearly increased with increase in the dissolved oxygen concentration ranging from 0 to 30 ppm.

References

1. F. Hine, "Electrode processes and electrochemical engineering", Plenum press, new York (1985), p175.

2. R.W. Grimshaw and C.E. Harland, "The Chemical Society Monographs For Teachers No. 29, Ion-exchange : Introduction to Theory and Practice", The Chemical Society Publications, London (1975), Chap. 3.

3. T. Kyu and A. Eisenberg, "Perfluorinated Ionomer Membranes", A. Eisenberg and H. L. Yeager (Eds.), ACS Symposium Series, No.180, American Chemical Society, Washington DC, (1982) Chap. 6.

4. Z. Ogumi, K. Nishino, and S. Yoshizawa, *Denki Kagaku*, **49**, 212 (1981).

5. K. Kihara, Y. Miyamoto, *Kagaku Kogyo*, **58**, 170 (1987).

6. M. Seko, J. Ohmura, and T. Hane, *Nihon kagaku kaishi*, **10**, 1904 (1985).

7. J. T. Wang and R. F. Savinell, *Electrochim. Acta.*, **37**, 2737 (1992).

8. G.G. Scherer, *Phys. Chem.*, **94**, 1008 (1990).

9. T. E. Springer, T.A. Zawodzinski, and S. Gottesfeld, *J. Electrochem. Soc.*, **138**, 2334 (1991).

10. E. A. Ticianelli, C.R. Derouin, A. Redondo, and S. Srinivasan, *J. Electrochem. Soc.*, **135**, 2209 (1988).

11. Z. Ogumi, K. Nishino, and S. Yoshizawa, *Electrochim. Acta.*, **26**, 1779 (1982).

12. Z. Ogumi, H. Yamashita, K. Nishino, Z. Takehara, and S. Yoshizawa, *Electochim. Acta.*, **28**, 1687 (1983).

13. Z. Ogumi, H. Yamashita, K. Nishino, Z. Takehara, and S. Yoshizawa, *Denki Kagaku*, **52**, 180 (1984).

14. Z. Ogumi, S. Ohashi, and Z. Takehara, *Nippon Kagaku Kaishi*, **1984**, 1788 (1984).

15. Z. Ogumi, S. Ohashi, and Z. Takehara, *Electrochim. Acta.*, **30**, 121 (1985).

16. Z. Ogumi, T. Mizoe, N. Yoshida, and Z. Takehara, *Bull. Chem. Soc. Jpn.*, **60**, 4233 (1987).

17. Z. Ogumi, T. Mizoe, and Z. Takehara, *Bull. Chem. Soc. Jpn.*, **61**, 4183 (1988).

18. Z. Ogumi, T. Mizoe, C. Zhen, and Z. Takehara, *Bull. Chem. Soc. Jpn.*, **63**, 3365 (1990).

19. Z. Chen, T. Mizoe, Z. Ogumi, and Z. Takehara, *Bull. Chem. Soc. Jpn.*, **64**, 537 (1991).

20. Z. Chen, T. Mizoe, Z. Ogumi, and S. Takehara, *Bull. Chem. Soc. Jpn.*, **64**, 1261 (1981).

21. Z. Ogumi, K. Inatomi, J. T. Hinatsu, and Z. Takehara, *Electrochim. Acta.*, **37**, 1295 (1992).

22. Z. Ogumi, M. Inaba, S. Ohashi, M. Uchida, and Z. Takehara, *Electrochim. Acta.*, **33**, 365 (1988).

23. M. Inaba, J. T. Hinatsu, Z. Ogumi, and Z. Takehara, *J. Electrochem. Soc.*, **140**, 706 (1993).

24. M. Inaba, Z. Ogumi, and Z. Takehara, *J. Electrochem. Soc.*, **140**, 19 (1993).

25. T. Hanai, "Maku to ion", Kagaku Dohjin, (1980).

26. H. Kimitsuka, "Ion no Makutouka", Kyoritsu shuppan, (1988).

27. T. Hanai, Kagaku Kogaku, **51**, *563*, (1987).

28. S. K. Sikdar, *J. membrane Sci.*, **23**, 83 (1985).

29. H. L. Yeager, *J. Electrochem Soc.*, **1283**, 1880 (1981).

30. F. G. Will, *J. Electrochem Soc.*, **126**, 36 (1979).

31. Z, Ogumi, Z. Takehara, and S. Yoshizawa, *J. Electrochem Soc.*, **131**, 669 (1984).

32. Z, Ogumi. T. Kuroe, and Z. Takehara, *J. Electrochem Soc.*, **132**, 2601 (1985).

33. T. Sakai, H. Takenaka, and E. Torikai, *J. Electrochem Soc.*, **133**, 88 (1986).

34. K. Matusi, E. Tobita, K. Sugimoto, and K. Kondo, *J. Appl. Polm. Sci.*, **32**, 4137 (1986).

35. Z. Twardowski, H. L. Yeager, and B. O'Dell, *J. Electrochem. Soc.*, **129**, 328 (1982).

36. H. L. Yeager, Z. Twardowski, and L. M. Clarke, *J. Electrochem. Soc.*, **129**, 324 (1982).

37. R. S. Yeo, *POLYMER*, **432**, 21 (1980).

38. R. S. Yeo, *J. Electrochem. Soc.*, **130**, 533 (1983).

39. T. C. Ward and A. V. Tobolsky. *J. Appl. Polym. Sci.*, **11**, 2403 (1967).

40. R. Longworth and D.J. Vaughan, *Nature(London)*, **2**, 85 (1968).

41. A. Eisenberg and M. Navratil, *J. Polym. Sci.*, **B10**, 537 (1972).

42. C. L. Marx, D. F. Caulfield, and S. L. Cooper, *Macromolecules*, **6**, 3 (1973).

43. R. S. Yeo and A. Eisenberg, *J. Appl. Polym. Sci.*, **21**, 875 (1977).

44. E. J. Roche, R. S. Stein, T. P. Russel, and W. J. Macknight, *J. Polym. Sci., Phys. Ed.*, **18**, 1497 (1980).

45. T. D. Gierke, G. E. Munn, and F. C. Wilson, *J. Polym. Sci., Polym. Phys. Ed.*, **19** (1981).

46. M. W. Verbrugge, *J. Electochem. Soc.*, **136**, 417 (1989).

47. R. S. Yeo, *J. Electrochem Soc.*, **130**, 533 (1983).

48. C. R. Chris Wang, J. W. Strojek, and T. Kuwana, *J. Phys. Chem.*, **91**, 3606 (1987).

49. H. L. Yeager, B. Kipling, and R. L. Dotson, *J. Electrochem Soc.*, **127**, 303 (1980).

50. A. Herrera, and H. L. Yeager, *J. Electrochem Soc.*, **134**, 2446 (1987).

51. H. L. Yeager and A. Steck, *J. Electrochem. Soc.*, **129**, 85 (1982).

52. H. L. Yeager and A. Steck, *Anal. Chem.*, **51**, 862 (1979).

53. H. L. Yeager and B. Kipling, *J. Phys. Chem.*, **83**, 1836 (1979).

54. A. Steck and H. L. Yeager, *Anal. Chem.*, **52**, 1215 (1980).

55. E. J. Taylor, E. B. Anderson, and N. R. K. Vilambi, *J. Electrochem. Soc.*, **139**, L45 (1992).

56. M. S. Wilson and S. Gottesfeld, *J. Electrochem. Soc.*, **139**, L28 (1992).

57. M. S. Wilson and S. Gottesfeld, *J. Applied. Electrochemistry*, **22**, 1 (1991).

58. Z. Poltarzewski, P. Staiti, V. Alderucci, W. Wieczorek, and N. Giordano, *J. Electrochem. Soc.*, **139**, 761 (1992).

59. H. Ukihashi, *polym. prepr. Am. Chem. Soc. Div. Polym. Chem.*, **20**, 195 (1979).

60. M. Suhara and Y. Oda, in "Ion Exchange", R.S. Yeo, and R.P. Buck, Editors, p. 290, The Electrochemical Socety Softbound Proceedings Series, Pennington, NJ (1981).

61. H. Ukihashi, *Chemtech*, 118 (Feburuary 1980).

Part I

Permeation Phenomena Through Perfluorinated Ion-Exchange Membranes

Chapter 1

Oxygen Permeation Through Perfluorinated Carboxylate Ion Exchange Membranes

1.1 Introduction

Solid polymer electrolyte (SPE®) composite electrodes have been extensively studied for use in water electrolyzers[1], brine electrolyzers[2], fuel cells[3], and organic syntheses[4–6]. In these applications, gas permeation through an SPE material results in a decrease in current efficiency. This has been observed in Kolbe-type reactions using a "both sides" SPE method[6] as well as in water electrolysis. A fundamental understanding of the gas permeation is needed to improve current efficiency. The permeation of diffusants depends strongly on the properties of SPE materials and on the conditions encountered. The understanding of the gas permeation may also provide useful information about the morphology of SPE materials.

The morphology of perfluorinated sulfonate and carboxylate ion exchange membranes has attracted much attention of many workers[7–13]. Gierke et al. proposed an ionic cluster model for perfluorinated sulfonate ion exchange membranes (Nafion® , E. I. du Pont de Nemours and Co.), in

which hydrophilic ion-exchange sites, counterions and water are phase-separated from hydrophobic fluorocarbon backbone material[7]. Yeager and Steck modified Gierke's spherical ionic cluster model, and proposed the presence of an interfacial region between the ionic cluster region and the hydrophobic fluorocarbon region of Nafion[10]. Ogumi et al. studied the permeation of hydrogen and oxygen through Nafion membranes, and determined solubilities and diffusion coefficients of hydrogen and oxygen in Nafion[14,15]. They reported that the solubilities of hydrogen and oxygen in Nafion were close to perfluorocarbon media, and that the diffusion coefficients were independent of water content of Nafion. From these results, they concluded that both gases permeate through an "interfacial region" which is not a simple interface, but consists of a flexible amorphous part of fluorocarbon backbones, and they proposed a three-phase model for Nafion[15].

In this chapter, oxygen permeation through perfluorinated carboxylate ion exchange membranes (Flemion®) donated by Asahi Glass Co. is investigated. The structure of Flemion is shown in Fig. 1.1[16]. Solubilities and diffusion coefficients of oxygen in the membranes of different counterions and EWs are determined. The diffusion path of oxygen through the membranes is discussed in terms of morphological properties of perfluorinated ion exchange membranes.

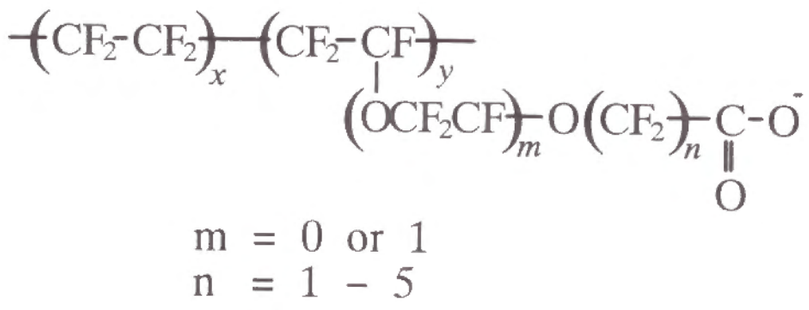

Figure 1.1 Structure of Flemion.

1.2 Experimental

1.2.1 Materials

Perfluorinated carboxylate ion exchange membranes (Flemion, Asahi Glass Co.) with nominal equivalent weights (EWs) of 700 and 800 (1.44 and 1.25 meq/g-dry polymer, respectively) and with different thicknesses were used for permeation studies. These membranes are referred to as A1, A2, B1 and B2 (see Table 1.1). The membranes were pretreated by soaking them in boiling water in Na^+-form for 30 min. After soaking, membrane thickness was measured with a micrometer. The values are listed in Table 1.1. Platinum was deposited on one side of the membrane using an electroless plating method described previously[3,14]. The prepared SPE composite electrode, referred to as Pt-Flemion, was equilibrated with 0.5 M (M = mol dm^{-3}) M_2SO_4 (M = Na, K and H) at 25 ℃ for 36 h.

Water contents of the membranes were determined as follows. After equilibration, a membrane sample (without Pt deposition) was quickly blotted between sheets of filter paper and weighed. After dried in vacuum at 100 ℃ for 48 h, the sample was weighed. The mass of water was determined by subtracting the mass of the dry polymer from the total mass. The water content was presented as grams of water uptaken/grams of dry polymer.

1.2.2 Chemicals

All chemicals were of reagent grade, and used without further purification. Oxygen was of purity higher than 99.8 %.

1.2.3 Electrolytic cell and permeation measurement

A schematic diagram of the experimental cell used for permeation

Table 1.1 Solubilities and diffusion coefficients of oxygen in Flemion membranes at 25 ℃.

Sample	EW	M^+	thickness /μm	water content*	c^0 / mM	$D \times 10^7$ /$cm^2 s^{-1}$
A1	700	Na^+	85	36.6	4.5	2.9
		K^+	85	30.0	3.8	3.7
		H^+	75	10.2	14.2	1.1
A2	700	Na^+	170	31.9	3.5	4.0
		K^+	169	30.8	2.8	5.3
		H^+	159	12.3	13.3	1.7
B1	800	Na^+	75	33.8	5.9	0.47
		K^+	73	13.2	5.0	0.61
		H^+	70	8.7	17.8	0.66
B2	800	Na^+	144	23.7	11.7	0.54
		K^+	142	19.5	10.6	0.55
		H^+	135	6.2	14.9	0.87

* In the unit of g H_20 / g dry polymer.

study is shown in Fig. 1.2. The cell was composed of two compartments, which were separated by Pt-Flemion. The effective geometric surface area of the SPE composite electrode was 3.1 cm^2. The volume of each compartment was 40 cm^3. Electrode potentials were measured as volts vs. Ag/AgCl (3.3 M KCl). The right-hand side (Fig. 1.2) compartment was filled with a solution of the same composition as that used for equilibration (0.5 M M_2SO_4, M = Na, K and H) to prevent the membrane from changing its water content during measurements. The entire cell was placed in a water bath maintained at 25 ℃. Oxygen permeation through the Flemion was monitored using an electrochemical technique described previously[14]. The left-hand side compartment was first filled with pre-humidified argon. Then, the gas was changed in stepwise to pre-humidified oxygen, and a build-up curve was obtained. The monitoring was carried out under the mass-transfer limiting conditions that all of oxygen molecules permeating through the membrane were reduced on the electrode. The electrode potential was set at -0.25 V vs. Ag/AgCl[14]. In a similar manner, a decay curve was obtained by changing the gas from pre-humidified oxygen to pre-humidified argon. The resulting data were analyzed by a technique described previously to determine diffusion coefficients and solubilities of oxygen in the membranes[14].

1.3 Results

1.3.1 Water content

The water content of ion exchange membranes affects their transport properties. Measured water contents of the Flemion membranes used in this study are listed in Table 1.1. The water content of the membranes decreased in the order Na^+-form > K^+-form > H^+-form. For a given counterion, the water content values of 700 EW membranes (A1 and A2) were higher than those of 800 EW membranes (B1 and B2).

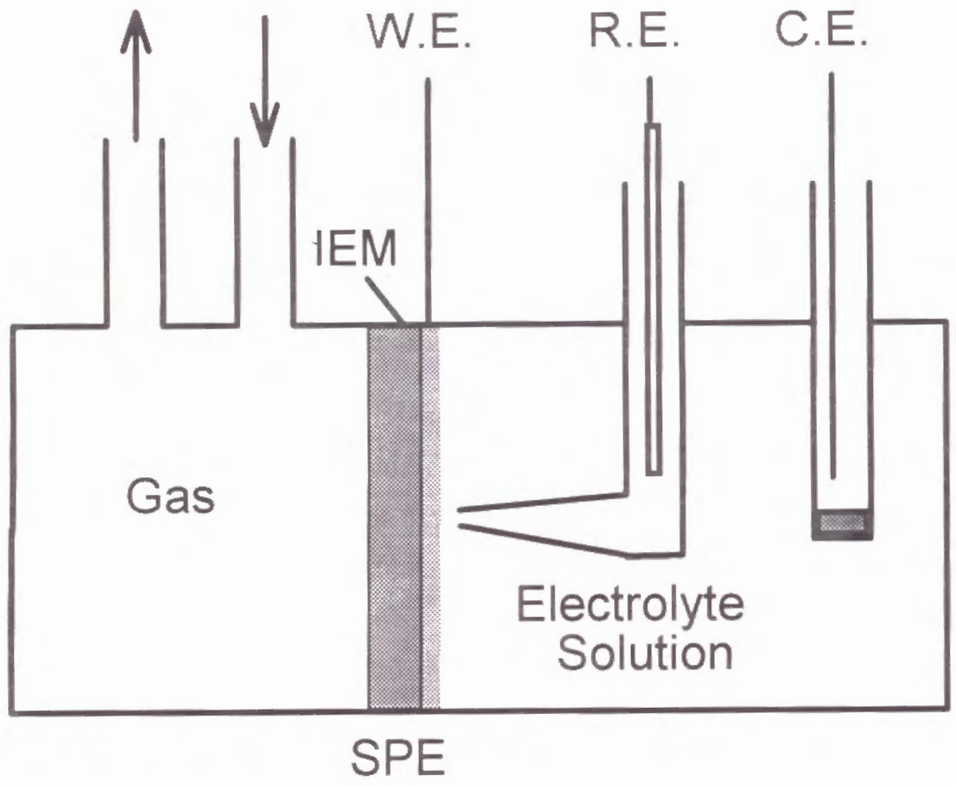

Figure 1.2 Schematic diagram of the electrochemical test cell using an SPE composite electrode.
WE = Pt-Flemion; CE = Platinum wire;
RE = 3.3M Ag/AgCl; IEM = Flemion.

1.3.2 Permeation of oxygen

Experimental transient curves of $J_t/J_\infty (= i_t/i_\infty)$ and theoretical ones for Fickian diffusion plotted against time (t) are shown in Fig. 1.3, where J_t, J_∞, i_t and i_∞ denote the oxygen flux at time t, the steady-state flux at $t \rightarrow \infty$, the current at time t, and the steady-state current at $t \rightarrow \infty$, respectively. Both build-up and decay curves were in good agreement with the theoretical ones. Solubilities (c^0) and diffusion coefficients (D) of oxygen were evaluated from the buildup and decay curves using the relations; $D = 0.138l^2/t_{1/2}$ and $j = nFDc^0/l$, where l is the membrane thickness, and $t_{1/2}$ is the time at which J_t/J_∞ reaches 1/2 (see ref [14] for details). The results are summarized in Table 1.1. Each value is an average of more than three measurements.

1.4 Discussion

1.4.1 Water content

The water content of Flemion membranes decreased in the order Na^+-form > K^+-form > H^+-form. This order is in agreement with the order obtained by Nakano et al. for Flemion membranes with ion exchange capacities of 1.25 and 1.80 meq/g[13]. Low water content values of H^+-form membranes should be attributed to low acidity of -COOH. The water contents of the Na^+-form Flemion membranes (EW = 700 and 800) are comparable with those of Na^+-form Nafion of EW = 1000 - 1100 [17].

1.4.2 Solubility of oxygen

Figure 1.4 shows the solubility values of oxygen in Flemion plotted against water/ion exchange site mol ratio (Nw), i.e., the number of water molecules per an ion exchange site. The solubility values in mem-

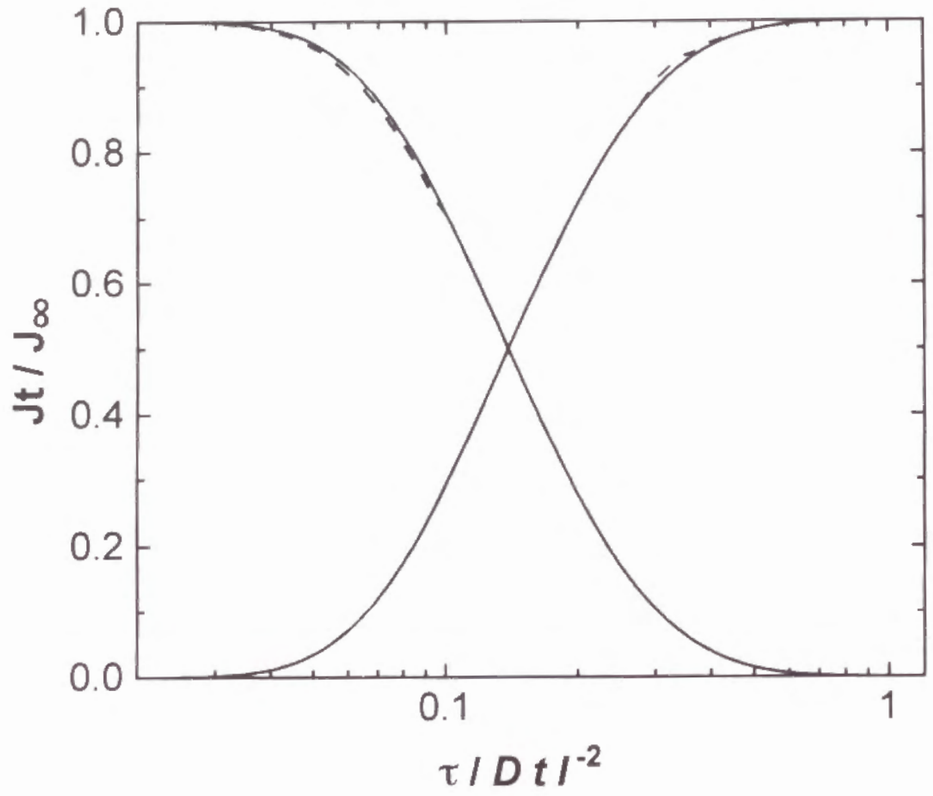

Figure 1.3 Oxygen permeation transient. Solid lines and circles : theoretical curves. Broken lines : experimental results for K^+-type Pt-Flemion at 25 ℃.

branes of different EWs fell on different straight lines. The solubility decreased with increasing Nw, i.e., increasing water content. For a given Nw, the solubility in 800 EW membranes was higher than that in 700 EW membranes. Table 1.2 shows solubility values of oxygen in various media[15,18–20]. It should be noted that the solubility values in Flemion membranes are much higher than that in water.

Ogumi et al. studied the permeation of oxygen and hydrogen through perfluorinated sulfonate ion exchange membranes, Nafion, of different counterions[15]. They observed that the solubility of oxygen in the Nafion membranes (about 10 mM) was independent of water content of the membranes, and that the solubility values were close to the values in perfluorocarbon media rather than to that in water (see Table 1.2). They also observed that the diffusion coefficient of oxygen in the Nafion membranes was independent of their water content. Similar results were reported for the solubility and diffusion coefficient of hydrogen in the Nafion membranes. From these observations, they concluded that oxygen and hydrogen permeate through a hydrophobic interfacial region which consists mainly of a flexible amorphous part of the fluorocarbon backbones of Nafion.

Tsou et al. studied the permeation of hydrogen through Dow's sulfonate and carboxylate ion exchange membranes, which have shorter side chains than Nafion and Flemion membranes[17]. The solubility values and the diffusion coefficients of hydrogen through the Dow's membranes were not close to the values either in water or in polytetrafluoroethylene. They also concluded that hydrogen permeates through interfacial areas located between the hydrophobic fluorocarbon backbones region and the hydrophilic ionic cluster region. However, they thought that a substantial portion of the "interfacial areas" is in the aqueous phase in their model.

Perfluorinated carboxylate ion exchange membranes are known to have a cluster-network structure similar to that of Nafion [12]. It is obvious

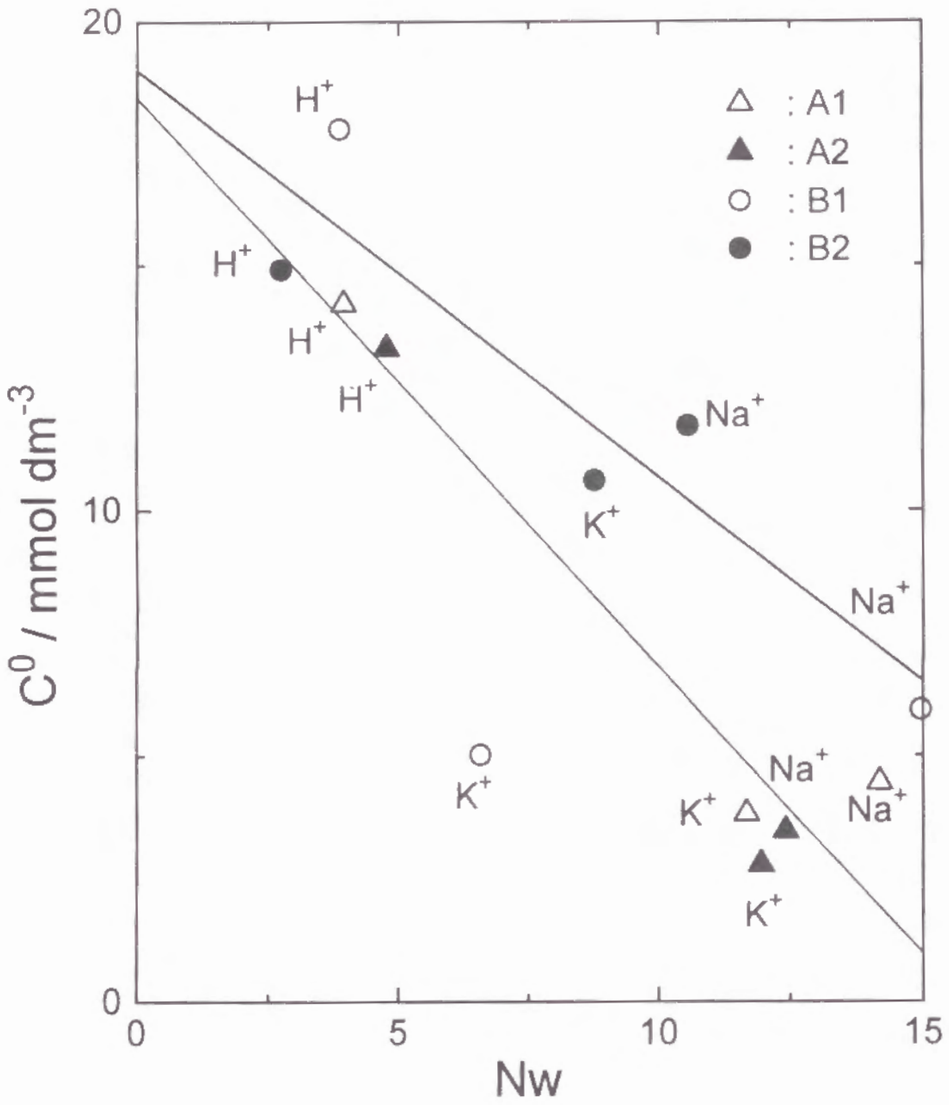

Figure 1.4 Oxygen solubilities in Flemion membranes plotted against Nw.
A1, A2, B1, and B2 denote the sample No. listed in Table 1.1.

from Table 1.2 that the solubility values of oxygen in Flemion membranes were much higher than that in water. In addition, the solubility decreased with an increase in water content. If the hydrophilic region served mainly to oxygen dissolution, oxygen solubility should increase with water content. These considerations lead to the conclusion that oxygen is dissolved mainly in the hydrophobic interfacial region of Flemion as is the case for Nafion.

The oxygen solubility decreased with water content for Flemion, while it was independent of water content for Nafion. These results indicate that the susceptibility of the hydrophobic interfacial region of Flemion to water is different from that of Nafion. From the permeation paths for gas molecules proposed by Ogumi et al.[15] and Tsou et al.[17], it is reasonable to consider that the interfacial region, in which gas molecules permeate, is composed of an amorphous part of the backbones and a part of the pendant side chains. The low acidity and the low water up-take of H^+-form Flemion show that the side chains of Flemion aggregate easily, in particular, in the H^+ form. The aggregated side chains are hydrophobic, and serve to compose the interfacial region. The degree of aggregation is dependent on water content. Therefore, the water-content dependency of oxygen for Flemion can be explained in terms of a change in degree of the side chain aggregation which serves to compose the hydrophobic interfacial region. An increase in water content increases hydration of the side chains, and decreases the degree of the side chain aggregation because well-hydrated side chains are considered to move into the hydrophilic ionic clusters. This leads to a decrease in volume of the interfacial region, i.e., a decrease in oxygen solubility. On the other hand, the sulfonate groups of Nafion are highly hydrated, and hence the water content of the Nafion membranes did not change as significantly as that of the Flemion membranes [15]. Therefore, the significant dependency of oxygen solubility on water content may not have been observed for Nafion

membranes.

The solubility in 800 EW membranes was higher than that in 700 EW membranes for a given Nw. A membrane of higher EW contains a larger volume of hydrophobic region per unit water volume, and hence contains a larger interfacial region in which oxygen can be dissolved. Therefore, solubility of oxygen increases with EW.

Table 1.2 Solubilities of oxygen in various media.

Medium	Temp. / ℃	c^0 / mM	Ref.
Nafion 125 Na^+-type	25	13.7	(15)
Nafion 117 Na^+-type	25	8.6	(15)
H_2O	25	1.3	(18)
0.5 M K_2SO_4	25	0.85	(18)
n-C_7F_{16}	25	26.8	(19)
n-C_8F_{18}	25	23.2	(19)
PTFE	20	26.8	(20)

1.4.3 Diffusion coefficient of oxygen

The diffusion coefficients of oxygen in Flemion membranes were much smaller than that in water ($2.08 \times 10^{-5} cm^2 s^{-1}$ [21]). This fact also suggests that oxygen permeate through the hydrophobic interfacial region rather than through the hydrophilic ionic clusters. However, the diffusion coefficients were smaller than those in Nafion membranes ($D = 4.3 \times 10^{-7}$ and $2.6 \times 10^{-7} cm^2 s^{-1}$ for Na^+-form Nafion membranes of EW = 1100 and 1200, respectively[15]). This indicates that the hydrophobic interfacial region in Flemion is less flexible than that in Nafion.

Figure 1.5 shows the diffusion coefficients of oxygen through Flemion membranes plotted against Nw. Opposite dependencies on Nw

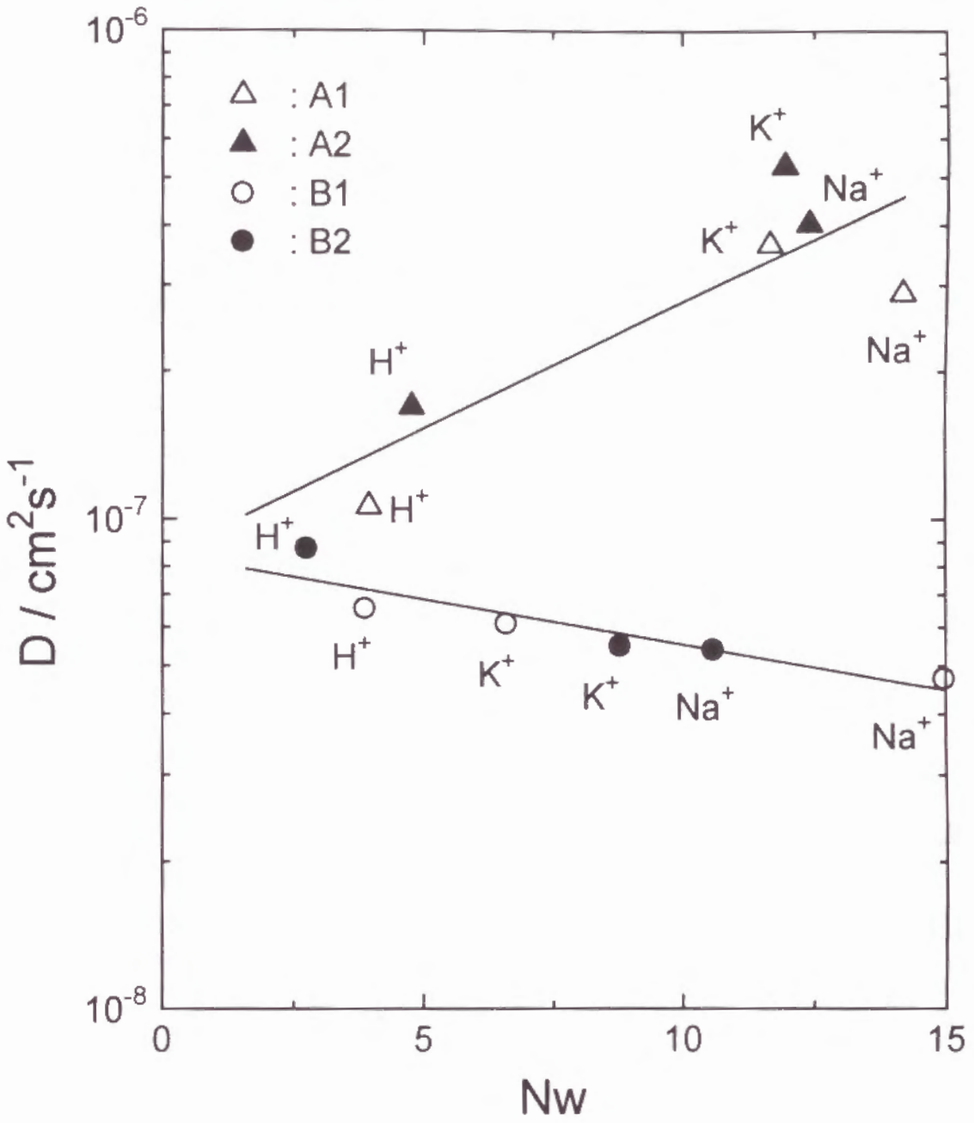

Figure 1.5 Oxygen diffusion coefficients in Flemion membranes plotted against Nw.
A1, A2, B1, and B2 denote the sample No. listed in Table 1.1.

were observed for Flemion membranes of different EWs. The diffusion coefficient in 700 EW membranes increased with Nw, while that in 800 EW membranes decreased slightly. The influence of water content, pretreatment, EW, etc. on the morphology of perfluorinated sulfonate and carboxylate ion exchange membranes have been extensively studied[12,22]. For example, a high water content decreases the crystallinity of the fluorocarbon backbones[12], and makes the hydrophobic region flexible. A high EW decreases the sizes of ionic clusters[12]. Although such morphology changes have not been studied well for Flemion, these tendencies are applicable to Flemion. The change in water content is therefore considered to affect the diffusion coefficient of oxygen in the following two different manners: (i) Water behaves as a plasticizer in the hydrophobic interfacial region and therefore an increase in water content leads to an increase in flexibility of the hydrophobic interfacial region. This enhances the diffusion coefficient of oxygen through the interfacial region in Flemion membranes, in particular, the region consisting of the aggregated side chains. (ii) The incorporation of water, plasticizer, into hydrophobic interfacial region may decrease the hydrophobicity of the region, i.e., it may decrease the volume of hydrophobic region. For example, a part of the side chains which has formed the hydrophobic interfacial region at a low water content may move to the hydrophilic ionic cluster region by increasing water content. The expansion of ionic clusters increases the tortuosity of oxygen diffusion path through the hydrophobic region, and decreases apparent diffusion coefficient. While the opposite dependencies of the diffusion coefficients in 700 EW and 800 EW membranes on Nw may be interpreted in terms of the former (i) and the latter (ii) effects, respectively, extensive investigation on the morphology of Flemion membranes is necessary to understand the detail reasons for the opposite dependencies of the diffusion coefficient.

1.4.4 Conclusions

Solubilities and diffusion coefficients of oxygen in perfluorinated carboxylate ion exchange membranes (Flemion, Asahi Glass Co.) of different counterions and equivalent weights were determined by an electrochemical monitoring technique using SPE composite electrodes. Oxygen solubility decreased with increasing water content of the membranes. The solubilities and the diffusion coefficients were close to the corresponding values in perfluorocarbon media rather than to those in water. These results lead to the conclusion that oxygen permeate mainly through a hydrophobic interfacial region which consists of a flexible amorphous part of the fluorocarbon backbones and an aggregated part of the side chains of the carboxylate membranes.

References

1. P. W. T. Lu and S. Srinivasan, *J. Appl. Electrochem.*, **9**, 269 (1979).

2. A. P. Laconti, *Japan TokkyoKakai*, 54 - 112398 (1979).

3. P. W. Eisman, *J. Power Sources*, **29**, 389 (1990).

4. Z. Ogumi, K. Nishio and S. Yoshizawa, *Denki Kagaku*, **49**, 212 (1981).

5. Z. Ogumi, K. Nishio and S. Yoshizawa, *Electrochim. Acta*, **26**, 1779 (1981).

6. Z. Ogumi, H. Yamashita, K. Nishio, Z. Takehara and S. Yoshizawa, *Electrochim. Acta*, **28**, 1687 (1983).

7. T. D. Gierke and W. Y. Hsu, in "Perfluorinated Ionomer Membranes", A. Eisenberg and H. L. Yeager (Eds.), ACS Sympo-

sium Series No. 180, Chap. 13, American Chemical Society, Washington DC (1982).

8. M. Falk, *Can. J. Chem.*, **58**, 1495 (1980).

9. N. Sivashinsky and G. B. Tanny, *J. Appl. Polym. Sci.*, **26**, 2625 (1981).

10. H. L. Yeager and A. Steck, *J. Electrochem. Soc.*, **128**, 1880 (1981).

11. H. L. Yeager, Z. Twardowski and C. M. Clarke, *J. Electrochem. Soc.*, **129**, 324 (1982).

12. T. Hashimoto, M. Fujimura and H. Kawai, in "Perfluorinated Ionomer Membranes", A. Eisenberg and H. L. Yeager (Eds.), ACS Symposium Series No. 180, Chap. 11, American Chemical Society, Washington DC (1982).

13. Y. Nakano and W. J. MacKnight, *Macromolecules*, **17**, 1585 (1984).

14. Z. Ogumi, T. Takehara and S. Yoshizawa, *J. Electrochem. Soc.*, **131**, 769 (1984).

15. Z. Ogumi, T. Kuroe and Z. Takehara, *J. Electrochem. Soc.*, **132**, 2601 (1985).

16. H. Ukihashi and M. Yamabe, in "Perfluorinated Ionomer Membranes", A. Eisenberg and H. L. Yeager (Eds.), ACS Symposium Series No. 180, Chap. 17, American Chemical Society, Washington DC (1982).

17. Y. Tsou, M. C. Kimble and R. E. White, *J. Electrochem. Soc.*, **139**, 1913 (1992).

18. Chemical Society of Japan, "Kagaku Binran, Maruzen", Tokyo (1975).

19. M'H. A. Hamza, G. Serratrice, M. J. Stebe and J. H. Delpuech, *J. Am. Chem. Soc.*, **103**, 3733 (1981).

20. T. D. Gibbs and D. Pletcher, *Electrochim. Acta*, **25**, 1105 (1980).

21. K. Asano, "Busshitsu Idouron", Kyoritsu Syuppan, Tokyo (1976) p 7.

22. W. G. Grot, G. E. Mann and D. N. Walwsley, *Paper 154 presented at the Electrochemical Society Meeting*, Houston, TX, May 7-11 (1992).

Chapter 2

Diffusion of Aniline through Perfluorosulfonate Ion-Exchange Membranes

2.1 Introduction

The perfluorosulfonate ion exchange membrane, Nafion® (E.I. du Pont de Nemours Co.) shows peculiar and very interesting properties[1,2], which make Nafion membranes very promising separators for use in electrolytic cells[3,4], SPE fuel cells[5], batteries[6,7], and even in cells for organic syntheses[8]. Results reported on the mechanical[9], structural[10], chemical[11,12] and transport[1,4] properties of Nafion membranes suggest that their peculiar properties depend mainly on two factors: the structure of the ion-cluster network in the polymer-solution phase and the polymer swelling properties which are influenced by the composition of the electrolyte contacting the Nafion. In Nafion, a hydrophobic backbone structure similar to poly-tetrafluoroethylene (PTFE) surrounds an ionic cluster which contains most of sulfonate groups and sorbed water. Ionic clusters 5 to 10 nm in diameter are connected by narrow channels.[1,4,10] In applications of these membranes, it is important to develop as detailed an understanding as possible about the underlying relationships between the

membrane structure and transport properties. Although many studies on the diffusion of inorganic ions and molecules through Nafion have been reported [13-17], only a few studies have been reported on the diffusion of organic compounds through Nafion.[18-20] Nafion has a larger affinity for hydrophobic cations than hydrophilic cations. For example, hydrophobic ruthenium bipyridine complex has an exchange selectivity of 6×10^6 over hydrophilic Na^+[21]. It has been reported from luminescence-probe and diffusivisity measurements that hydrophobic cations interact strongly with the hydrophobic sites in Nafion[22,23]. Aniline is fairly hydrophobic and therefore likely interacts with the hydrophobic regions when it diffuses through Nafion. In this chapter, the transport of aniline through Nafion 117 (equivalent weight=1100) under a concentration gradient is investigated.

2.2 Experimental

2.2.1 Ion-exchange selectivity

Three disks of Nafion 117 in the H^+ form were pretreated in boiling water for 1 h. The disks then were soaked in 0.1 M HCl solutions (M=mol dm^{-3}) of different volumes, containing 0.3-5.1 mM aniline, for 1 week in the dark and at 35 ℃. The partition coefficient of aniline into Nafion (k) then was determined spectroscopically by measuring the aniline content of the remaining solution. Using this k value, the ion-exchange selectivity of Nafion 117 for aniline over H^+, K_H^{AN}, was calculated by assuming that all of the aniline existed in the form of anilinium cation.

2.2.2 Diffusion of aniline

The apparatus used for diffusion measurements consisted of a simple diffusion cell having two PTFE chambers (Fig. 2.1). The source and receiver chambers were separated by Nafion 117 of 170 μm(dry) thickness. The exposed surface area for mass transport was 3.1 cm^2. A source solution (1 dm^3) and a receiver solution (50 cm^3) were recycled through the respective chambers at 9 $cm^3 min^{-1}$. The solution compositions are listed in Table 2.1. All chemicals were of reagent grade and were used without further purification. For the diffusion experiments with neutral aniline, purified water from a Nanopure water system (Barnstead Co.) was used as a receiver solution. Aniline transported to the receiver solution through the membrane was monitored on real time spectroscopically at 260-290nm, using a Hitachi model 200-10 spectrometer and a microflow cell which was set in the recycling line of the receiver solution. The wavelength was selected based on the absorption peak, which changed depending on the pH of solution. All experiments in this study were performed at 35 ℃, except where otherwise noted.

2.2.3 Aniline concentration and water sorption in Nafion

Three sheets of pretreated Nafion disk (2 cm in diameter) were immersed in each of the solutions that were used for the diffusion measurements(see Table 2.1), for 1 week in the dark and at 35 ℃. The concentration of the external solution was then measured spectroscopically. These measurements allowed us to calculate the total sorbed aniline (which included both the anilinium cation and neutral aniline) at pH 4.0. Water sorption into Nafion of different cationic forms, including the anilinium form, was measured by weighing the Nafion sheets before and after soaking in water. The weight difference gave the amount of water sorbed into the Nafion.

2.3 Results and Discussion

2.3.1 Ion-exchange selectivity of Nafion for anilinium cation.

Aniline is partly protonated in acidic solutions (pKb=9.30), and

Table 2.1 Composition of source and receiver solutions.

A:	source solution, 1 dm^3
	pH=4.0, I=0.3
	10 mM aniline
	83 mM M_2HPO_4 (M = Li, Na, K, Cs, Rb)
	59 mM citric acid
	37 mM M*Cl* (M = Li, Na, K, Cs, Rb)
B:	receiver solution, 50 cm^3
	pH=4.0, I=0.3
	83 mM M_2HPO_4 (M = Li, Na, K, Cs, Rb)
	59 mM citric acid
	42 mM M*Cl* (M = Li, Na, K, Cs, Rb)
or	
	pure water (resistivity > 18 MΩcm)

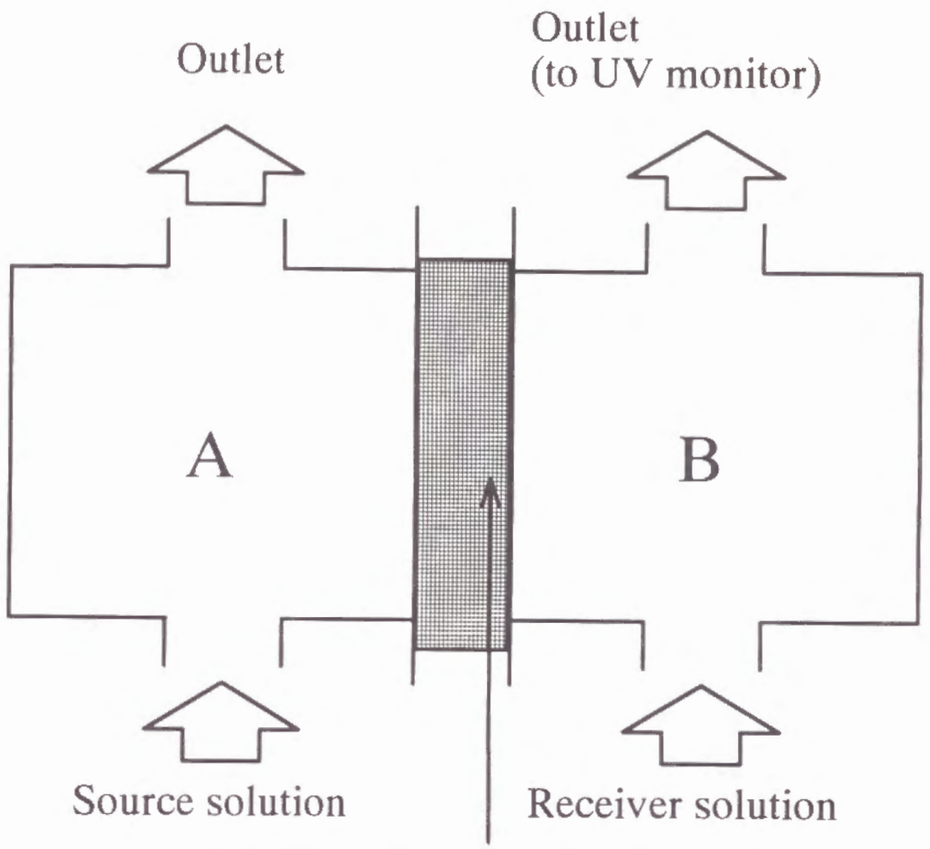

Figure 2.1 Schematic diagram of cell used for transport measurements.
A: source solution chamber, B: receiver solution chamber.
Solutions of both chambers were recycled at 9 cm^3 min^{-1}.

both the anilinium cation and neutral aniline can penetrate into Nafion. The amount of aniline absorbed into Nafion from diluted solutions of aniline in 0.1 M HCl is shown in Fig. 2.2 as a function of the aniline concentration in the external solution. In strongly acidic solutions such as 0.1 M HCl, most of the aniline exists as anilinium cations. The partition coefficient (k) can be obtained from the slope in the low concentration region of Fig. 2.2 (<0.4 mM):

$$\bar{c} = kc_0 \tag{2.1}$$

where $\bar{c}$ and c_0 are the concentrations of aniline inside and outside the Nafion, respectively. The slope in Fig. 2.2 yields a value of $k = 1.04 \times 10^3$, from which the ion-exchange selectivity of Nafion for anilinium cation over H^+, K_H^{AN} can be calculated as

$$K_H^{AN} = \frac{X_{AN} a_H}{X_H a_{AN}} \tag{2.2}$$

where X_{AN} and X_H are the mole fractions of aniline and proton respectively, inside the Nafion, and a_{AN} and aH are the activities of aniline and proton in the external solution. (Activities were assumed to be equal to concentrations.) A value of $K_H^{AN} = 69$ was obtained using Eq. (2.2). The value of K_H^{AN} is compared in Table 2.2 with the selectivity of Nafion for alkali metal cations over H^+. The value of K_H^{AN} is 1 to 2 orders of magnitude larger than that for alkali metal cations, but is much smaller than that reported for the hydrophobic ruthenium bipyridine complex cation[21]. This result suggests the existence of some interaction (hydrophobic interaction) between anilinium cations and Nafion, although this interaction is much weaker than that with hydrophobic complex cations such as ruthenium bipyridine.

Neutral aniline existing in the solution must be in equilibrium with the species in the Nafion membrane. The partition coefficient for neutral aniline, k_n, was also determined, and a value of $k_n = 2$ was obtained

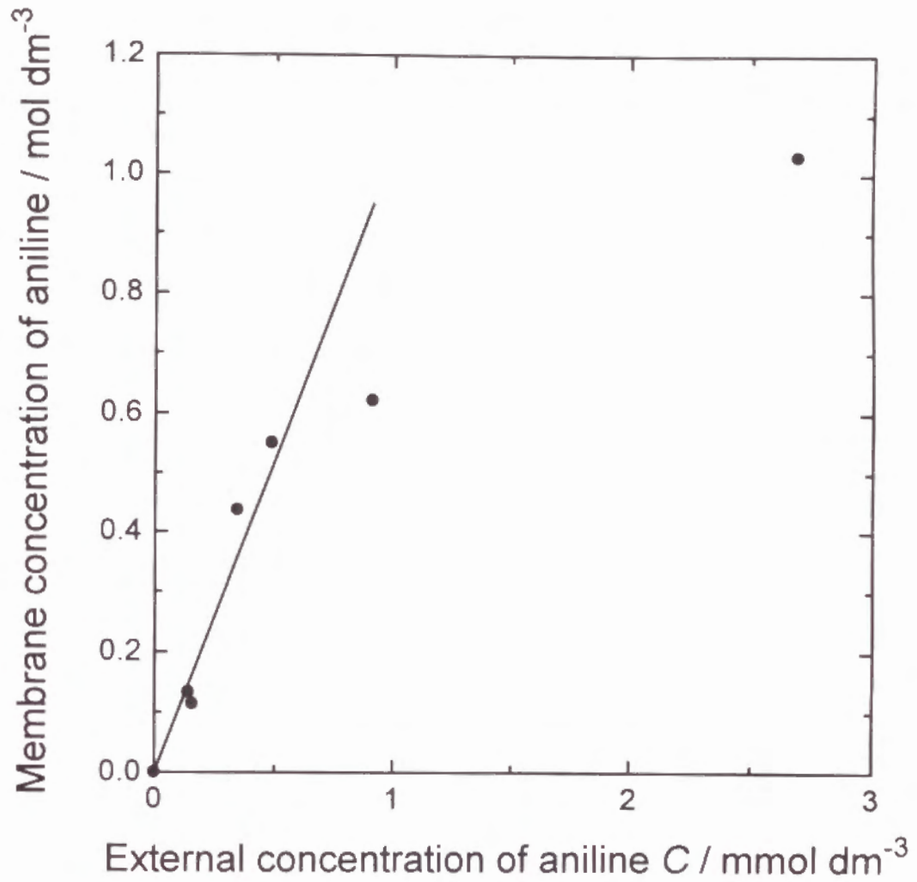

Figure 2.2 The ion exchange isotherm of aniline for Nafion in H^+ form. The external solution contained aniline and 0.1 M HCl.

Table 2.2 Selectivity coefficients and water contents of Nafion.

cation	K_H^M	N
Li^+	0.586*	22.3**
Na^+	1.18*	18.4**
K^+	3.48*	13.3**
Rb^+	4.71*	11.8**
Cs^+	7.06*	11.3**
aniline	69	10-11.5
*: from (11) **: from (12)		

for concentrations between 0.5 mM and 1.5 mM aniline in the external solution. This value larger than unity suggests that Nafion has some an affinity for neutral aniline, although much less than for anilinium cations.

2.3.2 Aniline concentration and sorbed water in Nafion

The concentration of anilinium cation in Nafion contacting solutions contacting various cations can be calculated using the values of K_H^M listed in Table 2.2. Using the value of pKb=9.30 for aniline in an aqueous solutions, it can be shown that for solution of pH 4.0 83.3 % of the aniline dissociates to anilinium cation and 16.7 % remains in the neutral form. When Nafion is in contact with a solution of pH 4.0 and an ionic strength of 0.3, and alkali metal cation is Na^+, for K_H^{AN}=69, the ratio of mole fractions inside the Nafion are

$$X_{AN} : X_{Na} : X_H = 5.7 \times 10^3 : 2.6 \times 10^3 : 1. \qquad (2.3)$$

Using a calculated value for the ion-exchange capacity of Nafion 117 of 1.7 mol dm^{-3}, the corresponding anilinium cation concentration in swollen Nafion is $c_{AN} = 1.14$ mol dm^{-3}.

The concentrations in Nafion of anilinium cation and the coexisting alkali metal cation for several other alkali metal cations (with 10 mM aniline in the contacting solution) are shown in Table 2.3. These values were calculated in the same manner as described above for Na^+, using the K_H^M values listed in Table 2.2.

Table 2.3 Concentration of aniline, C_{AN}, and co-existing cation, C_M, and apparent diffusion coefficient of aniline , D_{app}, in Nafion.
The external solution was solution A of Table 2.1.

cation	C_{AN}	C_M	$D_{app} \times 10^9$
	mol dm^{-3}	mol dm^{-3}	cm^2s^{-1}
Li^+	1.35	0.32	10.2
Na^+	1.14	0.54	11.8
K^+	0.75	0.92	6.7
Rb^+	0.63	1.04	4.9
Cs^+	0.50	1.17	3.2

The ion-exchange isotherm of aniline for Nafion in Na^+ form was measured spectroscopically and is shown in Fig. 2.3.

The amount of swelling water was measured for Nafion in the sodium and anilinium cation forms from the weight difference between before versus after swelling. The value for the anilinium form ranged from 10 to 11.5 mol H_2O per mol SO_3^-, which is reasonable when compared with the values for alkali-metal cations reported by Yeager et al[12]. (see Table 2.2). The fact that our measured value for sodium form Nafion is in good agreement with the previously reported value [12] indicates that our measuring techniques are reliable.

2.3.3 Diffusion of aniline through Nafion.

When discussing the diffusion of aniline through Nafion membranes,

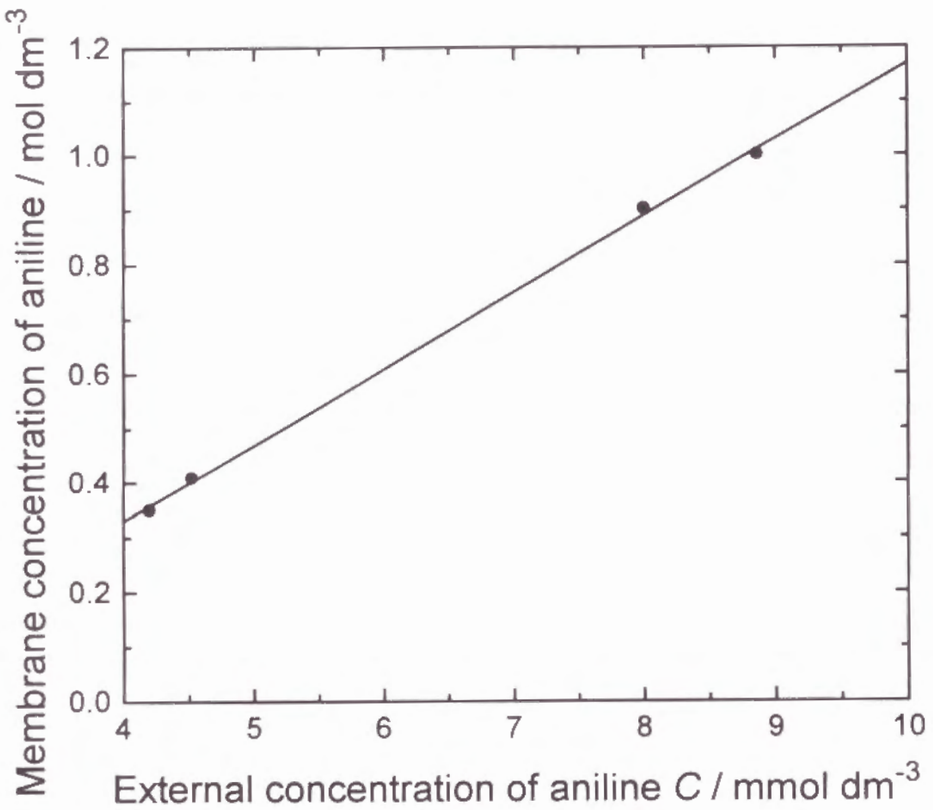

Figure 2.3 The ion exchange isotherm of aniline for Nafion in the presence of Na^+.
The external solution was the pH 4.0 solution of Table 2.1 (M=Na^+), but with various concentrations of aniline.

two diffusing species must be taken into consideration: cations (anilinium ion) and neutral molecules. Figure 2.4 shows the amounts of aniline transported from a source chamber containing solution A of Table 2.1 (10 mM aniline) to a receiver chamber containing either solution B of Table 2.1 (no added aniline, curve a) or pure water (curve b). The amount of aniline (the aniline concentration in the receiver solution) increased gradually due to its transport through the Nafion.

Curve a represents the total aniline transported through the Nafion membrane including both neutral molecules and anilinium cations, while curve b represents the neutral aniline molecules transported through the Nafion.

Many workers have reported that mass transport through ion-exchange membranes is complicated, and that in addition to diffusion, the influence of the potential distribution inside the membrane (i.e., migration effects) also should be taken into consideration[24,25]. Furthermore, even diffusion is complicated by a non-linear concentration distribution caused by the potential distribution inside the membrane. However, the conditions under which curve a was obtained permit a simple linear diffusion treatment, since the solution compositions in the two chambers contacting the membrane were almost the same (except that the receiver solution initially did not contain any aniline), and the concentration of aniline in the source solution was low.

2.3.4 Apparent diffusion coefficient, D_{app}, through Nafion.

The aniline diffusion coefficient was calculated from curve a, taking the equilibrium concentration of the species within the Nafion into consideration. As mentioned above, simple linear concentration gradients of aniline and anilinium ion through the Nafion under steady state conditions were assumed. The apparent diffusion coefficient of aniline D_{app}

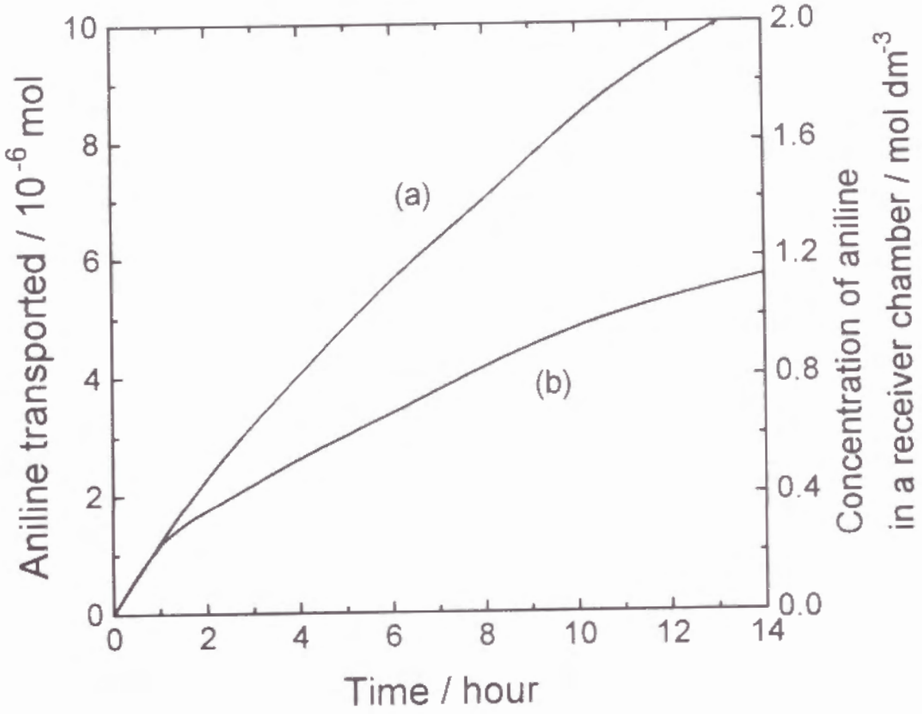

Figure 2.4 Changes in the amount of transported aniline.
The source solution is described in Table 2.1.
a: receiver chamber contained solution B of Table 2.1 (pH 4, M=Na^+).
b: receiver chamber contained pure water.

was estimated to be 1.2×10^{-8} $cm^2s^{-1}$by Fick's law using a source solution containing Na^+. This value includes the diffusion of both anilinium cations and neutral aniline, and is reasonable when compared with the values reported for alkali metal cations (1.1×10^{-6} $cm^2s^{-1}$for Na^+ and 3.7×10^{-8} $cm^2s^{-1}$for Cs^+)[26], H_2 (5×10^{-7} cm^2s^{-1})[17], and O_2 (2×10^{-7} cm^2s^{-1})[17] at 25 ℃.

The variation of D_{app}, with the cationic species in the solution also was investigated. D_{app} was dependent on the co-existing cationic species, as can be seen from the calculated values listed in Table 2.3. When the co-existing cation was changed, the circumstances inside the membrane had to change accordingly; the concentration of the anilinium ions and the co-existing cations and protons, as well as the water content in the membrane also must have changed. In particular, the fraction of the anilinium cation in the membrane was dependent on the co-existing cation because of the differences in the ion-exchange selectivity coefficients of the different cationic forms of Nafion.

For the transport of aniline within the membrane, molecular diffusion through the aqueous pores of the membrane structure was assumed, and since the pressure difference between the two compartments (including the osmotic pressure) was small under experimental conditions, contributions from convection were considered to be negligible. Migration effects also were neglected (see above). The Nafion membranes were assumed to be micro-porous films. The micro-pores correspond to the ionic clusters of Nafion which contain almost all of the water and ionic species and are thought to be responsible for the diffusion of anilinium cations[20]. This might not be the case for hydrophobic cations such as Cs^+ and Rb^+: it has been reported that Cs^+ exists at the interfacial region between the ionic clusters and the hydrophobic backbone, and that the diffusion constant of Cs^+ is independent of the water content of the

membrane[14]. Aniline and anilinium cation also are hydrophobic, and therefore one might expect that they also would exist at the interface. Contrary to this expectation, however, the value of D_{app} was dependent on the counter ion and on the water content (see below). This fact indicates that the above assumption of molecular diffusion through the micro-pores is acceptable for the particular case of transport of aniline through Nafion 117 under the conditions used in this study. It also was assumed that D_{app} is linearly proportional to the membrane porosity, and furthermore, that the membrane porosity is linearly proportional to the water content in the membrane. The water content of the membrane is a measure of the pore volume. The total water content in the membrane equilibrated with the source solution can be expressed as a linear combination of the water content for each cation existing within the membrane:

$$N = N_{AN}X_{AN} + N_M X_M \tag{2.4}$$

where N is the total water content in the membrane equilibrated with the source solution, N_{AN} and N_M are the water contents when all the counter ions are changed to anilinium and M^+ (alkali metal cation), respectively, and X_{AN} and X_M are the respective mole fractions in the membrane. The value of N_{AN} calculated based on Eq. (2.4) is 10.7 mol H_2O per mol SO_3^-. This value was obtained by using Eq. (2.4) to calculate the values of N for the different cations corresponding to various assumed values of N_{AN}. Since the experimental values of D_{app} for the different cations (listed in Table 2.3) were assumed to be linearly proportional to N, the value of N_{AN} corresponding to the best straight line plot of D_{app} versus N_{AN} was determined by trial and error. (The method of least squares was used to judge the linearity of the plots of D_{app} versus N.) The plot of D_{app} versus N for the best straight line is shown in Fig. 2.5. The corresponding value of $N_{AN} = 10.7$ mol H_2O per mol SO_3^- is reasonable when compared with the water content for the

other cations, and falls in middle of the range of 10-11.5 obtained from the weight change measurements described in the previous section.

2.3.5 Transport of aniline molecules through Nafion

The contribution from diffusion of neutral molecules was estimated from Curve b in Fig. 2.4, which was obtained by filling the receiver chamber with pure water. It was assumed that in this case only neutral molecules diffused through the membrane into the receiver solution. If anilinium cations had diffused through the membrane, then either some other cations had to have diffused in the opposite direction, or anions had to have diffused in the same direction, in order to prevent charge separation. However, since there were no cations in the receiver solution to be exchanged with anilinium cations from the source solution, therefore it was assumed that only neutral molecules could have diffused through the Nafion to the receiver compartment. It was also assumed that the diffusion of each species was independent and did not influence the diffusion of the other species. The apparent diffusion coefficient for neutral aniline, D_n, was estimated as 3.3×10^{-6} cm^2s^{-1}using the same method as that used to estimate D_{app}. This value is two orders of magnitude larger than D_{app} and one order of magnitude larger than the values for diffusion of oxygen, hydrogen, and bromine ($1\text{–}5 \times 10^{-7}$ cm^2s^{-1}) [6]. The value is comparable to the value for water ($1\text{–}4 \times 10^{-6}$ cm^2s^{-1}) [14] and would appear to be too high for a molecule as large as aniline. D_n was not affected by the co-existing cationic species in the Nafion. The anomalously high apparent flux of neutral aniline can be explained as follows. An equilibrium exists between anilinium cations and aniline within Nafion, although the equilibrium constant may differ from the value in bulk aqueous solution.

$$AN(\text{aniline}) + H^+ \rightleftharpoons ANH^+(\text{anilinium cation}) \tag{2.5}$$

This equilibrium may exist even at the interface between Nafion and the

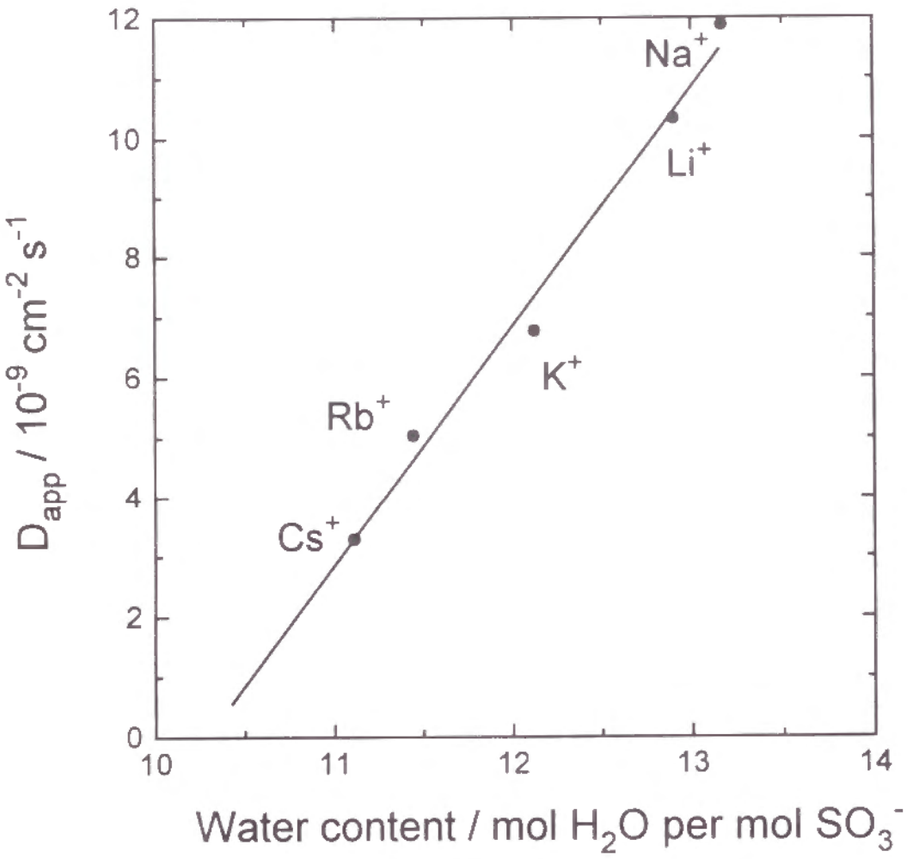

Figure 2.5 The relation between apparent diffusion constant of aniline, D_{app}, and water content of Nafion 117.
The co-existing cations, M^+, in the solutions are marked on the figure.
The solution compositions were as listed in Table 2.1.

receiver solution. Since the rate reaction (2.5) likely is very fast, it is not likely to be the rate determining step in the transport of neutral aniline, Accordingly, the apparent flux of neutral aniline should be equal to the flux of total aniline, if the assumptions used to calculate D_n are valid. However, the results in Fig. 2.4 show that the apparent flux of neutral aniline is half of the total aniline flux. This smaller flux may be due to the existence of a potential difference at the membrane/solution interface. In contrast to the conditions under which curve a in Fig. 2.4 was obtained, for curve b in Fig. 2.4, the compositions of the two solutions contacting the membrane were different; the ionic strength of the source solution was 0.3, but that of the receiver solution was nominally zero. The extremely low concentration of the receiver solution may have resulted in the formation of a large Donnan potential at the interface, which in turn may have influenced reaction (2.5).

Further investigation is required to elucidate the details of the mass transfer of neutral aniline through Nafion.

Refferences

1. H. L. Yeager and B. Kipling, *J. Phys. Chem.*, **83**, 1836 (1979).

2. G. Scibona, C. Fabiani, and B. Scuppa, *J. Membrane Sci.*, **16**, 37 (1983).

3. H. L. Yeager, B. Kipling, and R.L. Dotson, *J. Electrochem. Soc.*, **127**, 303 (1980).

4. R. S. Yeo, J. McBreen, G. Kissel, F. Kulesa, and S. Srinivasan, *J. Appl. Electrochem.*, **10**, 741 (1980).

5. E. Gileadi and S. Srinivasan, F. J. Salzano, C. Brann, A. Beaufrere, S. Gottesfield, L.J. Nuttal, and A.B. LaConti, *J. Power Sources*, **2**,

191 (1977).

6. F. G. Will, *J. Electrochem. Soc.*, **126**, 36 (1976).

7. F. G. Will and H. S. Spacil, *J. Power Sources*, **5**, 173 (1980).

8. R. S. Yeo, *J. Electrochem. Soc.*., **130**, 533 (1983).

9. A. Eisenberg and H. L. Yeager, "Perfluorinated Ionomer Membranes", ACS Symposium Series, Vol.180, Chap.6 American Chemical Society, Washington D.C., (1982).

10. T. D. Gierke, 152nd National Meeting, *Electrochem. Soc.*, Atlanta, (1977).

11. H. L. Yeager and A. Steck, *Anal. Chem.*, **51**, 862 (1979).

12. H. L. Yeager and A. Steck, *Anal. Chem.*, **52**, 1215 (1980).

13. A. Herrera and H. L. Yeager, *J. Electrochem. Soc.*, **134**, 2446 (1987).

14. H. L. Yeager and A. Steck, *J. Electrochem. Soc.*, **128**, 1880 (1981).

15. C. R. Cris Wang, J. W. Strojek, and T. Kuwana, *J. Phys. Chem.*, **91**, 3606 (1987).

16. Z. Ogumi, Z. Takehara, and S. Yoshizawa, *J. Electrochem. Soc.*, **131**, 769 (1984).

17. Z. Ogumi, T. Kuroe, and Z. Takehara, *J. Electrochem. Soc.*, **132**, 2601 (1985).

18. S. K. Sikdar, *J. Membrane Sci.*, **23**, 83 (1985).

19. S. K. Sikdar, *Ind. Eng. Chem. Res.*, **26**, 170 (1987).

20. M. W. Verbrugge, *J. Electrochem. Soc.*, **136**, 417 (1989).

21. M. N. Szentirmay and C. R. Martin, *J. Electrochem. Soc.*., **131**, 751 (1984).

22. M. N. Szentirmay and C. R. Martin, *Anal. Chem.*, **56**, 1898 (1984).

23. D. A. Buttry and F. C. Anson, *J. Am. Chem. Soc.*., **104**, 4824 (1982).

24. F. Helffrich, "Ion Exchange", McGraw-Hill, Inc., New York (1962).

25. N. Lakshminarayanaiah, "Transport Phenomena in Membranes", Academic Press, Inc., New York (1969).

26. M. Lopez, B. Kipling, and H. L. Yeager, *Anal. Chem.*, **49**, 629 (1977).

Chapter 3

Electrotransportation of Aniline Through Perfluorosulfonate Ion-Exchange Membranes

3.1 Introduction

A commercially available perfluorosulfonate cation-exchange membrane, Nafion, is chemically and thermally stable, and applied to a variety of processes such as electrolytic cells[1,2], polymer electrolyte membrane fuel cells[3], sensors[4], batteries[5,6], and cells for organic synthesis[7]. Results reported on its structure[8] and transport properties[1,9–11] reveal that Nafion is microscopically separated into two phases: an ionic cluster domain, which contains most of the sulfonate groups, cations and sorbed water, and a hydrophobic backbone domain similar to that of polytetrafluoroethylene (PTFE), which surrounds the ionic cluster. This characteristic structure gives Nafion peculiar and interesting properties in swelling, ion-exchange selectivity, etc.

While organic cations are reported to interact strongly with the hydrophobic micro-domain in Nafion[12,13], few studies have been reported on the permeation of organic compounds through Nafion[14–16]. In the previous chapter, the effects of various alkali cations on permeation phenomena

of aniline through Nafion in the presence of concentration gradient across a Nafion membrane have been diccused[17]. The apparent diffusion coefficients of anilinium cation and neutral aniline were determined and it was found that they are strongly affected by the water content of the Nafion membrane. However, permeation behavior of anilinium cation under application of DC current still remains to be clarified. Research on permeation behavior of organic species under current passage, electrotransportation, would give useful information on the perm selectivity of Nafion and hydrophobic interaction between organic species and Nafion. In this chapter, the attention is focused on the electrotransportation of aniline through Nafion 117 (Equivalent Weight : EW=1100).

3.2 Experimental

3.2.1 Membrane treatments

A perfluorosulfonate cation-exchange membrane, Nafion 117, was used in this study. Nafion samples in H^+-form (3 cm in diameter in the dry state) were pre-treated in boiling water for more than 1 h. The sample was then soaked in a source solution shown in Table 3.1 for c.a. 24 h in the dark at 35 ℃. During this treatment swelling and ion exchange between the Nafion and the source solution were brought into equilibrium.

3.2.2 Measuring cell

The permeation measurements under a flow of DC current were carried out using a cell shown in Fig. 3.1. The cell was composed of four compartments made of PTFE. The volume of compartments A (anode compartment) and D (cathode compartment) was c.a. 10 cm^3, and that of B and C was c.a. 3 cm^3. Compartments B and C were separated by the Nafion membrane which had been equilibrated with the source solution. Compartments A and D were fitted with a DSA-type anode plate and a

Table 3.1 Composition of source and receiver solutions.

Source solution
pH 4.2
10 mmol dm^{-3} Aniline
83 mmol dm^{-3} M_2HPO_4
59 mmol dm^{-3} Citric acid
37 mmol dm^{-3} MCl
(M = Na, K, Cs)
Receiver, anode and cathode solutions
pH 4.2
83 mmol dm^{-3} M_2HPO_4
59 mmol dm^{-3} Citric acid
42 mmol dm^{-3} MCl
(M = Na, K, Cs)

Ni cathode plate, respectively. Hydrocarbon-type anion-exchange membranes (Selemion® AMV, Asahi Glass Co.) separated compartments A and B, and compartments C and D in order to prevent anilinium cation from penetrating into compartments A and D. The exposed surface area of the Nafion membrane was 3.1 cm^2.

3.2.3 Permeation measurements

The compositions of the source and receiver solutions used for electrotransportation measurements are listed in Table 3.1. The source (1000 cm^3) and receiver (50 cm^3) solutions containing a common alkali cation (M^+) were circulated separately through compartments B and C at 0.15 $cm^3\ s^{-1}$, respectively. Since the volume of the source solution was 20 times larger than that of the receiver solution, the decrease in aniline concentration in the source solution was small; hence, the aniline concentration in the source solution was assumed to be constant during each permeation measurement. An external DC current was applied galvanostatically across the DSA type anode and the Ni cathode using a potentio/galvanostat (Hokuto Denko model HA301). The amount of aniline transported to the receiver solution through the Nafion membrane was monitored as a change in spectroscopic absorbance at 280 nm, using a Hitachi model 200-10 spectrometer equipped with a micro-flow cell, which was set in the circulating line of the receiver solution. Since the increase in aniline concentration in the cathode compartment, D, was less than 1

3.2.4 Absorbance change of aniline solution with pH

The source solution was diluted to 10-fold volume with water, and a solution containing 1 mM aniline was obtained. A small volume of 1 M HCl or 1 M NaOH was added to the solution to change its pH. The absorbance of the resulting solutions of various pHs was measured using

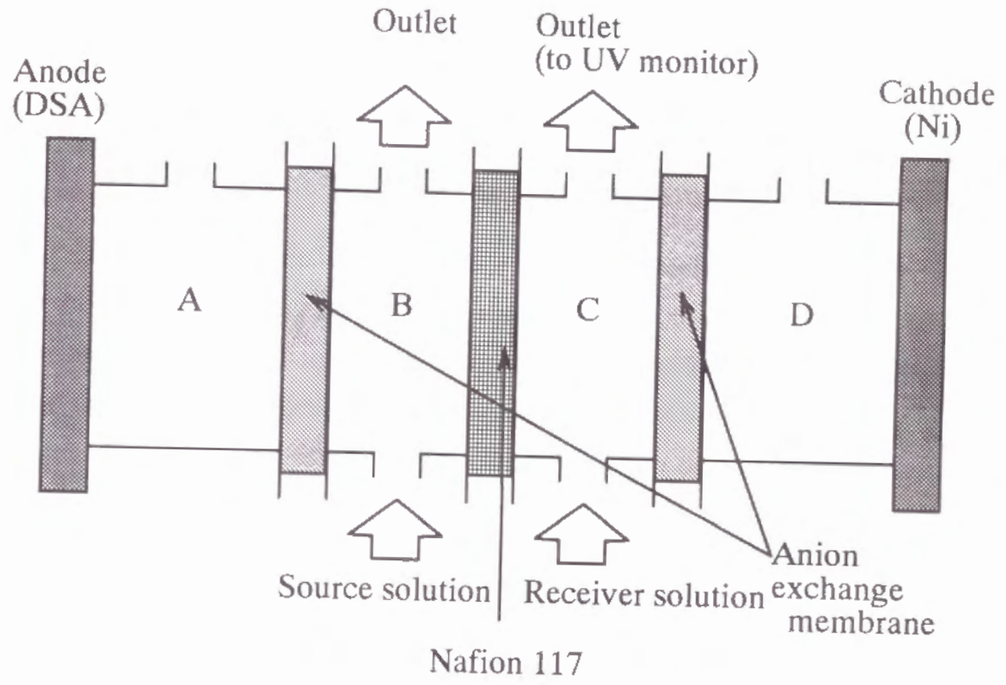

Figure 3.1 Schematic diagram of the cell used for permeation measurements.
A: anode compartment; B: source solution compartment; C: receiver solution compartment; D: cathode compartment.
The solutions in B and C were circulated at 0.15 $cm^{-3}\ s^{-1}$.

the UV/VIS spectrometer described above.

3.3 Chemicals

All chemicals were of reagent grade and were used without further purification. Water (> 18MΩ, nominally) was obtained from a NANO pure water purifying system (Barnstead Co.).

3.4 Results and Discussion

3.4.1 Variation in spectroscopic absorbance of aniline with pH

Spectroscopic absorbance of solutions containing aniline species of various pHs was measured at 280 nm, and the variation in the absorbance with pH is shown in Fig. 3.2. The absorbance at 280 nm changed drastically with pH. In acidic solutions a following reaction (3.1) reaches the equilibrium:

$$AN(\text{aniline}) + H^+ \rightleftharpoons ANH^+(\text{anilinium cation}) \qquad (3.1)$$

While neutral aniline absorbs light of 280 nm, protonated aniline (anilinium cation) does not. Hence the absorbance at 280 nm can be used as a measure of the content of neutral aniline in a solution. The dependency of the measured absorbance on the solution pH in Fig. 3.2 was in good agreement with the absorbance dependence calculated from the neutral aniline concentration using a pKa value of aniline, 4.7, and pHs of the solutions.

3.4.2 Electrotransportation of aniline through Na^+-form Nafion

The permeation of aniline was measured under a flow of DC current using Na^+-form Nafion and the solutions containing Na^+ cation (see Table 3.1). Figure 3.3 shows the absorbance changes at 280 nm of

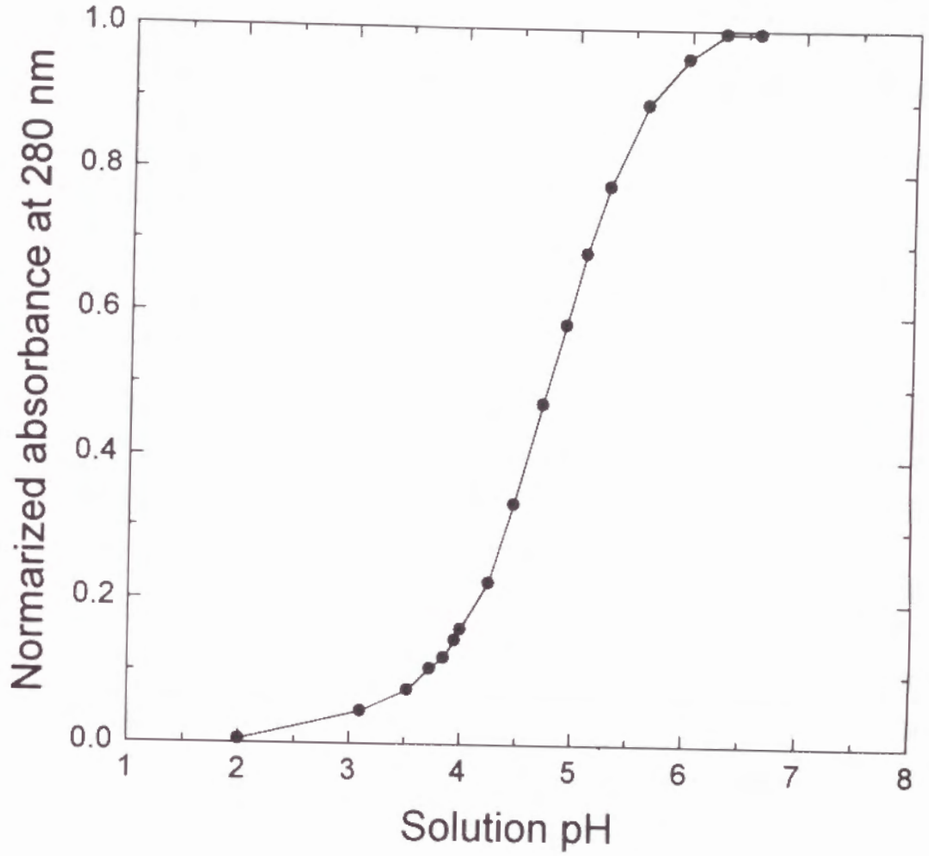

Figure 3.2 Absorbance change at 280 nm of solutions containing 1 mM aniline with pH.

the receiver solution with time at various current densities. The current density means here the magnitude of a DC current per unit surface area of the separator membrane, Nafion. During each run the pH of the receiver solution increased slightly with an increase in charge passed. The pH changes with charge passed are shown in Fig. 3.4. As is discussed above, a pH change affects the equilibrium between neutral aniline and anilinium cation in Eq. (3.1). In order to obtain the total amount of aniline transported to the receiver solution, the amount of anilinium cation must be taken into consideration in addition to neutral aniline obtained spectroscopically. Hence the total content of aniline species in the receiver solution was calculated using the data in Figs. 3.2 and 3.4. Figure 3.5 shows the calculated concentration changes of the total aniline in the receiver solution at various current densities.

The slope of each curve means the aniline flux under the corresponding conditions. The flux decreased with an increase in charge passed through the Nafion. Aniline was transported by migration under a potential field across the membrane and by diffusion due to a concentration gradient between the two solutions. Since the driving force for diffusional transport decreased with the passage of time because of accumulation of aniline in the receiver solution, the decrease in aniline flux observed in Fig. 3.5 is attributable to a decrease in diffusional contribution at a prolonged permeation time.

3.4.3 Influence of co-existing alkali metal cation

Similar permeation measurements were carried out using K^+- and Cs^+-form Nafion and the corresponding solutions listed in Table 3.1. Changes of total aniline concentration in the receiver solution are shown in Figs. 3.6-(i) and 3.6-(ii) for K^+- and Cs^+-form Nafion membranes, respectively. The tendencies were similar to that for Na^+-form Nafion,

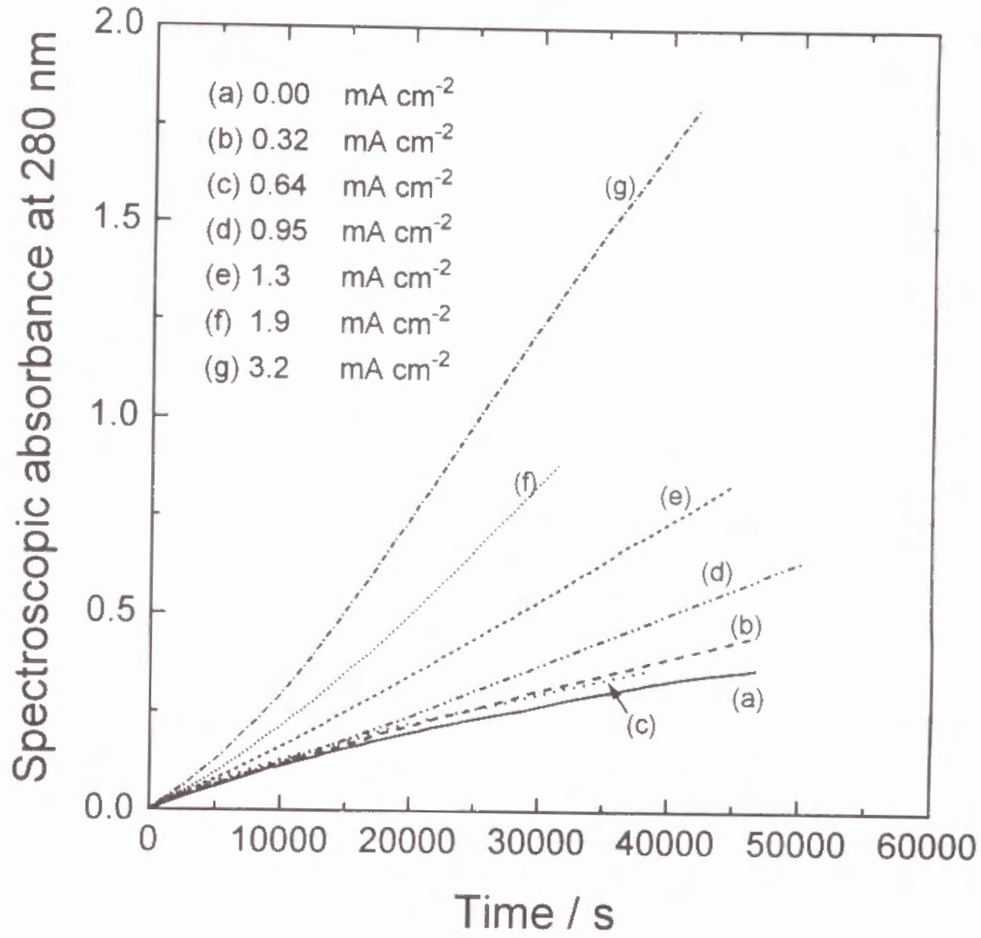

Figure 3.3 Changes in absorbance of the receiver solution at 280 nm for Na^+-form Nafion at current densities of (a) 0.0, (b) 0.32, (c) 0.64, (d) 0.96, (e) 1.3, (f) 1.9 and (g) 3.2 A cm^{-2}.

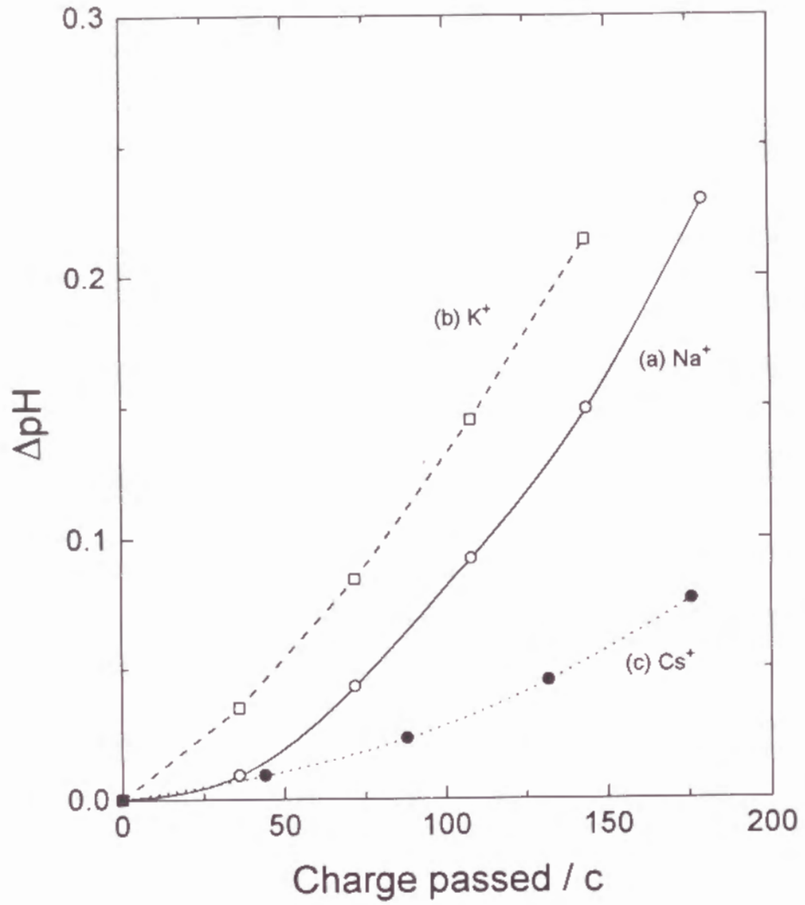

Figure 3.4 Changes in pH of receiver solution for (a) Na^+, (b) K^+ and (c) Cs^+ forms of Nafion with charge passed.

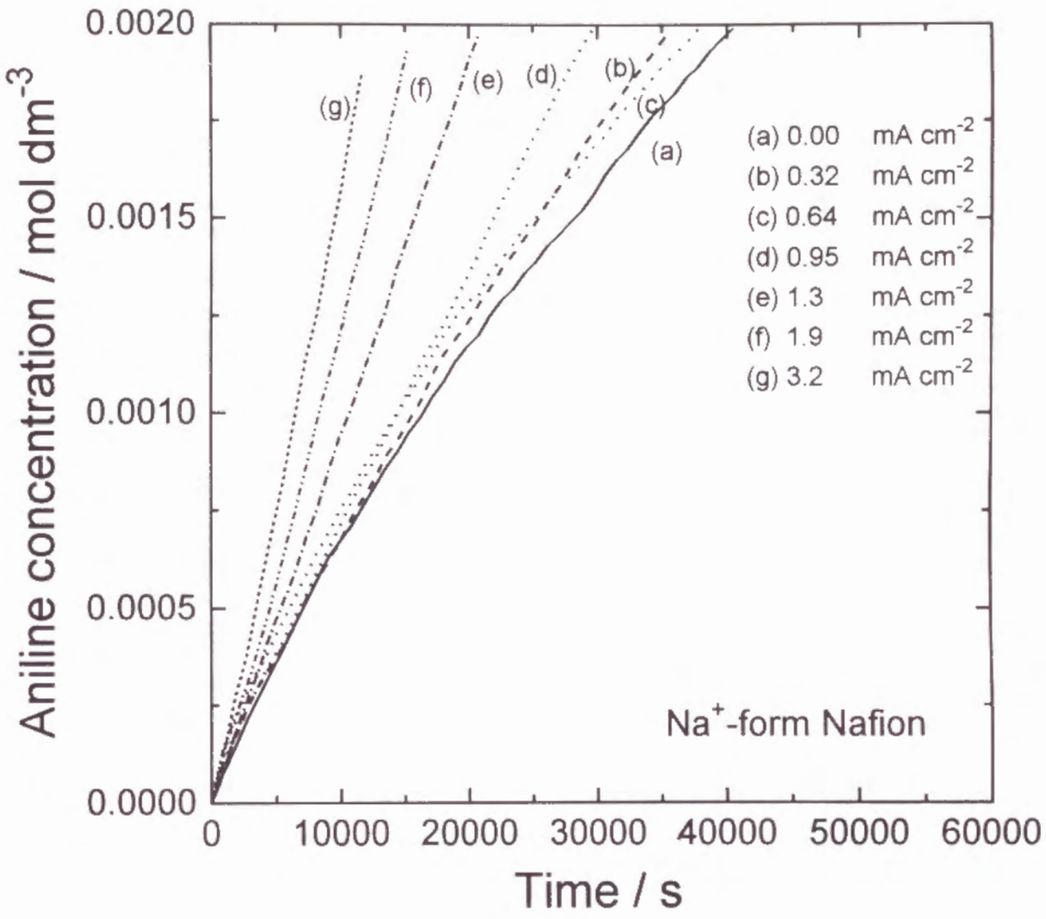

Figure 3.5 Calculated concentration changes of total aniline species in the receiver solution for Na^+- form Nafion at current densities of (a) 0.0, (b) 0.32, (c) 0.64, (d) 0.96, (e) 1.3, (f) 1.9 and (g) 3.2, A cm^{-2}.

although the aniline concentration for K^+- and Cs^+-forms increased less remarkably than that for the Na^+- form Nafion.

3.4.4 Influence of current density on aniline flux

The dependency of aniline flux through Nafion on current density is of primary interest of this study. Since aniline flux decreased with an increase in aniline concentration in the receiver solution as mentioned above, aniline fluxes at various current densities were compared using the values at a fixed aniline concentration (0.6 mM) in receiver solutions. At this concentration a pH change in the receiver solution was negligibly small (see Fig. 3.4). It is acceptable to assume that the fluxes due to the diffusional transport at the fixed aniline concentration difference were equal to one another because the driving force for diffusional transport was independent of the current density. On the basis of this assumption, the aniline fluxes were calculated from the data in Figs. 3.5 and 3.6, and are plotted in Fig. 3.7. Although the values in Fig. 3.7 are still not free from a contribution from the diffusional transport, they are assumed to be independent of current density. In each form the slope of aniline flux increased abruptly in the current density range from 0.3 to 1.3 A cm^{-2}. The aniline flux was highest for Na^+-form Nafion. At low current densities aniline flux for Cs^+-form was lowest. However, the increase in aniline flux for Cs^+-form was slightly larger than that for the K^+-form.

3.4.5 Transport number of anilinium cation

Since the ionic strength of the external solutions was much smaller than that inside the Nafion membrane, the Donnan exclusion works well and the absorption of anions inside the Nafion membrane can be neglected under the present experimental conditions. Hence three species, i.e., anilinium cation (AN^+), alkali metal cation (M^+) and proton (H^+),

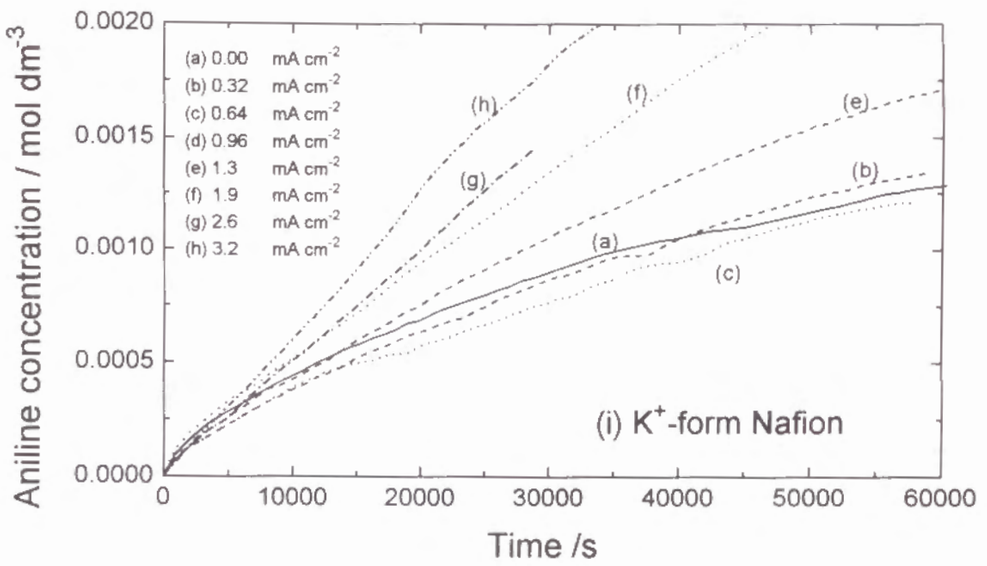

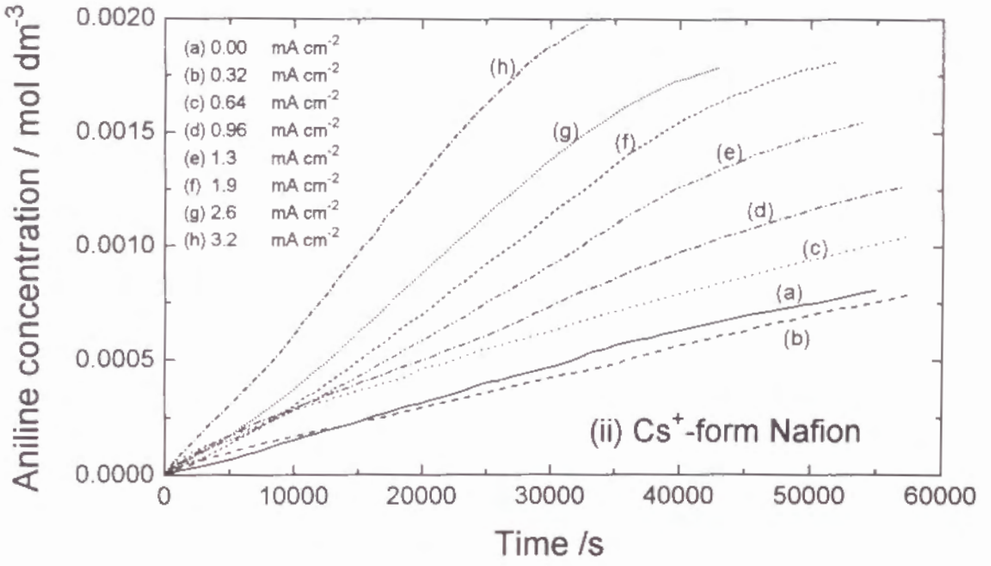

Figure 3.6 Calculated concentration changes of total aniline species in the receiver solution for (i) K^+- and (ii) Cs^+-forms of Nafion at current densities of (a) 0.0, (b) 0.32, (c) 0.64, (d) 0.96, (e) 1.3, (f) 1.9, (g) 2.6 and (h) 3.2 A cm^{-2}.

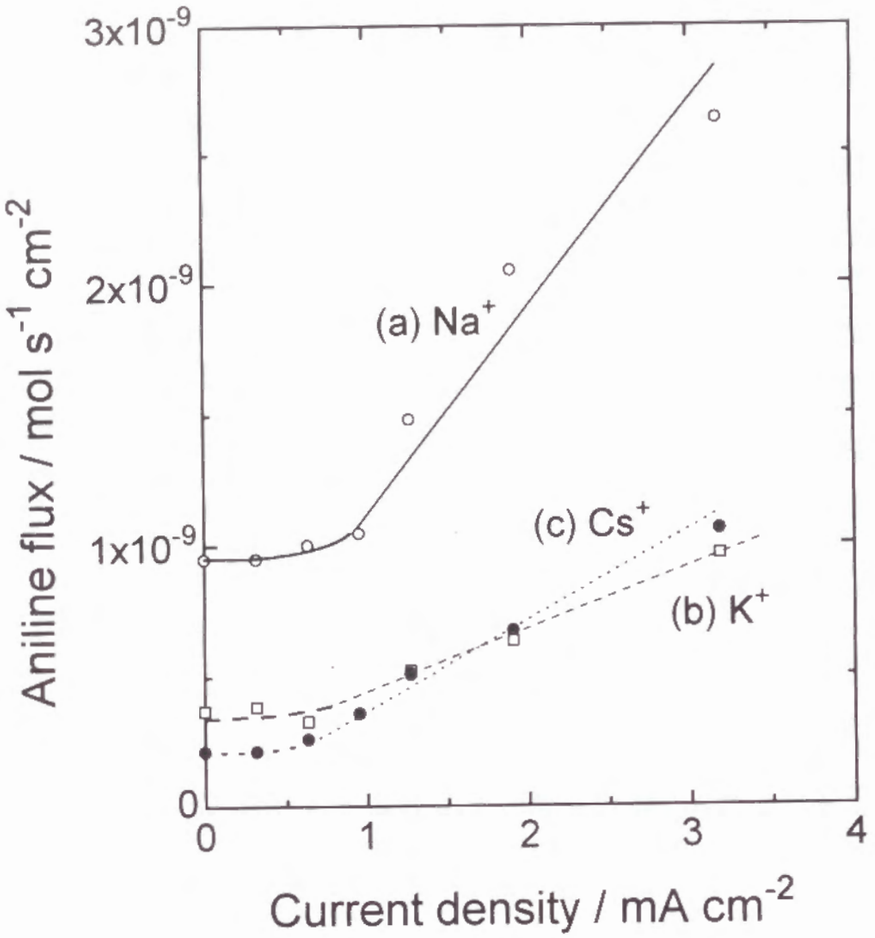

Figure 3.7 Aniline fluxes at an aniline concentration of 0.6 mM in the receiver solution against current density for (a) Na^+-, (b) K^+- and (c) Cs^+-forms of Nafion.

are supposed as mobile ionic species in Nafion. In other words, these three cations are the charge carriers inside Nafion. Total ionic conductivity, σ_t, of the Nafion is expressed as

$$\sigma_t = \sum_i t_i \sigma_t \tag{3.2}$$

$$= \sum_i \sigma_i \tag{3.3}$$

where t_i and σ_i denote the transport number and conductivity of individual charged species. The conductivity of individual charged species having uni-valency is expressed as

$$\sigma_i = F^2 C_i u_i = \frac{F^2 C_i D_i}{RT} \tag{3.4}$$

where C_i, D_i, and u_i denote the concentration, diffusion coefficient, and mobility of the individual charged species in Nafion, and F and R are the Faraday and gas constants.

Electrotransported aniline flux was estimated subtracting the diffusional aniline flux (the aniline flux at zero current density in Fig. 3.7) from the total aniline flux. The resulting transport numbers were plotted in Fig. 3.8 against current density. In each form, transport number increased in the range from 0.3 to 1.3 A cm^{-2}, and reached a constant value at higher current densities. However, these transport numbers of AN^+ were small, and most of the charge was therefore carried by the other cations in Nafion. The concentration changes of H^+ in the source and receiver solutions were small during the measurements (for example, see Fig. 3.4). In addition, the proton concentration inside Nafion was much lower than those of other cations because of the low H^+ concentration in the solutions (10^{-4} M) and of the low H^+-selectivity coefficient of Nafion. Hence, the charge carried by proton can be neglected, and most of the charge was carried by M^+ in Nafion.

As shown in Fig. 3.8, the magnitudes of transport number of AN^+ in the plateau region in Na^+-, Cs^+- and K^+-form Nafion membranes de-

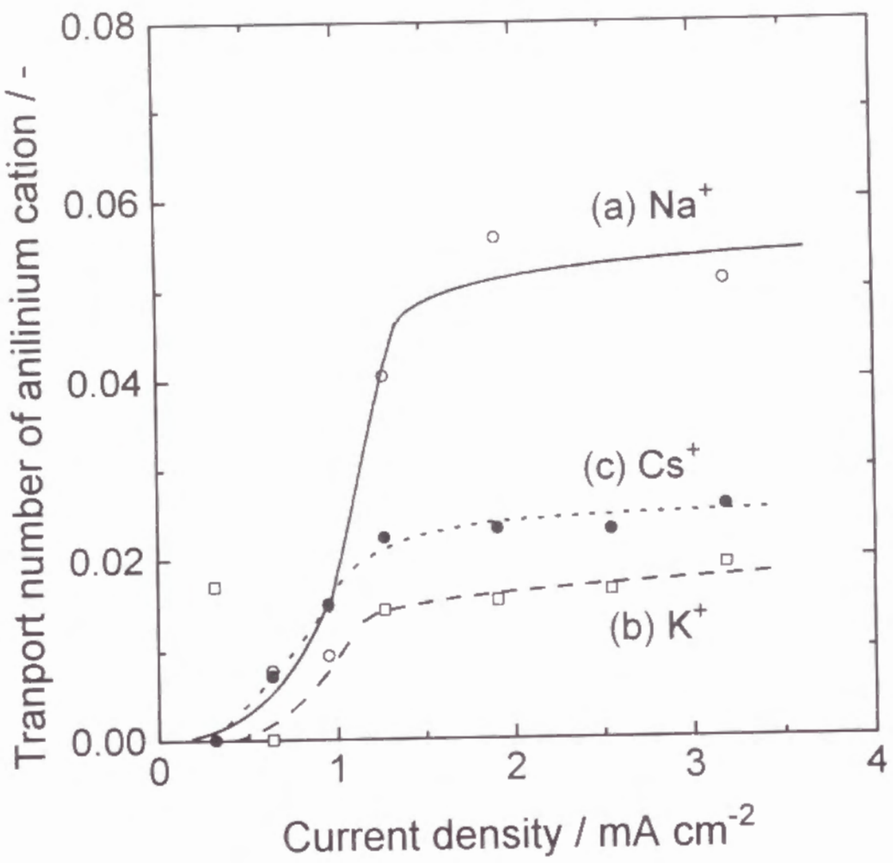

Figure 3.8 Changes in transport number of anilinium cation in Nafion with current density for (a) Na^+-, (b) K^+- and (c) Cs^+-forms of Nafion.

creased in that order. From Eq. (3.4) the individual conductivity should be proportional to C_i and D_i. The diffusion coefficients and concentrations of aniline in Na^+, K^+ and Cs^+-forms of Nafion 117 in contact with a solution of the same composition as the source solution had been reported and are summarized in Table 3.2[17]. (The diffusion coefficients of alkali metal cations are the values reported for Nafion 120). The products of C_{AN^+} and D_{AN^+} for each form Nafion is also shown in Table 3.2. From the values one would expect that the magnitudes of transport number of AN^+ should to follow the order in Na^+- > in K^+- > in Cs^+-forms. However the order was not the case. The transport number of AN^+ (t_{AN^+}) in the plateau region for Na^+-form in Fig. 3.8 was about three times larger than that for K^+-form, which is in good agreement with the ratio of the products, $C_{AN^+} \times D_{AN^+}$, for Na^+- and K^+-forms. However, t_{AN^+} in Cs^+-form was much larger than the value expected from the product. Hydrophobic properties of Cs^+ seems to cause the higher transport number in Cs^+ than in K^+-form Nafion, and this will be discussed in the following sections.

3.4.6 Electrotransportation of aniline without concentration gradient

To eliminate the contribution from the diffusional transport, permeation measurements were carried out using a buffer solution of pH 4 containing Na^+ and 2 mM aniline as both source and receiver solutions. The change in aniline concentration in the receiver solution was monitored for 20 min. In this experiment, a contribution from the diffusional transport can be neglected because there was almost no concentration gradient of aniline. The aniline concentration in the receiver solution increased linearly with time. The calculated aniline flux change is shown in Fig. 3.9. While the tendency was similar to those in Fig. 3.7, the flux at a given current density was much smaller than those in Fig. 3.7, and

Table 3.2 Diffusion coefficient and concentration of aniline in Nafion.

Ionic form		Na^+	K^+	Cs^+
$D_{M^+}^{Nafion}/10^{-7}$ [8]	25 ℃	9.8		1.9
cm^2s^{-1}	40 ℃	15.0		2.7
Water contents [19]				
		11.9	8.8	6.6
(mol H_2O/mol -SO_3^-)				
$K_{H^+}^{M^+}$ [20]		1.18	3.48	7.06
D_{AN^+} $/10^{-9}$ [17]		11.8	6.7	3.2
cm^2s^{-1}				
$C_{AN^+}^{Nafion}$ [17]	equilibrated	1.14	0.75	0.50
(mol dm^{-3})	with the			
$C_{M^+}^{Nafion}$ [17]	source	0.54	0.92	1.17
(mol dm^{-3})	solution			

the transition region of aniline flux shifted somewhat to a lower current density range (from 0.3 to 1.0 A cm^{-2}). The lower aniline concentration (2 mM) may be responsible for the smaller flux. The shift of the transition region suggests that the observed change in t_{AN^+} in the transport number is dependent on the AN^+ concentration in the Nafion membrane.

3.4.7 Causes for the aniline flux change

Gluga and Dindi reported that deprotonation of anilinium cation at the Nafion/water interface is the rate determining step in the permeation of aniline from an acidic solution to pure water through H^+-form Nafion.[22] They concluded that the rate of the ion-exchange process at the solution/Nafion interface is faster than the rate of deprotonation process at the Nafion/water interface. In the present case, pHs of both receiver and source solutions were about 4, and interfacial reactions such as protonation and deprotonation seem not to have a significant influence to total aniline transportation. Hence the phenomena observed here seem to be attributable to bulk properties of Nafion.

The phenomena may be explained in terms of the following two possibilities. (i) The change of the ionic cluster network structure is caused by an application of a DC current. The movement of cations and water may distort the microscopically phase-separated structure of Nafion and make the channels connecting the ionic clusters wider. (ii) The hydrophobic interaction between aniline and Nafion may be decreased due to the mass transport caused by a flow of DC current .

It is difficult to separate (i) and (ii). The transport number of anilinium cation in Cs^+-form in Fig. 3.8 was larger than that expected from the product of C_{AN^+} and D_{AN^+}. Cesium ion is known to be located in the interfacial region between the ion cluster region and the PTFE-like backbone region inside Nafion[10]. Since anilinium cation interacts strongly

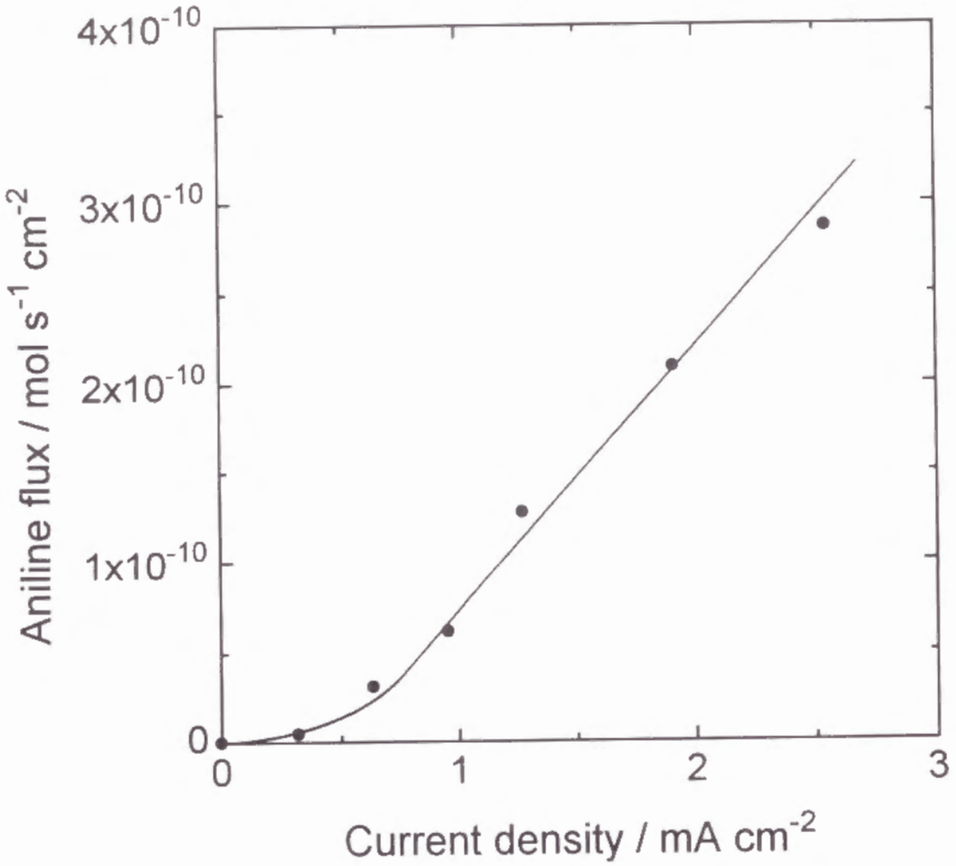

Figure 3.9 Aniline fluxes at the aniline concentrations of 2 mM in the both source and receiver solutions against current density for Na^+-form of Nafion.

with the hydrophobic region in Nafion[17], it is reasonable to consider that the anilinium cation is located in and permeates through the interfacial region as Cs^+ does. When Cs^+ moves in Nafion, it disturbs and decreases hydrophobic interaction between anilinium cation and Nafion. Then, the mobility of anilinium cation may increase to lead to an increase in t_{AN^+}. In addition, the movement of Cs^+ through the interfacial region of Nafion may cause friction in the interfacial region of Nafion, and this friction also leads to a distortion of the ionic cluster structure, i.e., the channels of Nafion, which is considered to affect the mass transport in Nafion[23], are broadened. This broadening enhances the mobility of anilinium cation which moves most slowly among the cations examined in this study, and then the transport number of anilinium cation may be increased.

Sandeaux et al. reported that an external applied voltage accelerated the permeation of acetate ion through the anion-exchange membrane, Selemion AMV, more than that of chloride ion[22]. They suggested that this acceleration was caused by a higher value of the "transfer coefficient" (a measure of the permeation rate through the interface between a membrane surface and the adjacent solution) of acetate ion. They proposed the hydrophobic character of acetate ion as one possible reason why the acetate ion movement was enhanced by the application of external current. Although the situation is different from present system, this type of influence should be also taken into consideration in the system for further discussion because the interaction between anilinium cation and Nafion is much stronger than that between acetate ion and Selemion AMV.

3.5 Conclusion

The transport phenomena of aniline through several ionic forms of

a perfluorosulfonate ion-exchange membrane, Nafion 117, under a flow of DC current were investigated. In each form, an increase in transport number of anilinium cation was observed in the current density range from 0.3 to 1.3 A cm^{-2}. The transport number of anilinium cation in Cs^+-form Nafion was larger than that expected from the concentration and diffusion coefficient in Cs^+-form Nafion. These phenomena may be attributed to a decrease in hydrophobic interaction between anilinium cation and Nafion or to a change in the ion cluster network structure due to the mass transport caused by the flow of DC current.

References

1. H. L. Yeager, B. Kipling and R. L. Dotson, *J. Electrochem. Soc.*, **127**, 303(1980).

2. R. S. Yeo, J. McBreen, G. Kissel, F. Kulesa and S. Srinivasan, *J. Appl. Electrochem.*, **10**, 741 (1980).

3. E. Gileadi, S. Srinivasan, F. J. Salzano, C. Brann, A. Beaufrere, S. Gottesfeld, L. J. Nuttal and A. B. Laconti, *J. Power Sources*, **2**, 191 (1977).

4. K. Katakura, Z. Ogumi, A. Noma and Z. Takehara, *Chem. Lett.*, 1291 (1990).

5. F. G. Will, *J. Electrochem. Soc.*, **126** 36 (1979).

6. F. G. Will and H. S. Spacil, *J. Power Sources*, **5**, 173 (1980).

7. R. S. Yeo, *J. Electrochem. Soc.*, **130**, 533 (1983).

8. T. Kyu and A. Eisenberg, "Perfluorinated Ionomer Membranes", A. Eisenberg and H. L. Yeager (Eds.), ACS Symposium Series, No.180, American Chemical Society, Washington DC, (1982) Chap 6.

9. H. L. Yeager and B. Kipling, *J. Phys. Chem.*, **83**, 1936 (1979).

10. H. L. Yeager and A. Steck, *J. Electrochem. Soc.*, **128**, 1880 (1981).

11. G. Scibona, C. Fabiani and B. Scuppa, *J. Membrane Sci.*, **16**, 37 (1983).

12. M. N. Szentirmay and C. R. Martin, *Anal. Chem.*, **56**, 1898 (1984).

13. D. A. Buttry and F. C. Anson, *J. Am. Chem. Soc.*, **104**, 4824 (1982).

14. S. K. Sikdar, *J. Membrane Sci.*, **23**, 83 (1985).

15. S. K. Sikdar, *Ind. Eng. Chem. Res.*, **26**, 170 (1987).

16. M. W. Verbrugge, *J. Electrochem. Soc.*, **136**, 417 (1989).

17. Z. Ogumi, K. Toyama, Z. Takehara, K. Katakura, and S. Inuta, *J. Membrane Sci.*, **65**, 205 (1992).

18. H. L. Yeager and A. Steck, *Anal. Chem.*, **51**, 862 (1979).

19. H. L. Yeager and A. Steck, *Anal. Chem.*, **52**, 1215 (1980).

20. A. Herrera and H. L. Yeager, *J. Electrochem. Soc.*, **134**, 2426 (1987).

21. H. Ohya, *Kagaku Kogaku*, **51**, 563 (1987).

22. P. B. Gluge and K. Dindi, *J. Membrane Sci.*, **28**, 311 (1986).

23. T, D, Gierke, "Proceedings of 152nd National Meeting", Electrochemical Society, Atlanta, 1977.

Part II

Application of Porous Metal-Solid Polymer Electrolyte Composite Electrode

Chapter 4

Microelectrode Simulation of Anode in Polymer Electrolyte Membrane Fuel Cells

4.1 Introduction

Polymer electrolyte membrane fuel cells (PEMFC) have recently been a focus of much attention because of their very high discharge current densities and power densities[1,2]. Porous gas-diffusion electrodes are usually used in fuel cells to increase their output current density and decrease their overpotential[3]. Although fairly high performance at a low platinum loading has been achieved by localizing platinum catalyst in a thin layer of porous electrodes close to the solid polymer electrolyte in PEMFC[4,5,6], even higher catalyst utilization is still required for applications such as power sources for electric vehicles to decrease its cost. The configuration of the active sites of electrodes, i.e., the three phase regions in PEMFC differs from those in the porous electrodes of fuel cells that use liquid electrolytes, such as aqueous solutions and molten salts. With liquid electrolytes, a thin film (meniscus) is formed at the three-phase region, and the characteristics of the meniscus are governed by the physical properties of the gas, the liquid and the electrode. The meniscuses

that form in pores of gas-diffusion electrodes limit current production by restricting the effective reaction region, i.e., the region with both fast gas diffusion and high ionic conductivity, to only a small portion of the meniscus. This is because on the one hand, near the bulk electrolyte, the meniscus is too thick for rapid diffusion of the reactant gases through the electrolyte to the electrode, and on the other hand, the opposite end of the meniscus is very thin, therefore the ionic conductivity being very low.

With solid polymer electrolytes, such meniscuses are not formed, because water is fixed in the matrix of the polymer as swelling by water. Consequently, in the case of PEMFC electrodes, the effective reaction region is not limited by meniscus formation. This opens up different possibilities for electrode design and placement of the platinum electrocatalyst. For example, it is possible that spreading the catalyst throughout an extended reaction zone might result in increased catalyst utilization, since the gases would have access to the entire surfaces of the catalyst particles, and the ionic conductivity would not be a limiting factor.

In this chapter, the author presents the results of some preliminary experiments in order to clarify the effective depth to which active sites of the reaction locate inside the solid polymer electrolyte. The anodic oxidation of hydrogen at platinum electrode in Nafion® (E. I. Dupont de Nemours and Company) was used as a model electrode reaction, since the reaction has a high exchange current density, and therefore should give a more definitive indication of diffusion limitations than the case of oxygen reduction reaction[7]. The depth to which the active reaction zone is extended into the Nafion (effective depth) was investigated by inserting a conical platinum micro-electrode into a Nafion NR50 particle to different depths under a hydrogen atmosphere. A mathematical model was also designed and solved by a numerical method.

4.2 Experimental

Working electrodes were platinum wires (0.3 mm in diameter) that had been electrically polished to a fine conical tip in aqueous $NaNO_2$, using a modified method of Silver[8]. A SEM micrograph of the tip of a typical electropolished wire is shown in Fig. 4.1. The electropolished working electrodes were cleaned immediately before use in the hydrogen oxidation experiments, using Fenton's reagent (hydrogen peroxide - ferrous sulfate)[9], followed by potential cycling in 0.1 M H_2SO_4under Ar atmosphere.

The solid polymer electrolyte consisted of particles of Nafion NR50 (1.2 to 1.3 mm in diameter and 2 to 3 mm in length, equivalent weight (EW) = 1200). The as received yellowish colored Nafion was first converted to a H^+ form by immersion in 1.0 M H_2SO_4, and then it was converted to a Li^+ form by immersion in 0.5 M LiOH. The surface of the Nafion particles was then rendered smooth by heating the Nafion in a solution of 1:1 (by volume) propanol:water to about 190 ℃ in autoclave for 3 to 4 hours, followed by recrystallization at about 120 ℃ for about 2 hours, and then cooling under ambient conditions to room temperature. Fine platinum wires (70 μm diameter) were inserted into the resulting swollen Nafion particles to serve as a hydrogen reference electrode. The swollen Nafion particles were subsequently reshrunk by immersion in 0.1 M H_2SO_4, and were then treated to decompose organic impurities by lightly boiling in potassium permanganate solution. The permanganate was removed by overnight immersion in 0.1 % aqueous hydrazine, followed by boiling in hot aqueous 1 M HNO_3, and then boiling in deionized water from a Barnstead Nanopure® water system. The resulting Nafion particles were colorless.

The cell assembly is shown in Fig. 4.2. The Nafion particle was inserted into the glass capillary cell, which in turn was inserted into the

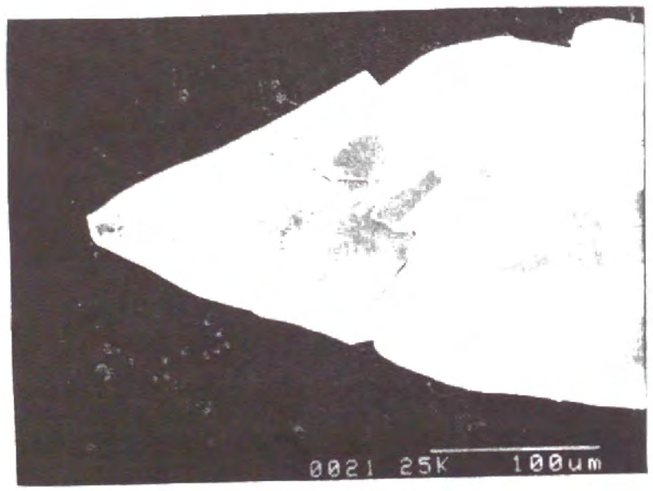

Figure 4.1 SEM photograph of a typical platinum tip electrode.

gas-tight methylmethacrylate cell housing. The capillary was filled with 0.1 M H_2SO_4, and a platinum wire counter electrode was placed inside the capillary. Either argon or hydrogen, humidified at room temperature (ca. 23℃), was passed through the cell container. The depth of penetration of the tip of the platinum micro-electrode into the Nafion was varied using a micrometer head. The cell was viewed under an optical microscope during the experiments.

Electrochemical measurements were carried out using a Yanaco P-1100 polarographic analyzer and a Watanabe WX 441 X-Y recorder. SEM micrographs were taken using a Hitachi S-510 scanning electron microscope.

4.3 Mathematical Model

F. G. Will studied the oxidation of hydrogen at a meniscus formed on a platinum electrode immersed partially in aqueous sulfuric acid[10]. He concluded that the rate of the hydrogen oxidation reaction at the platinum gas diffusion electrode in acidic media was dominated by the rate of hydrogen diffusion through the electrolyte film rather than its surface diffusion on platinum. Following his results, we assumed that diffusion of hydrogen through polymer electrolyte is a rate determining step of the anode reaction of PEMFC. A cylindrical diffusion model shown in Fig. 4.3 was used to represent the experimental model. In this model, a conical platinum micro-electrode was partially inserted into a polymer electrolyte particle under hydrogen atmosphere. The overall hydrogen oxidation process proceeds as follows. First, hydrogen gas dissolves into the Nafion particle and diffuses through it toward a platinum electrode surface. Next, the hydrogen is oxidized electrochemically at the platinum/electrolyte interface. It is assumed that the hydrogen diffusion in the gas phase and the hydrogen penetration at the gas/electrolyte in-

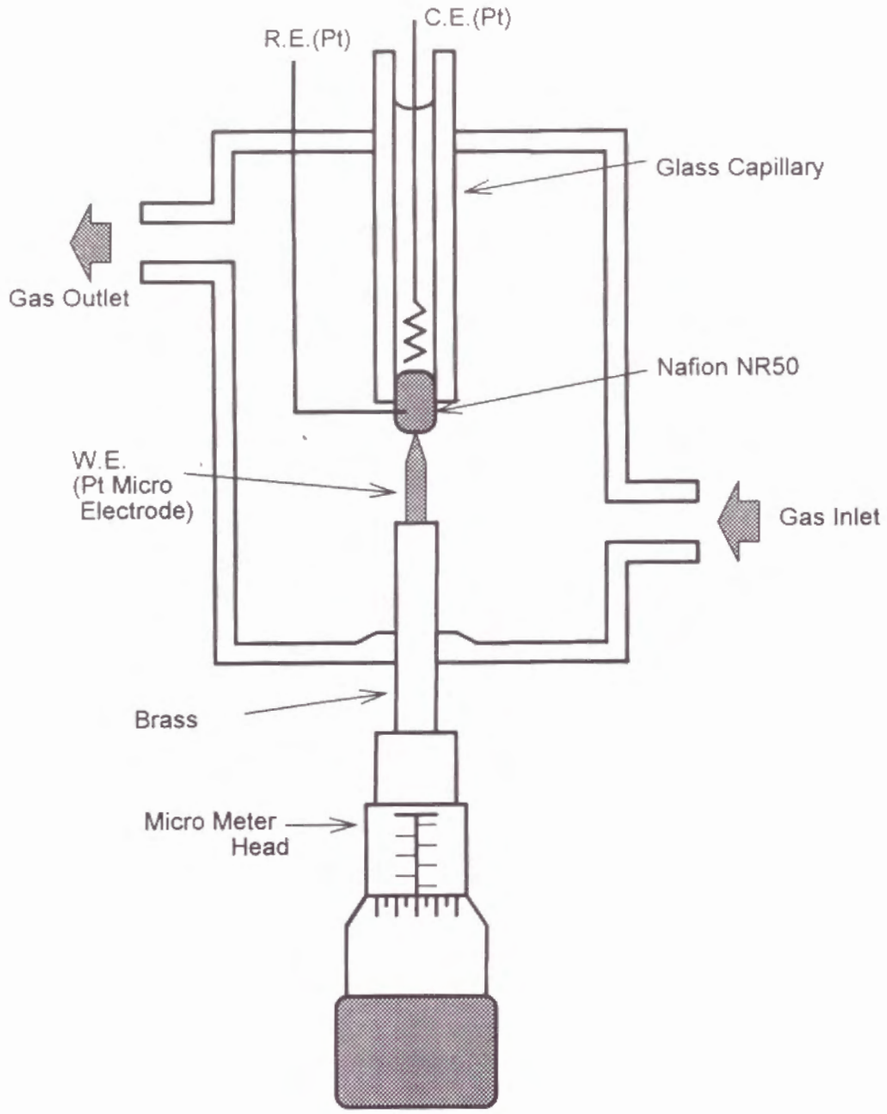

Figure 4.2 Schematic diagram of an apparatus for hydrogen oxidation experiments.

terface are so rapid that hydrogen concentration at the surface of the polymer electrolyte is in equilibrium with the gas phase. Furthermore, electrochemical oxidation of hydrogen at the platinum electrode is also so rapid that the rate of the mass transfer of hydrogen through the Nafion solely limits the overall reaction. Thus, hydrogen oxidation current at the conical tip electrode is decided by the hydrogen flux to the electrode/electrolyte interface governed by diffusion.

Diffusion of hydrogen through the Nafion is expressed by the following three dimensional cylindrical diffusion equation:

$$\frac{\partial C}{\partial t} = \frac{1}{r}\frac{\partial}{\partial r}\left(Dr\frac{\partial C}{\partial r}\right) + \frac{\partial}{\partial z}\left(D\frac{\partial C}{\partial z}\right) + \frac{1}{r}\frac{\partial}{\partial \theta}\left(\frac{D}{r}\frac{\partial C}{\partial \theta}\right) \qquad (4.1)$$

Since the present model has a rotation symmetry along with the z axis, $\partial C \ / \ \partial \theta = 0$, and the third term of right hand of equation (4.1) is omitted. Hence, equation (4.1) becomes equation (4.2),

$$\frac{\partial C}{\partial t} = \frac{1}{r}\frac{\partial}{\partial r}\left(Dr\frac{\partial C}{\partial r}\right) + \frac{\partial}{\partial z}\left(D\frac{\partial C}{\partial z}\right) \qquad (4.2)$$

The initial and boundary conditions which satisfy the above conditions are expressed as follows:

at t = 0

$$C(r\ ,\ z) = C_0 \qquad (4.3)$$

at t > 0

$$\left.\frac{\partial C}{\partial r}\right|_{r\,=\,0} = \left.\frac{\partial C}{\partial r}\right|_{r\,=\,r_{max}} = \left.\frac{\partial C}{\partial z}\right|_{z\,=\,z_{max}} = 0 \qquad (4.4)$$

$$C(r\ ,\ 0) = C_0 \qquad (4.5)$$

where C_0 denotes the hydrogen concentration in Nafion which is equilibrated with hydrogen in the gas phase.

The differential equation was solved numerically using a control volume method and the concentration profile of hydrogen inside a polymer electrolyte particle was determined. Hydrogen oxidation current at

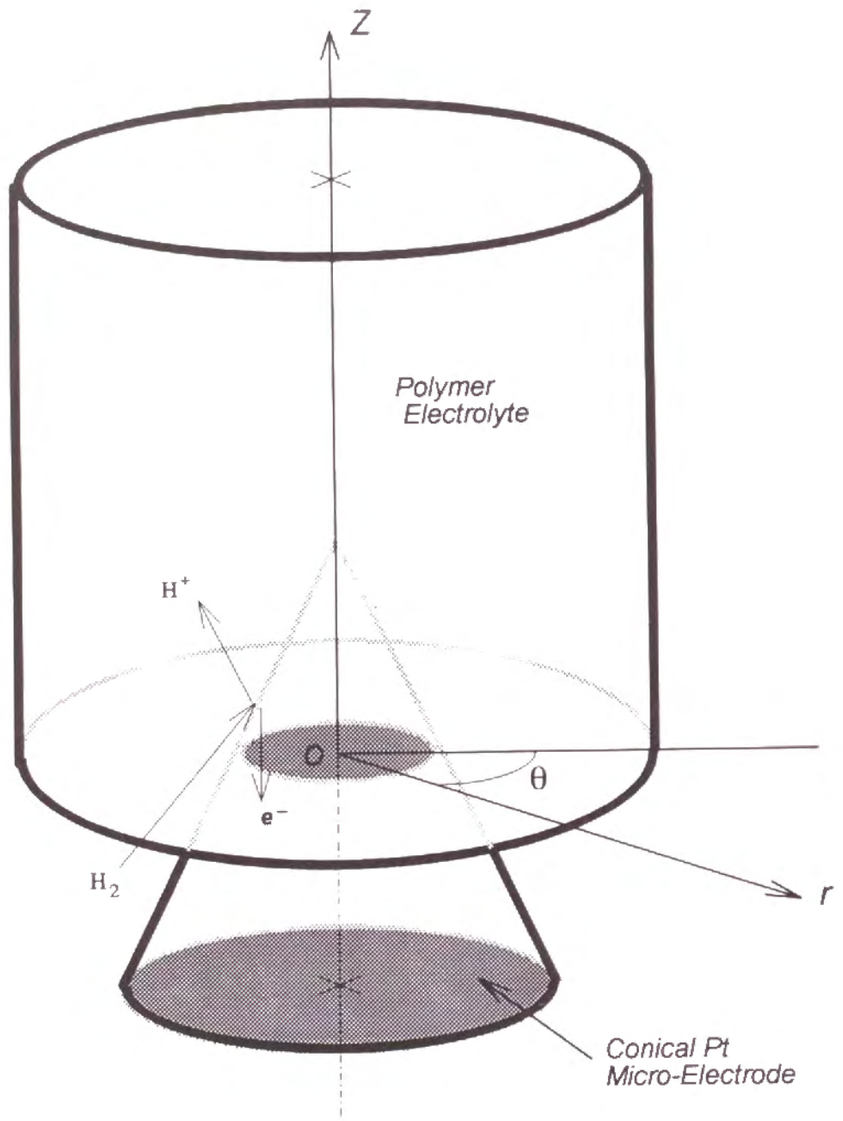

Figure 4.3 Mathematical diagram of the system used in the computer calculation.

various electrode insertion depths was also calculated using the hydrogen concentration profile around the electrode surface. The computer simulation results were compared with the experimental ones.

4.4 Results and Discussion

4.4.1 Experimental results

The catalyst utilization in PEMFC is dependent on the depth to which the reactant gases diffuse through the polymer electrolyte and reach active sites on carbon-supported platinum catalyst (Fig. 4.4 (a)).

In order to obtain an estimate of the depth to which the reaction zone can be extended, we have simulated the oxidation of hydrogen gas at anodes in PEMFC by inserting platinum wires polished to a fine conical tip into Nafion under hydrogen atmosphere (Fig. 4.4 (b)). The depth of insertion of the platinum micro-electrodes into the Nafion was varied, thereby catalyst layers of different depths being simulated.

Before hydrogen oxidation experiments, the purity of the system was checked by cyclic voltammetry under argon atmosphere. A typical cyclic voltammogram, obtained with the tip of the micro-electrode inserted into the Nafion to a depth of 100 μm, is shown in Fig. 4.5. Although a slight shoulder peak at about +0.1 V vs. RHE and the slightly rising currents at higher anodic potentials indicate that the system was not completely free of organic impurities, the voltammogram is well-defined, and is typical of voltammograms for platinum in acidic media. This voltammogram for Pt in bulk Nafion (Fig. 4.5) is similar to those reported by previous workers for Pt in bulk[11], recast[12], and solution-processed[13] Nafions. The inserted surface areas of the platinum micro-electrode were determined from the charge associated with the hydrogen desorption peaks. The inserted surface areas at different insertion depths are shown in Fig. 4.6, along with the corresponding geometric sur-

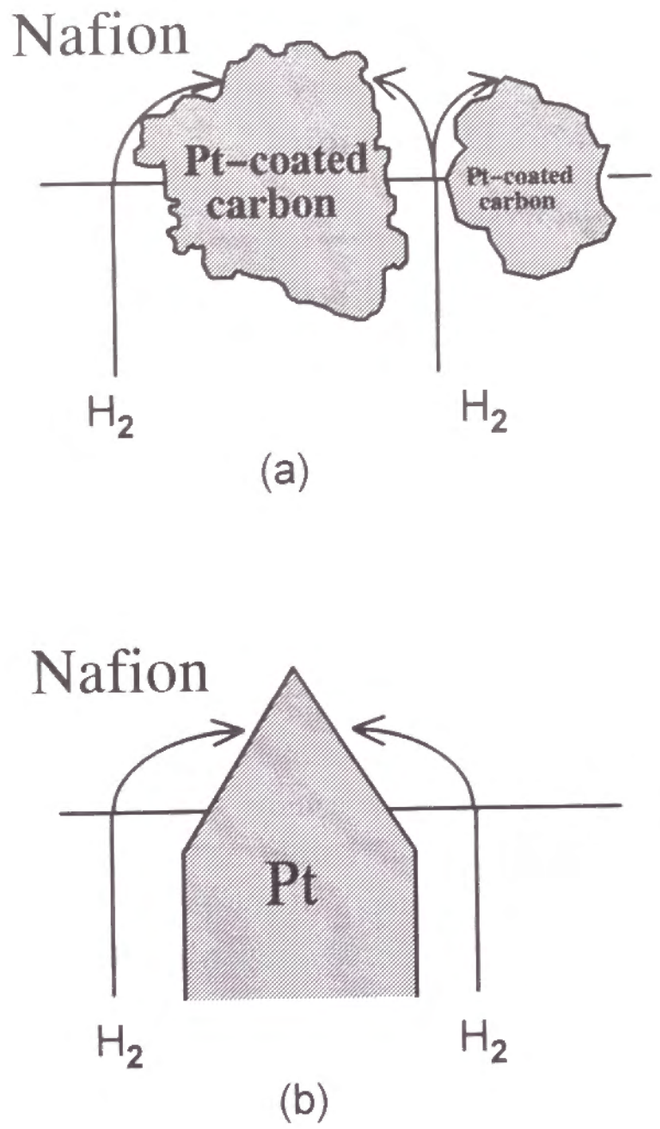

Figure 4.4 Schematic diagram of a three phase region (a) in practical PEMFC anode and (b) in present simulation model.

face areas. The similarity of the two curves in their shapes indicates that there was a good electrical contact between the electrode and the Nafion, and that the measured insertion depths were accurate. The actual surface areas are greater than the geometric surface areas by an average factor of about 2, which represents the surface roughness factor for the Pt/Nafion interface.

In order to get indication of the depth to which the active sites for hydrogen oxidation extended into the Nafion, the limiting hydrogen oxidation currents were measured with the Pt micro-electrode inserted into the Nafion to different insertion depths. In order to obtain the limiting current, the potential was scanned at 5 mV s^{-1}, and the current of a flat peak observed at 0.3 to 0.6 V vs. RHE was adopted (Fig. 4.7). Similar voltammograms were observed for platinum wire meniscus electrodes inserted in 0.05 M H_2SO_4. The current decrease (after the peak maximum) that was observed at potentials higher than about 0.6 V can be attributed to inhibition by anion adsorption on the platinum electrode[14] or partial coverage of the electrode surface by oxides. The peak current corresponds to the limiting current for hydrogen oxidation.

The limiting current values at different insertion depths are plotted in Fig. 4.8. As shown in this figure, the oxidation current increased rapidly with increasing platinum electrode insertion depth up to about 50 μm. At greater insertion depths, however, the rate of increase of the measured currents decreased.

4.4.2 Computer calculation results

According to equations (4.2) to (4.5), concentration profile of hydrogen around the platinum tip electrode inserted into Nafion and hydrogen flux at the electrode surface were evaluated using a numerical calculation technique. The hydrogen oxidation current was calculated from the

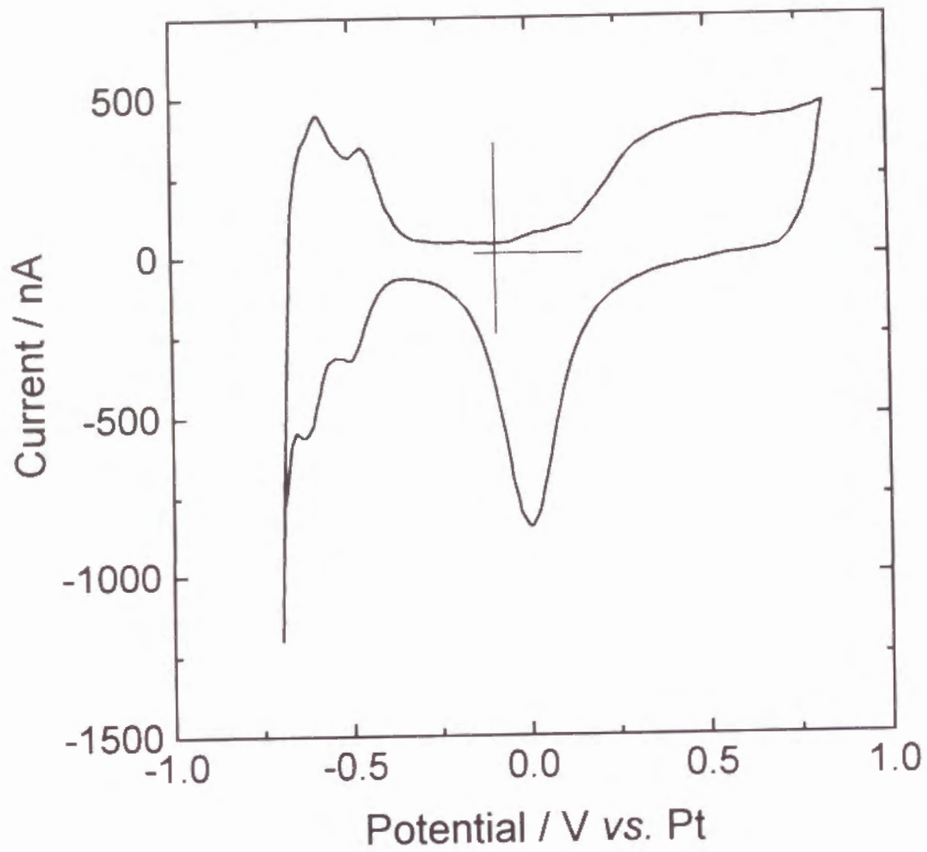

Figure 4.5 A typical cyclic voltammogram of the Pt microelectrode inserted into Nafion NR50 under argon atmosphere.

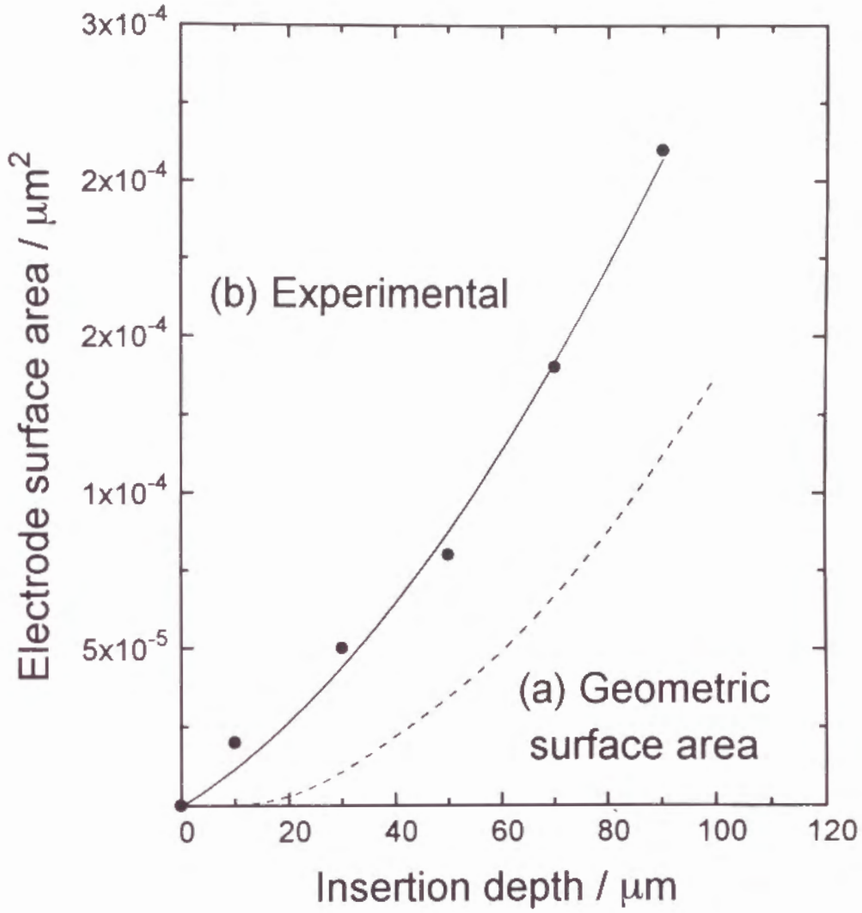

Figure 4.6 Dependencies of the inserted surface area of the Pt micro electrode on the electrode insertion depth.
(a) calculated from the electrode geometry. (b) calculated from hydrogen desorption peaks of the cyclic voltammograms.

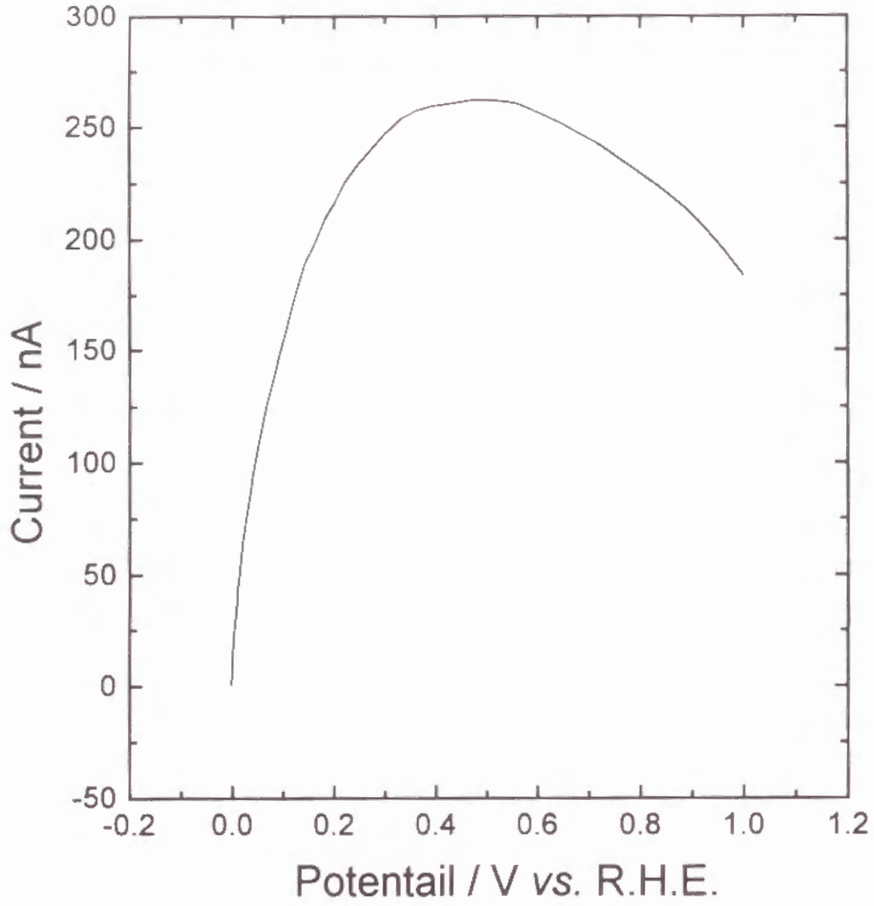

Figure 4.7 Steady state polarization curve on Pt micro electrode under hydrogen atmosphere. Sweep rate of the electrode potential was 5 mVs^{-1}.

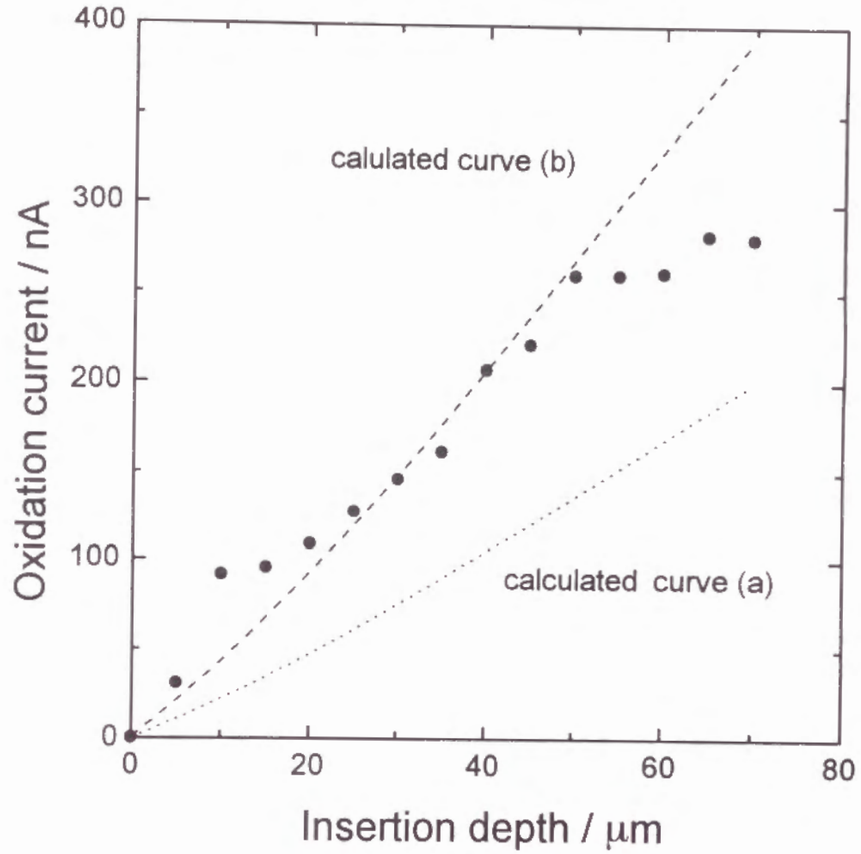

Figure 4.8 Dependencies of hydrogen oxidation current on Pt electrode insertion depth.
Closed circles denote the experimental data. Curve (a) and (b) show the computer calculation results using the cylindrical diffusion model. For curve (a), the hydrogen permeability value reported by Yea et al.[15] was adopted. For curve (b), hydrogen permeability value was adjusted to experimental results.

evaluated hydrogen flux at the electrode surface. The tip angle (47°) of the conical platinum micro-electrode was measured from the SEM micrograph in Fig. 4.2.

Hydrogen diffusion flux through the electrolyte is dependent on the separation between neighboring electrodes, because the Nafion surface even far from the Pt electrode can contribute to the flux, especially to the flux to a deeper part of the Pt electrode. When the separation becomes larger, the hydrogen flux should be independent of the separation distance. In the present model in Fig. 4.3, the glass wall surrounding the Nafion is an insulating wall and this is equal to the middle point between the neighboring electrodes from a symmetry consideration. Hence, when the Nafion electrolyte radius becomes larger, the concerning electrode can be treated as an isolated electrode. The electrolyte radius achieving this consideration was first examined.

The diffusional flux is time dependent. In the present simulation, model fitting was conducted under steady state conditions. Therefore, the time when hydrogen diffusion can be assumed as in a steady state was also examined.

In these calculations, diffusion coefficient $D = 6.6 \times 10^{-7}$ cm^2 s^{-1} and solubility $C = 2.45 \times 10^{-5}$ mol cm^{-3} [15] were used as the physical parameters. The calculation results indicated that when the electrolyte size was over 3 times larger both in radius and in length than the inserted electrode, the hydrogen oxidation current was independent of the electrolyte size. Therefore, the dependency of the hydrogen oxidation current on the insertion depth of the conical tip electrode into Nafion particle was calculated, setting the Nafion particle size as 400 μm in diameter and 400 μm in length. In these calculations, the hydrogen oxidation current initially decreased with time, and a steady state current was attained within 20 s at an electrode insertion depth of 100 μm. The relationship between the

calculated steady state hydrogen oxidation current and insertion depth of the conical tip electrode was superimposed on the experimental results in Fig. 4.8 with doted curve (theoretical curve (a)). This figure reveals that the theoretical curve had a tendency similar to experimental one up to c.a. 50 μm, although the calculated hydrogen oxidation currents were smaller than the experimental values.

Permeability ($D \times C$) of hydrogen and oxygen in Nafion under various conditions have been extensively studied by many workers[12,15–18]. The reported permeability values varies widely depending on the workers and the experimental conditions. For example, hydrogen permeability values in the recast Nafion contacted with 85 % H_3PO_4 are ranging from 3.5 $\times 10^{-12}$ mol cm^{-1}s^{-1} to 8.6 $\times 10^{-12}$ mol cm^{-1}s^{-1} [17]. In Nafion 120 which contacted with 14% HCl, P = 1.6 $\times 10^{-11}$ mol cm^{-1}s^{-1} was reported[15]. For oxygen, Gottesfeld et al[12]. reported for the recast Nafion that the permeability value contacting with 0.5 M H_2SO_4 was approximately 10 times higher than that contacting with 85 % H_3PO_4. It is reasonable to consider that hydrogen permeability in Nafion contacting with 0.1 M H_2SO_4 is higher than that contacting with 85 % H_3PO_4. Furthermore, in the present experiment, the Nafion NR50 particle was precedingly swollen in propanol at 190 ℃. Therefore, the hydrogen permeability in the used Nafion should be higher than the value used in the present computer calculation, the value through the Nafion 120 membrane contacted with 14 % HCl.

Permeability coefficient of hydrogen in the Nafion NR50 was adjusted until obtained curve was fitting well to experimental results. The resulting theoretical curve was superimposed in Fig. 4.8 as a curve (b). The adopting permeability value was ca. 2 times higher than the value reported by Ogumi et al.

Based on the above discussion, this permeability value may be reasonable for Nafion NR50 contacting with 0.1 M H_2SO_4. The experimental

values at the insertion depth ranging from 10 to 15 μm deviated from the curve (b). As shown in Fig. 4.6, the electrode surface area at the insertion depth ranging from 10 to 15 μm also deviated from geometric surface area. Thus the deviation may be caused by the irregularity of the conical platinum tip electrode shown in Fig. 4.3.

Therefore, theses results indicated that the hydrogen oxidation reaction at the Nafion/platinum interface proceeded under hydrogen diffusion limiting conditions expressed by the cylindrical diffusion model in equations (4.2) to (4.5).

The simulation results indicate that the oxidation current should be increases with increasing the insertion depth even at the deeper insertion depths ($> 50\ \mu m$). Willson et al. reported that the active sites for hydrogen oxidation in PEMFC extended to ca. 4 μm inside the polymer electrolyte[4,5]. At the catalytic layers in actual PEMFC electrodes, the distance between two neighboring platinum particles (or carbon particles supporting platinum black catalyst) is close to each other and hydrogen cannot access the deep portion of the catalyst electrode in polymer electrolyte. In the experiments, however, single platinum electrode tip was used. The distance between two neighboring platinum particles is assumed to be infinite. Furthermore the shape of the electrode used in this study might be different from that of the practical electrodes in PEMFC anodes (see Fig. 4.4). The present results exhibit that hydrogen can access the deep portion of the inserted electrode. Thus, with a large distance between neighboring two platinum particles, a high platinum catalyst utilization would be achievable, although the practical apparent current densities may be decreased. The large electrode particle spacing may also enhance an ionic conductivity of the polymer electrolyte at the cost of the efficiency loss of the fuel-cell system due to the permeation of reactant gases through the electrolyte membrane. The large particle spacing leads to the high mass transport rate through the porous catalyst electrodes of PEMFC. In designing the practical carbon supported platinum electrode for PEMFC, these factors have to be taken into consideration.

4.5 Conclusion

The depth of the active site for hydrogen oxidation on platinum electrodes in Nafion solid polymer electrolyte was investigated by inserting platinum micro-electrodes into Nafion to different depths under hydrogen atmosphere and measuring the corresponding hydrogen oxidation currents. The experimental results were well fitted with the mathematical calculation results using cylindrical diffusion model. These results indicated that hydrogen oxidation reaction on anode in PEMFC proceeded under hydrogen diffusion limiting conditions. Furthermore, the results also indicated that the three-dimensional reaction zone extended fairly deeply inside the Nafion, and therefore suggested criterion for catalyst loading in PEMFC; namely, loading the catalyst throughout the reaction zone, with relatively wide particle spacing to allow for good gas permeation as well as good ionic conductivity.

References

1. S. Srinivasan, D. J. Manko, H. Koch, M. A. Enayetullah and A. J. Appleby, *J. Power Sources*, **29**, 367 (1990).

2. S. Srinivasan, E. A. Ticianelli, C. R. Derouin and A. Redondo, *J. Power Sources*, **22**, 359 (1988).

3. J. Giner and C. Hunter, *J. Electrochem. Soc.*, **116**, 1124 (1969).

4. M. S. Wilson and S. Gottesfeld, *J. Electrochem. Soc.*, **139**, L28 (1992).

5. M. S. Wilson and S. Gottesfeld, *J. Appl. Electrochem.*, **22**, 1 (1992).

6. E. J. Taylor, E. B. Anderson and N. R. K. Vilambi, *J. Electrochem. Soc.*, **139**, L45 (1992).

7. W-K Paik, T. E. Springer and S. Srinivasan, *J. Electrochem. Soc.*, **136**, 644 (1989).

8. I. A. Silver, *Med. Electron. Biol. Eng.*, **3**, 377 (1965).

9. C. Walling and S. Kato, *J. Am. Chem. Soc.*, **93**, 4275 (1971).

10. F. G. Will, *J. Electrochem. Soc.*, **110**, 145 (1963).

11. A. Parthasarathy, C. R. Martin and S. Srinivasan, *J. Electrochem. Soc.*, **138**, 916 (1991).

12. S. Gottesfeld, I. D. Raistrick and S. Srinivasan, *J. Electrochem. Soc.*, **134**, 1455 (1987).

13. D. R. Lawson, L. D. Whiteley, C. R. Martin, M. N. Szentirmay and J. I. Song, *J. Electrochem. Soc.*, **135**, 2247 (1988).

14. S. Schuldiner, *J. Electrochem. Soc.*, **115**, 362(1968)

15. R. S. Yeo and J. McBreen, *J. Electrochem. Soc.*, **126**, 1682 (1979).

16. Z. Ogumi, T. Kuroe and Z. Takehara, *J. Electrochem. Soc.*, **132**, 2601 (1985).

17. S. D. Fritts, D. Gervasio, R. L. Zeller III, and R. F. Savinell, *J. Electrochem. Soc.*, **138**, 3345 (1991).

18. T. Sakai, H. Takenaka, and E. Torikai, *J. Electrochem. Soc.*, **133**, 88 (1986).

Chapter 5

A New Type Oxygen Sensor Composed of Tightly Stacked Membrane/Electrode/Electrolyte

5.1 Introduction

Recently, many different types of electrochemical oxygen sensors, such as solid electrolyte type ones and Clark type ones, have been developed. Yttria stabilized zirconia (YSZ) and carcia stabilized zirconia (CSZ), which exhibit fairly high oxygen-ion conductivity at the elevated temperature, are utilized for the electrolytes of solid state oxygen sensors. In these sensors, oxygen is detected as an electro motive force between two porous electrodes deposited on each side of YSZ or CSZ membrane which separates two phases, a reference phase of fixed oxygen partial pressure and a test phase of unknown oxygen partial pressure. The electromotive force is proportional to the logarithmic of oxygen partial pressure of test phase. However, these oxygen sensors are limited to the use only at the temperature higher than ca. 400 ℃[1,2] except for a few sensors which are lately reported to be able to operate at room temperature[3,4].

Oxygen dissolved in aqueous solutions and gaseous oxygen at room temperature are usually determined by Clark type oxygen sensors. In

Clark type sensors, oxygen is reduced electrochemically under diffusion limiting conditions at a cathode which is separated from sample gas or sample solution by a hydrophobic oxygen transport limiting (OTL) membrane. Oxygen is reduced at the electrode and the magnitude of the reduction current is a measure of oxygen content and directly proportional to the oxygen concentration of the sample bulk.

Clark type and modified Clark type oxygen sensors are used also as a component of bio-sensors; Different kinds of enzyme are, for example, immobilized on the OTL membrane of the Clark type oxygen sensor. Furthermore, applications of the Clark type oxygen sensor become increasing more and more.

Clark type oxygen sensors, however, have some draw backs; e.g. difficulties in miniaturization and stability under conditions where the pressure may change. These draw backs difficulties originate from its principle that the sensor contains a liquid layer between a cathode and a OTL polymer film through which the gas to be detected permeates.

Previously, Ogumi et al. reported that oxygen was reduced on an SPE (Solid Polymer Electrolyte) composite electrode which was prepared by electroless deposition of porous platinum electrode on Nafion(Pt-Nafion). via a 4 electron process[5].

$$O_2 + 4H^+ + 4e^- \longrightarrow 2H_2O \qquad (5.1)$$

In this chapter, the author proposes a new type amperometric oxygen sensor operating at room temperature which is composed of SPE composite electrodes. Fundamental properties of the sensor are mainly examined.

5.2 Principle of the new type oxygen sensor

One of the most important applications of an SPE composite elec-

trode is a H_2-O_2 Polymer Electrolyte Membrane Fuel Cells (PEMFC)[6,9]. In PEMFC, the SPE composite electrode is used as a cathode and an anode. The cathode reaction in PEMFC is oxygen reduction which is the same as that of oxygen sensing reaction in a Clark type oxygen sensor. As described earlier, Ogumi et al. reported that, oxygen reduction at the SPE composite electrode contacting with acidic media proceeds fast.[5] In this type of electrode, even if the electrode bound on a polymer electrolyte is tightly covered with oxygen permeable polymer film(shown Fig. 5.1), oxygen can diffuse to electrode surface through the polymer film and be reduced electrochemically by the equation (5.1). Therefore, the SPE composite electrode covered with an appropriate polymer film can be utilized for an oxygen sensor.

The structural model of the new type oxygen sensor is schematically described in Fig. 5.1. A polymer electrolyte behaves as both an electrolyte and a support for the sensing electrode. This structure enables us to use a thin OTL membrane and it enhances a sensor response. A counter electrode is set either on the opposite side of the polymer electrolyte membrane (a) or in the electrolyte solution contacting the polymer electrolyte (b). In the latter case, the above oxygen reduction can be forced to proceed potentiostatically. In this chapter, the latter case is focused. Oxygen in test fluids permeates through the OTL membrane and reaches the sensing electrode bound on the Nafion which is set at the potential at which oxygen is reduced rapidly following the above equation. If the oxygen is reduced under diffusion limiting conditions through the OTL membrane as in the case of Clark type sensors, the current will be proportional to the oxygen content in the test fluid. In comparison with a Clark type sensor, no solution is required to exist between a sensing electrode and a OTL membrane. This structure not only enable the reduction of gap between the sensing electrode and the OTL membrane, but also en-

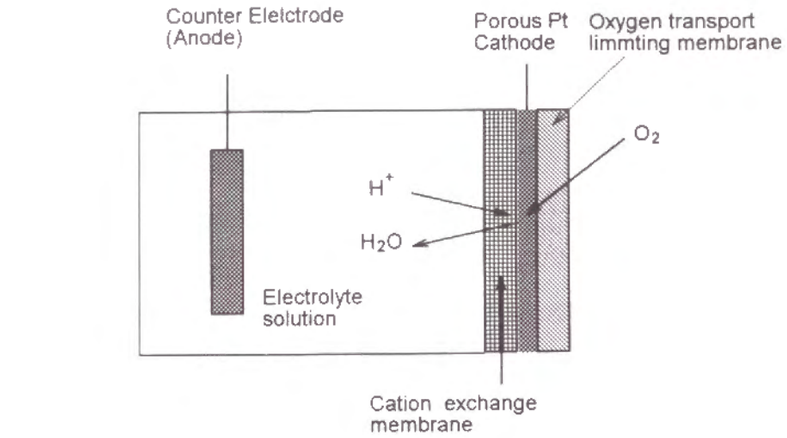

(b) Counter electrode is set in the electrolyte solution.

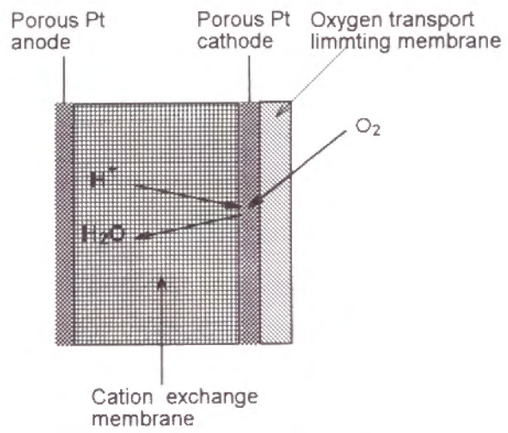

(a) Counter electrode is set on the opposite side of the membrane.

Figure 5.1 A principles of an oxygen sensor utilizing tightly stacked membrane/electrode/electrolyte.

hances the stability and reliability of the sensor[10] and therefore, enable its miniaturization.

5.3 Experimental

5.3.1 Preparation of an OTL membrane covering SPE composite electrode

In the present work, a sensor having 3 electrodes was prepared (Fig. 5.2). A perfluorosulfonate cation-exchange membrane, Nafion 117, was used as an SPE material because of its chemical and thermal stability. A porous platinum sensing electrode was deposited directly on the Nafion surface (Pt-Nafion) by the method previously reported[11]. High density polyethylene (PE) film (MITSUI chemicals) having 10 μm in thickness was chosen as an OTL membrane and it was directly bound on the sensing electrode by hot-pressing at ca.100 ℃ applying desirable pressure (PE-Pt-Nafion). Figure 5.3 shows a scanning electron micrograph of the cross-sectional view of the PE-Pt-Nafion. This micrograph shows that the OTL membrane covers and contacts well with the rough surface of the porous cathode and that its thickness is fairly uniform. An outer surface of the PE-film is smooth and no pinhole is observed. The thickness of the OTL membrane was controlled by changing the numbers of PE-films.

5.3.2 Measuring cell

The PE-Pt-Nafion was mounted in the cell shown in Fig. 5.2. The bare Nafion surface of this composite electrode faced against a liquid electrolyte in which a counter electrode (platinum wire) and a reference electrode (sat. Ag/AgCl) were immersed. Since 0.5 mol dm^{-3} sulfuric acid was used as an electrolyte, oxidation of water proceeds on the counter electrode. Test gases containing oxygen were introduced into a gas compartment of the cell at 1.7 cm^3 s^{-1}.

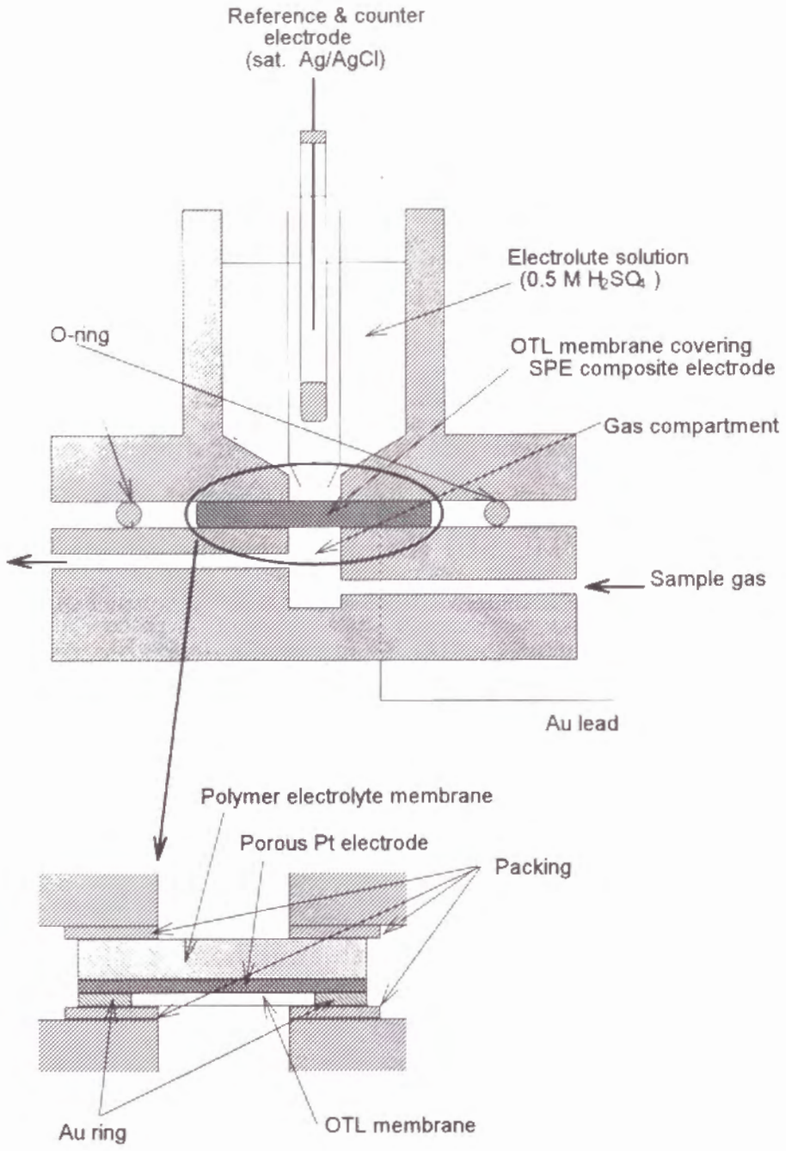

Figure 5.2 Schematic diagram of an oxygen sensor and an arrangement of the measuring apparatus.

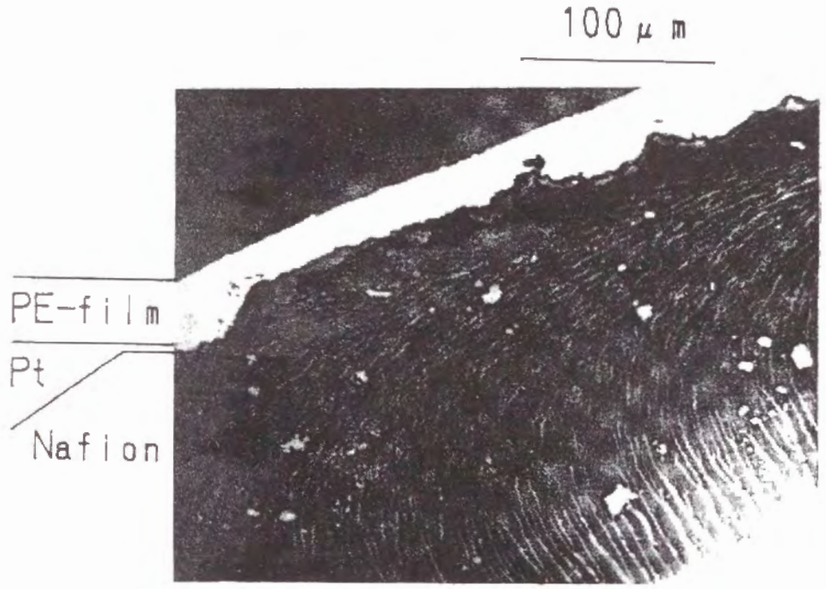

Figure 5.3 A scanning electron micrograph of the cross section of the oxygen sensor.

5.3.3 *Measuring procedure*

The thickness of the OTL varied from 16 to 60 μm. The dependency of the oxygen reduction current on the oxygen content was examined changing the content from 0 to 100 %. The response time was examined by changing stepwise the gas composition from Ar to 100 % oxygen and from 100 % oxygen to Ar.

A sensing electrode (cathode) potential was controlled using a potentiostat (Hokuto Denko Model HA301). The electrode potential was scanned using a function generator (Hokuto Denko Model HB-111). The potential-current relationships were recorded on an X-Y recorder (Graphtec Model WX2400). To compare with the Pt-Nafion coated with a OTL layer, bare Pt-Nafion was also examined.

All experiments were carried out at room temperature.

5.3.4 *Chemicals*

All chemicals except hydrazine were of reagent grade. Hydrazine as a reductant for platinum plating was of chemical pure grade. Chemicals were used without further purification. Solutions were prepared with distilled water. Argon was of 99.998 % purity and oxygen of 99.995 % purity.

5.4 Result and Discussion

5.4.1 *Oxygen reduction at Pt-Nafion covered with an OTL membrane*

The electrochemical behavior of the OTL membrane covering Pt-Nafion (PE-Pt-Nafion) was examined. Initially, potential of the platinum electrode of the PE-Pt-Nafion was set at 0.6 V and was swept cathodically to 0.0 V with the scan rate of 1.0 mV s^{-1}. Obtained polarization curves are shown in Fig. 5.4. As shown in this figure, when the potential

became lower than 0.4 V, a limiting current was observed under 100 % O_2 atmosphere. On the other hand, on bare Pt-Nafion any clear limiting current was not observed. These facts indicate that the PE film bound on the porous platinum electrode behaves as an OTL layer.

When the oxygen reduction proceeds under diffusion limiting condition, a linear relationship between bulk oxygen concentration and oxygen reduction current should be observed. Therefore, the electrode potential was set at 150 mV and the steady state oxygen reduction currents were measured under various oxygen concentration of gas samples. For every OTL membrane thickness, the background current measured in Ar was less than 2 % of the current at 100 % oxygen concentration.

The dependencies of the oxygen reduction current on the oxygen concentration were shown in Fig. 5.5. As shown in this figure, for every thickness of OTL membranes, the linear relationships were observed at the oxygen concentration ranging from 0 to 100 %. The slope of the lines in Fig. 5.5 decreased with increasing OTL membrane thickness.

5.4.2 *Influence of the thickness of OTL membranes*

When the oxygen reduction occurs under diffusion limiting conditions, the reduction current is represented by the following equation:

$$i = nFAD\frac{sP_{O_2}}{\delta} \tag{5.2}$$

where, n is a number of transferred electrons, 4, F is faradaic constant, A is a surface area of the electrode, D is a diffusion coefficient of oxygen through the OTL membrane, s is a solubility coefficient of oxygen in OTL membrane, P_{O_2} is a pressure of oxygen, and δ is a thickness of OTL membrane.

The dependencies of the oxygen reduction current on the thickness of OTL membrane at 100 % oxygen are shown in Fig. 5.7. As shown in this figure, for the thickness of OTL membranes ranging from 16 μm to

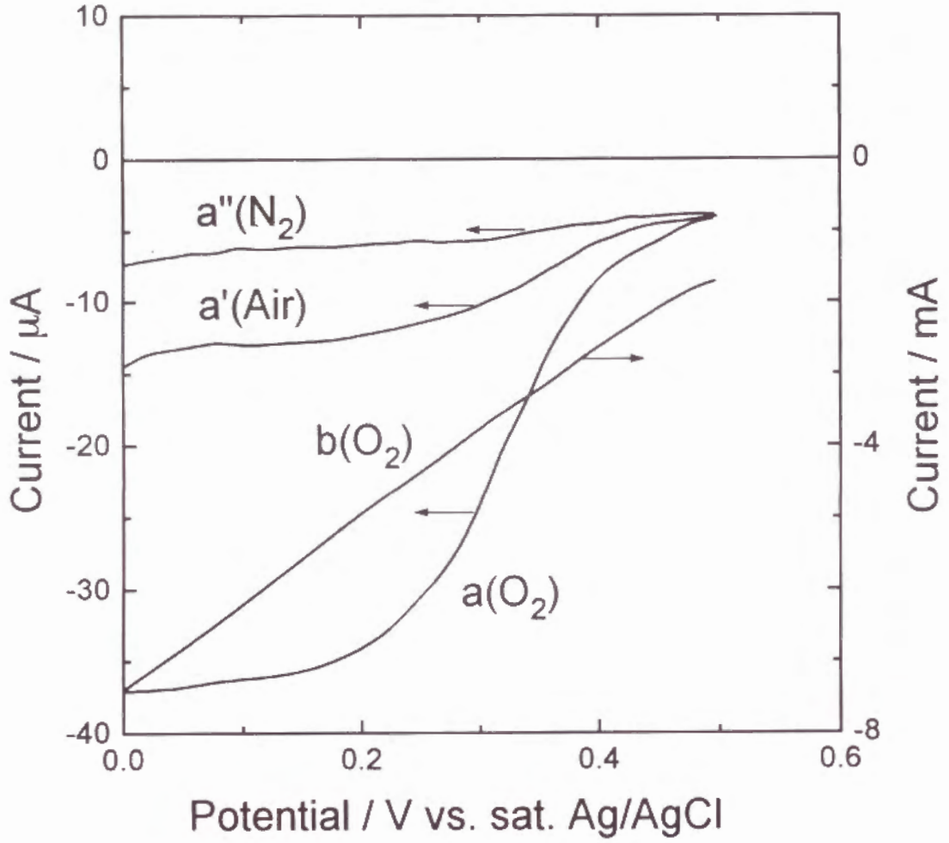

Figure 5.4 Polarization curves of the oxygen sensor (a) and bare Pt-Nafion (b) at various oxygen concentration with potential sweep rate of 5 mV s^{-1}.

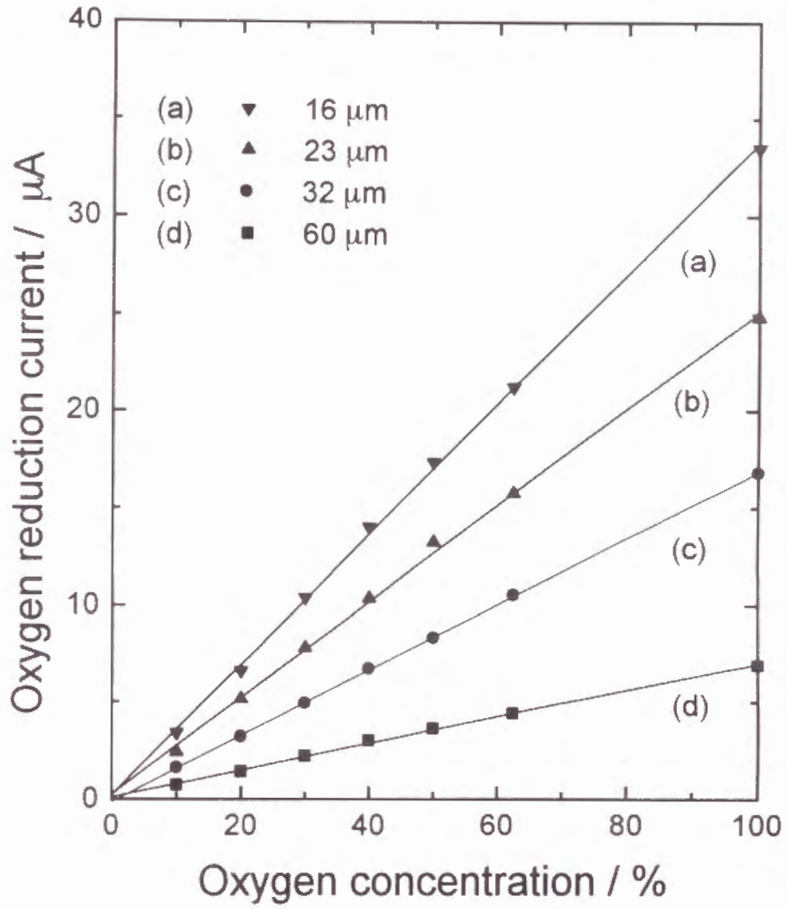

Figure 5.5 The relationships between the oxygen reduction current of an oxygen sensor and oxygen concentration in sample gas.
The thickness of PE film covering the platinum is (a) 16 μm, (b) 23 μm, (c) 32 μm, (d) 60 μm.

60 μm, a linear relationship between inverse of the thickness and cathodic current was observed. This linear relationship indicates that the oxygen reduction current (rate of oxygen reduction reaction) follows the equation (5.2) and that the PE-Pt-Nafion can be utilized for an oxygen sensor.

Table 5.1 Permeability and diffusion coefficients of oxygen in PE film.

OTL film thickness δ	Detected current I	Permeability $\mathbf{P}_{O_2}$	Diffusion coefficient D	90 % response time Exp.	Calc.
μm	μA	cm^3 (STP) $cm^{-1}s^{-1}$ $cmHg^{-1}$	cm^2s^{-1}	s	s
16	33.5	2.1×10^{-10}	2.0×10^{-7}	6	3.0
23	24.8	2.2×10^{-10}	2.0×10^{-7}	13	8.0
32	16.8	2.1×10^{-10}	2.0×10^{-7}	21	15.6
60	6.9	1.6×10^{-10}	2.0×10^{-7}	50	49.7

According to equation (5.2), a permeability of oxygen through OTL membrane ($\mathbf{P}_{O_2}$), which is defined as a product of a diffusion coefficient and a solubility coefficient of oxygen in OTL membrane ($D \times s$), was calculated. The permeability for each thickness of the OTL membrane is summarized in Table 5.1. As expected from the linear relationship in Fig.

5.6, obtained permeability were almost same value. The permeability values were comparable to the value for a low density PE film (2.89×10^{-10}) rather than the value for a high density PE film (4.1×10^{-11}). Since recrystalization of the polyethylene film occurred during the hot-pressing, oxygen permeability might be increased.

5.4.3 Responsibility

Responsibility of the sensor is one of the most important properties. When the sample gas was changed from Ar to 100 % O_2 or changed from 100 % O_2 to Ar, abrupt change in the oxygen reduction current was observed. The time response curve for the PE-Pt-Nafion having 16 μm thick OTL membrane is shown in Fig. 5.7. Build-up (from Ar to O_2) and decay (from O_2 to Ar) of the curve in this figure show that the steady state current was reached within 15 s in both cases. An average 90 % transient time for each OTL membranes were listed in Table 5.1. As listed in this table, the 90 % transient time for the OTL membrane of 60 μm thickness was c.a. 50 s and for the 16 μm thickness was c.a. 6 s. This response time (6 s) of the sensor is fast in comparison with that for typical Clark-type oxygen sensors[13].

To elucidate the diffusion mechanism of oxygen through the OTL membrane covering Pt-Nafion, the current response curves were calculated from theoretical diffusion model and were compared with the experimental ones. Solving the Fick's 2nd low (5.3) under the initial and boundary conditions in equations (5.4) or (5.5), the theoretical curves were obtained.

$$\frac{\partial C}{\partial t} = D\frac{\partial^2 C}{\partial x^2} \tag{5.3}$$

for build up

$$C(x,0) = 0.0,\ C(0,t) = C_0,\ C(\delta,t) = 0.0\ (t > 0, 0 <= x <= \delta) \tag{5.4}$$

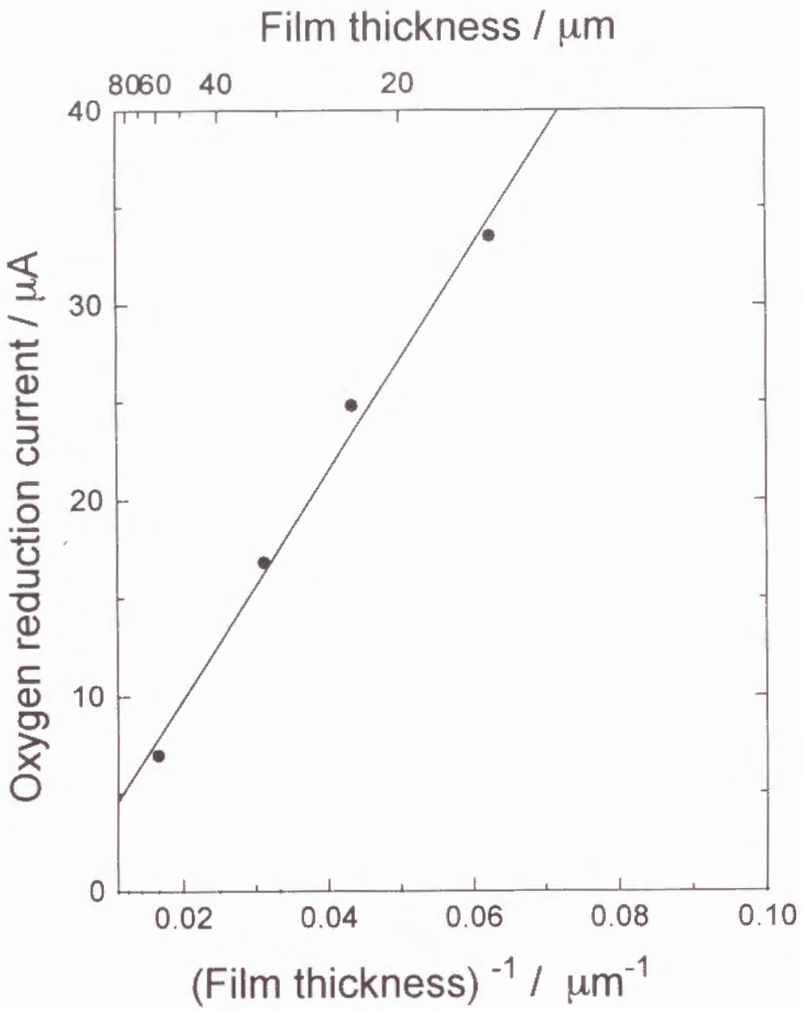

Figure 5.6 Dependencies of sensing current for 100 % oxygen gas on the thickness of OTL membrane.

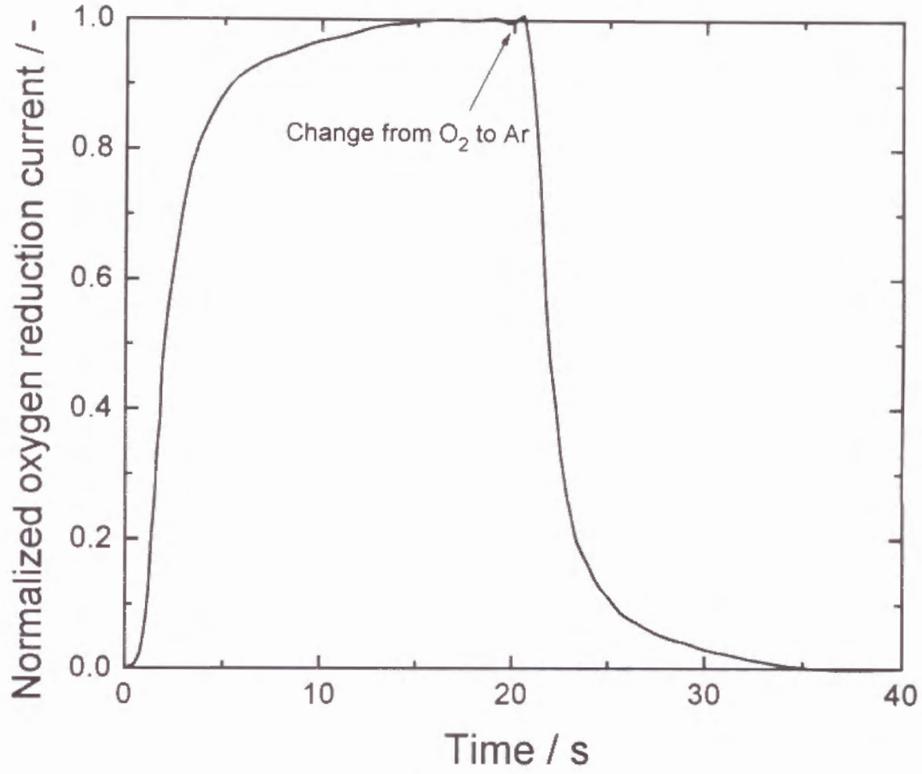

Figure 5.7 Time response curve of the oxygen signal current of the oxygen sensor, when the thickness of OTL membrane (PE) was 16 μm.

for decay

$$C(x,0) = C_0,\ C(0,t) = 0.0,\ C(\delta,t) = 0.0\ (t > 0, 0 <= x <= \delta) \quad (5.5)$$

At the OTL membrane/sample gas interface, $x = 0$ and at the electrode/OTL membrane interface, $x = \delta$.

The fitted curves for OTL membrane thickness of 16 μm were shown in Fig. 5.8. In this figure τ denotes the dimensionless time defined as followed:

$$\tau = \frac{Dt}{\delta^2} \quad (5.6)$$

As shown in this figure, the curves fitted well to the theoretical ones up to the 80 % of the final current changes. Over 80 % change, however, the response delayed. The deviation from the theoretical curves become less remarkable when the thickness of OTL membrane increases.

In the theoretical calculation using the boundary conditions of equations (5.4) and (5.5), both surfaces of the OTL membrane were assumed as flat plane (flat plane model). As shown in Fig. 5.3, however, the electrode side of the OTL layer was rough. Therefore, the influence of surface roughness on time response of the current was examined. Since rigorous description of the surface roughness of the OTL membrane was difficult, the roughness was assumed as a grating pattern (grating model). In this model, OTL membrane has pits whose width and depth are 10 % of the original membrane thickness. The pits are arranged with a space of those width.

Using the grating model, equation (5.3) was solved numerically using control volume method. In these calculations, original thickness of the OTL membrane which is the same as that in a flat plane model was adapted for δ in τ (equation (5.6)). Resulting theoretical curve is shown in Fig. 5.9 (a). As shown in this figure, the shape of the response curve of the grating model is identical to that of the flat plane model (b), except that the τ in the grating model is smaller than that in the flat plane

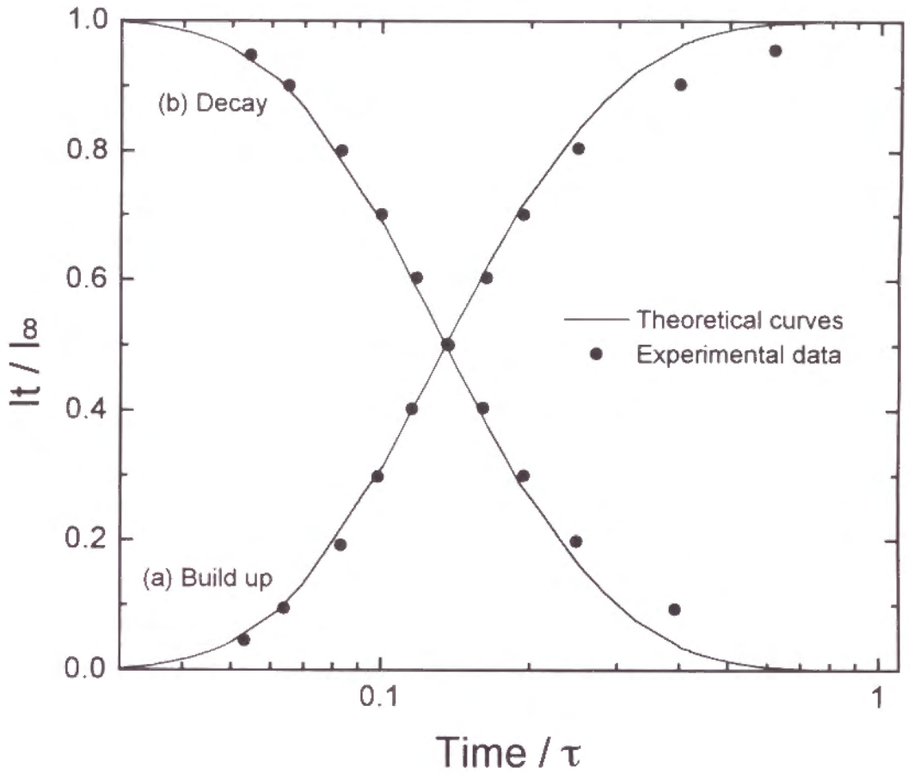

Figure 5.8 Comparison of the experimental time response data of the oxygen sensor with theoretical curves.

model. Since the effective film thickness in the grating model should be thinner than that in a flat plane model, the membrane thickness thinner than that of original one was adapted. As shown in Fig. 5.9 (c), the theoretical curve obtained for the membrane thickness 7 % thinner than the original membrane is in good agreement with that for grating model.

The thickness of OTL membrane estimated from the micrograph in Fig. 5.3 varies from place to place, so that the thickness were averaged. Therefore, the diffusion coefficient in the equation (5.3) was calculated using flat plane model. When τ becomes 0.138, the normalized current become 0.5 for a flat plane model in Fig. 5.8. The diffusion coefficients of oxygen in each thickness of OTL membranes were calculated using a flat plane model.

The diffusion coefficients obtained from grating model were comparable to those from flat plain model.

These values are comparable to that of a low density PE film 4.6 $\times 10^{-7}$ cm^2 s^{-1} and that of a high density one 1.7 $\times 10^{-7}$ cm^2 s^{-1} [12]. These results indicate that the new type oxygen sensor behaves almost theoretically.

For each thickness of OTL membranes, 90 % response time was calculated using the diffusion coefficient and listed also in Table. 5.1. In the case of OTL thickness was 60 μm, the 90 % response time was in good agreement with the theoretical value. In other cases the experimental response time were longer than the calculated values.

5.5 Conclusion

From the above results it is concluded that PE-Pt-Nafion behaves as an amperometric type oxygen sensor and the current is in proportion to the oxygen content ranging from 0 to 100 %. The sensor performance almost follows theoretically expected from the Fick's diffusion model and

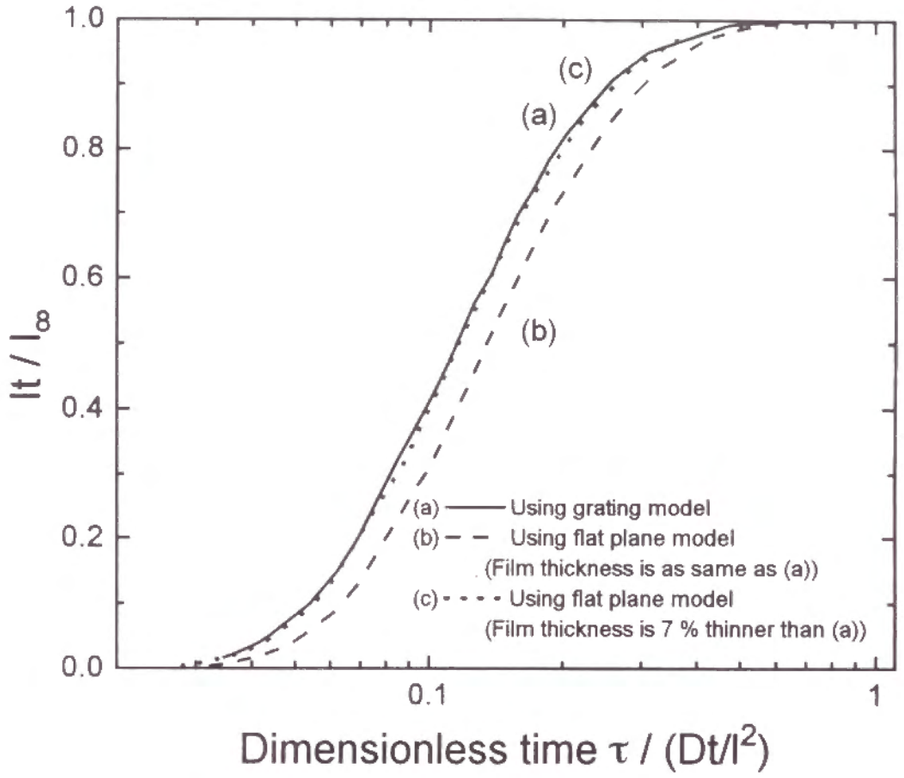

Figure 5.9 Fitting the theoretical response curve for the grating model (a) to those for flat plane model (b, c). In curve (b), thickness of the OTL membrane is the same as the original thickness of the grating model. In curve (c), OTL membrane whose thickness is 7 % thinner than the original membrane is adapted.

fast response time was obtained from the new type sensor. This new sensor is expected to be miniaturized and to be used as a base component of many types of enzyme sensors.

References

1. N. Yamazoe and N. Miura, *Denki Kagaku*, **55**, 200 (1987).
2. W. C. Maskell and B. C. Steele, *J. Appl. Elec. Chem.*, **16**, 475 (1986).
3. S. Kuwata, N. Miura, and N. Yamazoe, *Chemistry Letters*, **1988**, 1197.
4. N. Yamazoe, J. Hisamoto, and N. Miura, *Sensor and Actuators*, **12**, 415 (1987).
5. Z. Ogumi, N. Yoshida, Z. Takehara, and S. Yoshizawa, *Denki Kagaku*, **52**, 503 (1984).
6. E. A. Ticianelli, C. R. Derouin, A. Redondo, and S. Srinivasan, *J. Electrochem. Soc.*, **135**, 2209 (1988).
7. T. E. Springer, T. A. Zawodzinski, and S. Gottesfeld, *J. Electrochem. Soc.*, **138**, 2334 (1991).
8. Z. Poltarzewski, P. Staiti, V. Alderucci, W. Wieczorek, and N. Giordano, *J. Electrochem. Soc.*, **139**, 761(1984).
9. M. S. Wilson, and S. Gottesfeld, *J. Applied Electrochemistry*, **22**, 1 (1992).
10. Z. Ogumi, Z. Takehara, and S. Yoshizawa, *J. Electrochem. Soc.*, **131**, 769 (1984).
11. D. P. Lucero, *Anal. Chem.*, **41**, 613 (1969).

12. M. Nakagaki, "Makugaku Nyumon", Kitamisyobo, Tokyo (1982), p.281.
13. "Kankyo Keisokuki Guidebook", Nihon Denki Keisoku Kogyokai, Kogai Taisaku Gijutsu Doyukai, Tokyo (1985), p.123.

Chapter 6

Preparation and Performance of An Oxygen Sensor Composed of Tightly Stacked Membrane/Electrode/Electrolyte

6.1 Introduction

Recently, different kinds of electrochemical oxygen sensors operating at room temperature have been investigated[1-3]. Clark type sensors of an amperometric type are most extensively investigated and in practical use today. However, this type of sensors is difficult to be miniaturized because of its structure[4]. In the preliminary communication we have previously reported a new type of oxygen sensor[5]. This sensor is comprised of an oxygen-transport-limiting (OTL) layer which is tightly bound on a solid-polymer-electrolyte (SPE) composite electrode. The SPE composite electrode is composed of a porous platinum electrode directly deposited on an SPE material, usually a cation-exchange membrane. Since this sensor does not require any liquid between the OTL layer and the sensing electrode, it is capable to miniaturize it in principle and a stable performance is expected under conditions of pressure difference. In this chapter, preparation of a small sensing probe of ca. 1.2 mm diameter and its performance are investigated.

6.2 Experimental

6.2.1 Preparation of the oxygen sensor

The structure of the sensor prepared in this work is schematically described in Fig. 6.1. The sensor was composed by two electrodes. One of them was a sensing electrode and the other was a counter electrode. The sensing electrode was porous platinum and directly bound on the SPE material by an electroless plating method, the details of which was reported elsewhere[6]. Since the SPE material contacts directly with a sensing electrode as shown in the figure, a high chemical stability is required for the material. From this point of view, Nafion NR50, perfluorosulfonate cation-exchange resin of a cylindrical lump of ca.1.2 mm diameter and 3 mm length in average, which is widely used as a solid super acid catalysts, was used as an SPE material of the composite electrode comprising an oxygen sensor.

A borosilicate glass tube with an internal diameter of 1.2 mm, an outer diameter of 7.0 mm, and a length of ca. 50 mm was used as a sensor body. Gold was sputter-deposited on a cross-sectional surface of the glass tube to get an electrical contact with the sensing electrode. A Nafion NR50 lump was inserted into the capillary of the glass body followed by a deposition of the porous platinum layer which contacted with the gold layer to give electrical contact during deposition. This composite electrode is termed henceforth as Pt-Nafion. An OTL layer was then coated on the porous platinum electrode by the method described below. As an electrolyte, 1 mol dm^{-3} hydrochloric acid was filled in the room of the glass capillary and silver wire of 0.5 mm diameter was inserted into the solution for use as a counter electrode. Immersed length of the silver wire was about 40 mm.

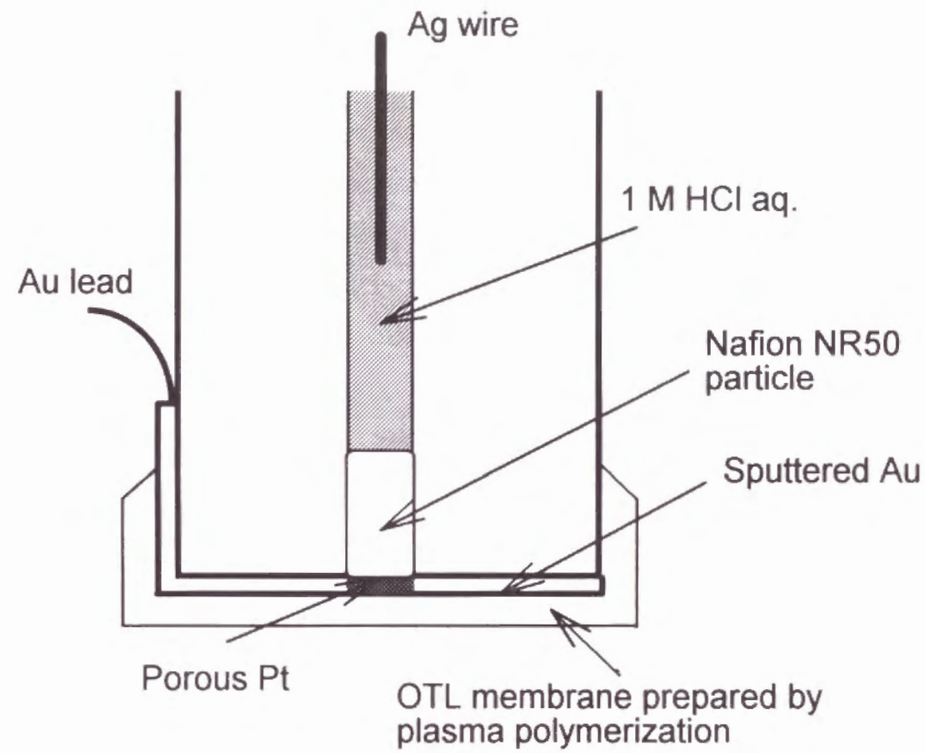

Figure 6.1 Schematic diagram of the sensor.

6.2.2 *Coating of OTL films*

Since an OTL layer contacts directly with the sensing electrode, it is required for the layer to have enough chemical and mechanical stability to prevent from contamination of the sensing electrode and to obtain a stable performance. This requirement is severer for the sensors of the present investigation than for Clark type sensors because the film directly contacts with the sensing electrode in the case of the former sensor. Although polyethylene films were used in our previous work, perfluoro-polymer was selected here as the OTL layer. The thickness of the OTL layer has a remarkable influence on the sensor performance both in response time and signal magnitude. The thinner the thickness, the faster the response is and the larger the magnitude is. Since perfluorocarbons show high oxygen solubility[7], a larger signal current and higher oxygen selectivity are expected for them than those for polyethylene. The film is also required to tightly adhere on the electrode and to be free from pinhole and uniform in thickness for the high sensor performance. Since it is very difficult for conventional coating methods to satisfy these requirements, a plasma-polymerization technique was selected because this technique is known to give an ultrathin, pinhole-free, and uniform film adhering tightly on a substrate from different kinds of precursor. As described in Fig. 6.2, an apparatus for the plasma polymerization was constructed from a borosilicate glass cylinder with two side arms. The reactor contains a couple of stainless steel disk electrodes placed parallelly with 2.5 cm gap. On these electrodes, an RF power was applied from an RF power supply (Samco Model FG-200) via a matching network to generate plasma. A substrate which was the glass tube inserted with the composite electrode was set in the after-glow region, at the downstream from the plasma electrodes. The distance from ends of the electrode was changed to obtain a desirable coating. After introducing argon to the glass chamber evacuated

by a rotary pump, plasma was ignited by applying an RF power of 15 W. After generating a stable plasma a precursor gas for plasma polymerization, hexafluoropropene (Daikin), was introduced into the chamber at 3 cm^3 min^{-1}. A pressure in the glass chamber was kept at 0.5 Torr by controlling a main valve. Polymerization was carried out for 6 hours. The details on the influences of plasma parameter on the properties of plasma polymer will be discussed elsewhere. IR spectra (Shimadzu Model FT-IR4100) and XPS (Matsushita Techno Research) measurements were carried out to characterize the plasma-polymerized film.

6.2.3 *Test cells*

Sample solutions containing oxygen were prepared and filled in a glass test cell shown in Fig. 6.3. Argon and oxygen mixture was introduced into the cell. A test sensor was immersed into the sample solution. Prior to the measurement, the sample solution was bubbled with the gas for half an hour. Concentration of the dissolved oxygen was controlled by changing of the oxygen partial pressure of the mixed gas from 0 to 1 atm. Dissolved oxygen was simultaneously monitored with a commercial DO meter (Horiba DO-Meter DO-8F) (not shown in the figure). The solution bubbled with the mixed gas was magnetically stirred during measurement in order to eliminate the formation of a depletion layer at the interface between the OTL layer and a test solution.

6.2.4 *Measuring procedure*

Using a potentiostat (Hokuto Denko Model HA301), constant voltage was applied between a sensing electrode (cathode) and a counter electrode (anode) of the sensor. The applied voltage was scanned using a function generator (Hokuto Denko Model HB-111). The voltage-current relationships was recorded on an X-Y recorder (Graphtec Model

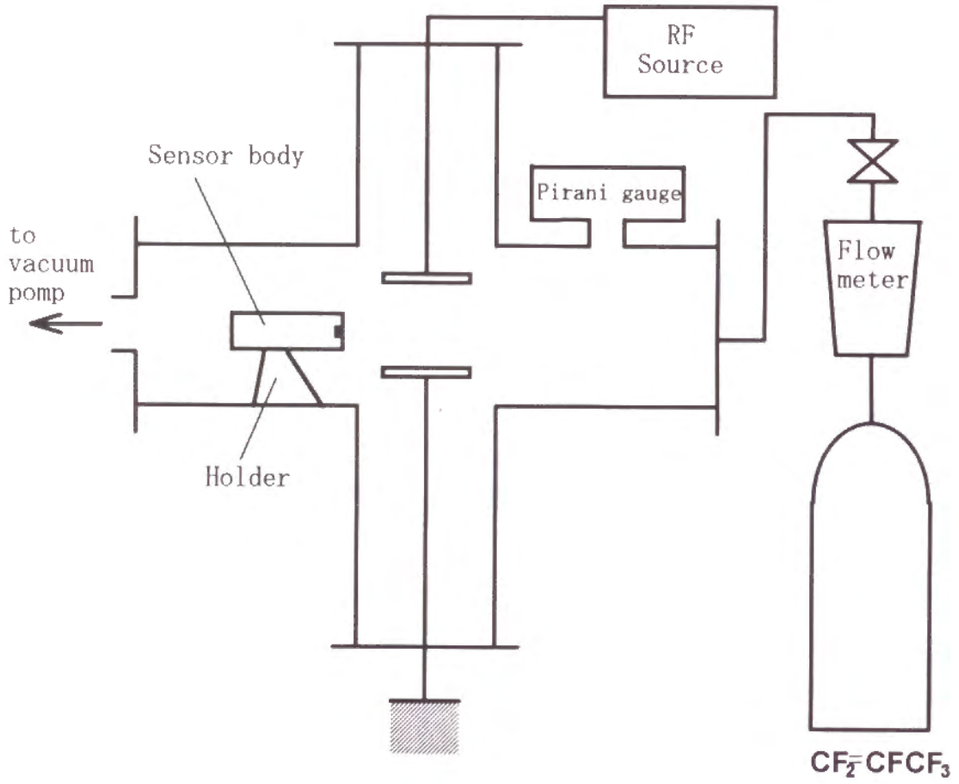

Figure 6.2 Schematic diagram of the plasma polymerization reactor.

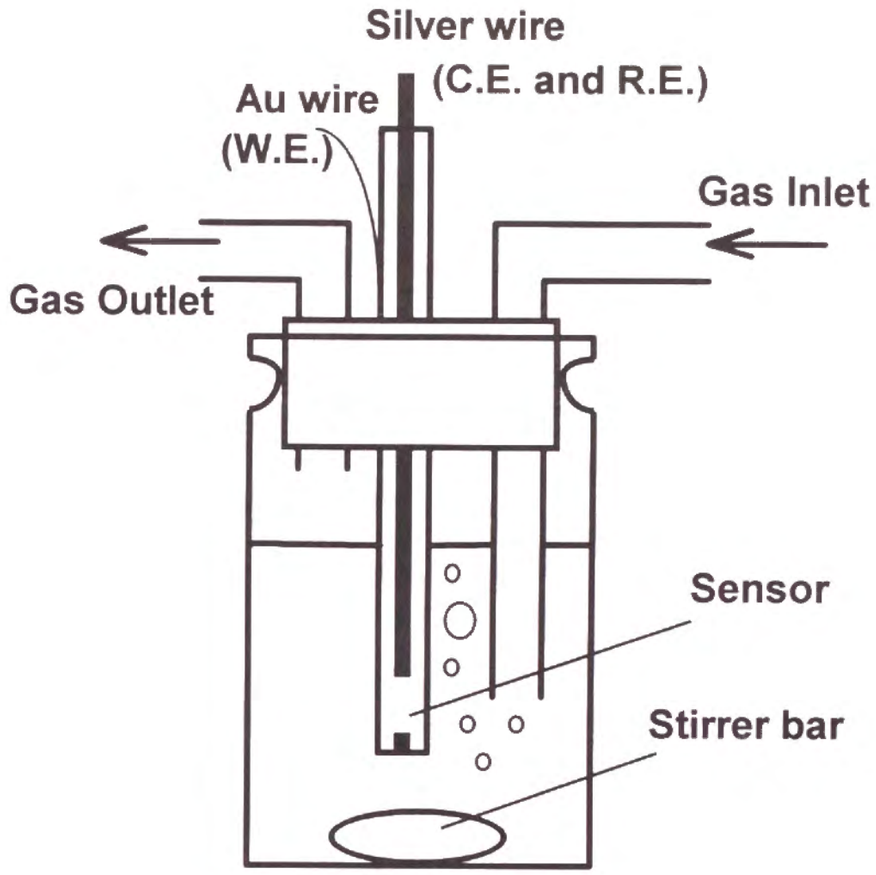

Figure 6.3 Measuring cell of the sensor characteristics.

WX2400). To compare with the sensor coated with an OTL layer, bare Pt-Nafion was also examined, which had the same composition as the sensor except that a porous electrode deposited on Nafion NR50 was not covered with a plasma-polymer layer and contacted directly with a test solution. All experiments were carried out at room temperature.

6.2.5 Chemicals

All chemicals except hydrazine were of reagent grade. Hydrazine as a reductant for platinum plating procedure was of chemical pure grade. Chemicals were used without further purification. Solutions were prepared with distilled water. The purity of argon was 99.998 % and of oxygen was 99.995 %.

6.3 Results and Discussion

6.3.1 Characterization of the plasma polymerized film

Plasma polymerization was first examined in order to obtain a good OTL layer. A gold sputtered glass plate was used as a substrate. Plasma polymerization was carried out for 6 hours under the plasma conditions mentioned above. The substrate covered with a thin plasma-polymer layer was examined by IR spectroscopy and XPS measurements. An IR spectrum was obscure but very similar to that of a co-polymer chemically produced from tetrafluoroethylene and hexafluoropropene except an absorption peak at 1730 cm^{-1} ascribed to C=O stretching. The distance of the substrate from the electrode edge did not give a significant influence on the IR spectrum. The layer thickness was measured by SEM observation. The weight of the plasma polymerized layer was measured by a microbalance. From these measurements density of the plasma polymer was calculated and the value was 1.75 g cm^{-3} which was smaller than the value of chemical co-polymer (2.12-2.17 g cm^{-3}). From C_{1s} peaks of XPS

spectrum of the plasma-polymer the existence of CF_3, CF_2, CF(COO), C-CF_n(C-O), and CF-CF(C=O) was suggested. That is, some oxygen was introduced into the plasma-polymer. This oxygen might be introduced from residual water in the reactor. An XPS spectrum suggested that the ratio of oxygen to fluorine was less than 0.04. From these results it was concluded that the structure of plasma-polymerized film was similar to the one of the radical co-polymer except that a small amount of oxygen containing functional groups existed and the polymer was cross-linked. The oxygen permeation rate through cross-linked perfluoro-polymers is expected to be faster than the rate through uncross-linked polymers[8]. Furthermore, the more the contents of CF3 in the polymer, the smaller the surface energy of the polymer is. The small surface energy retards contamination and results in high oxygen solubility[8]. A SEM photograph of Fig. 6.4 shows that a plasma polymerized film covered well the porous platinum electrode of Pt-Nafion and is free from pinhole and uniform. The plasma-polymerized OTL layers of 10 and 3.5 μmin thickness were deposited on the Pt-Nafion surface.

6.3.2 Polarization curves

Figure 6.5 shows current voltage curves obtained by a linear voltage sweep method in the range between 0.6 V and -0.2 V at a sweep rate of 1 mV s^{-1}. Curve (a) was obtained under argon bubbling. This curve shows the background current. Curves (b), (c), and (d) were obtained using a solution saturated with pure oxygen. Both curves (b) and (c) were obtained with the oxygen sensor which was not coated with a plasma-polymer layer (bare Pt-Nafion). The stirring rate of the test solution was faster for curve (b) than that for curve (c). Curve (d) was for the oxygen sensor coated with a plasma-polymer layer at the stirring rate of the same as for curve (b). On each of these three curves, a plateau region

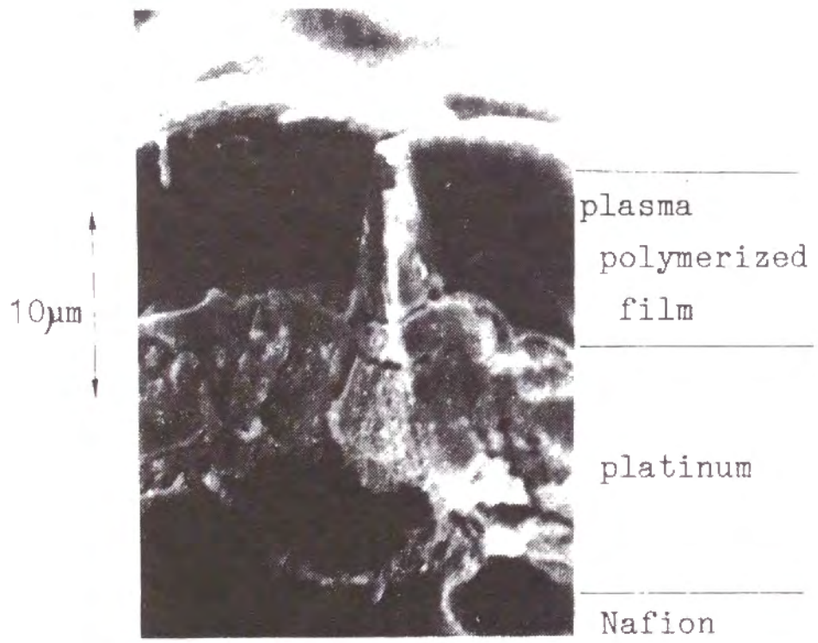

Figure 6.4 SEM photograph of the cross section of film coated electrode.

was observed in a potential range between 0.4 V and 0 V where oxygen was reduced via a 4 electron process[9].

$$O_2 + 4H^+ + 4e^- \rightarrow 2H_2O \tag{6.1}$$

In this plateau region, oxygen reduction is expected to proceeds under diffusion limiting conditions. On curve (b), plateau current was not stable and its magnitude was smaller than that of the curve (c). This suggest that the stirring affected the reduction current on the bare Pt-Nafion. This is because an oxygen diffusion layer was formed between the porous platinum cathode and the solution bulk and it was not stable. On the other hand, smaller but more stable reduction current than curves (b) and (c) was observed for the sensor coated with the plasma-polymer layer.

This result shows that the plasma-polymer coating film behaved well as a mass-transport-limiting layer on the porous platinum sensing electrode of the sensor. These polarization curves resembled the curve on the previously reported oxygen sensor[5] which was composed of PE-film/Pt-cathode/Nafion117. Although the present sensor was composed of two electrodes and constant voltage was applied between the two electrodes, the previous reported sensor had a three electrode structure and was operated under potentiostatic conditions. The above resemblance suggests that the present sensor behaved as if potentionstatically controlled one. This should be ascribed to that the potential of silver electrode remained at certain stable value under conditions of low current density electrolysis and that an ohmic drop in the electrolyte was small at a low detection current[10]. These conditions kept the potential of sensing electrode at fairly stable value and the potential was indirectly controlled by an applied voltage. The anode reaction was inferred as a formation of silver chloride from the color of electrode surface.

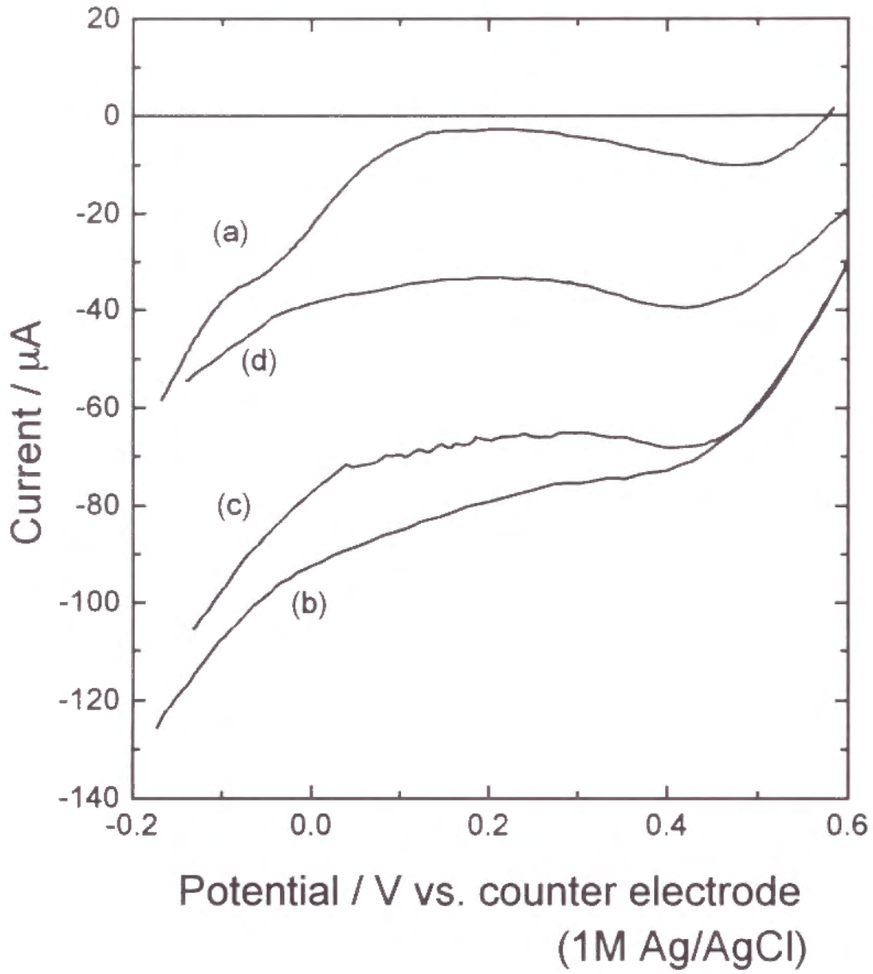

Figure 6.5 Current-voltage characteristics of the sensor.
(a) : residual current (b), (c): bare electrode, (stirring speed (b)<(c))
(d) : film coated electrode

6.3.3 Sensor performance

Using a sensor covered with an OTL layer of 3.5 μm thickness, the sensor performance was examined. As shown in Fig. 6.6, sensing current on the sensor set at 0.2 V at room temperature increased with increase in the oxygen concentration in a test solution. The deviation from the linearity at a higher oxygen concentration range might be ascribed to the slow rate of oxygen reduction on the sensing porous platinum electrode. The details on this point is now under investigation. Using a sensor covered with a 10 μm thick film, a similar relationship was observed. Figure 6.7 shows the stability of the sensor. The output current of the sensors was measured after storing under following 2 conditions. In the first condition, the sensor was stored in water except measuring time. In the second condition, the sensor was stored under atmosphere. Curve (a) in the figure shows the results in the first, and curve (b) in the second.

The sensing current fell down during storing for initial 1 or 3 days and after that the value remained almost constant for 10 days. The initial fast falling down of the output current may be caused by residual reducible substances introduced into the sensor during preparation. In each case, the temperature of test solution was not controlled. The fluctuation in the output currents observed on each sensor should be due to the change in the measuring temperature.

6.4 Conclusion

An oxygen sensor composed of tightly stacked plasma-polymerized-perfluoro-film/Pt-cathode/Nafion was prepared and it was applied to the detection of a dissolved oxygen. A perfluoro-polymer prepared by a plasma polymerization forms a thin uniform film and it is well bound on the porous Pt cathode. This polymer film acts as an oxygen-transport-limiting layer of an oxygen sensor. Oxygen reduction current increased

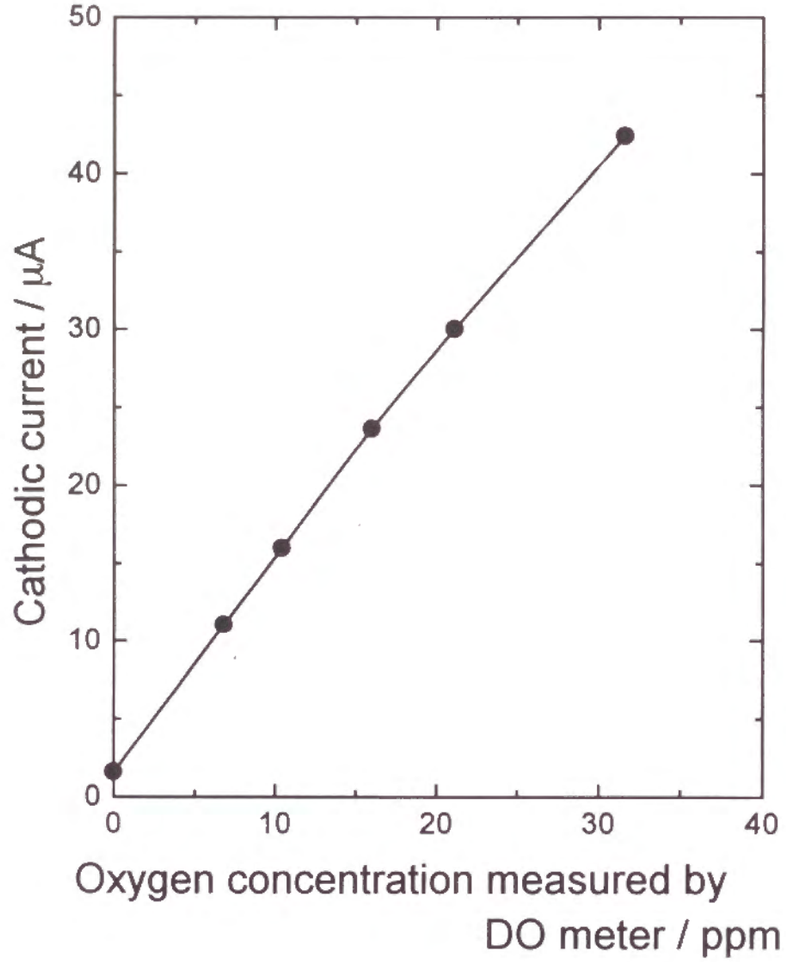

Figure 6.6 Relationship between cathodic current and concentration measured by DO meter.

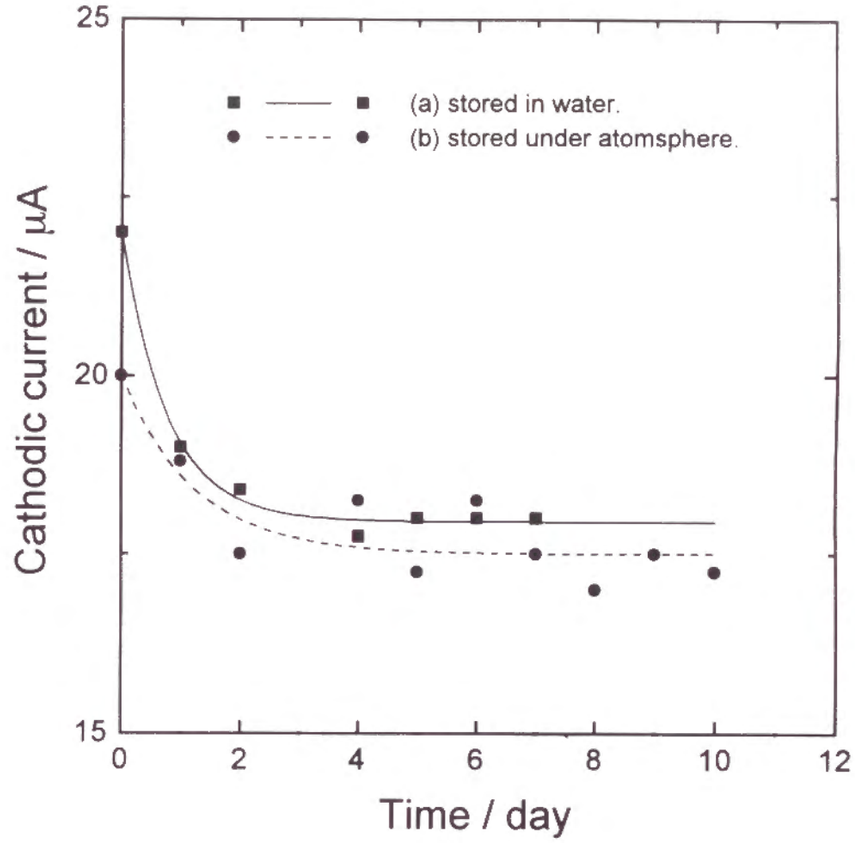

Figure 6.7 Stability of the sensor.

with increasing in dissolved oxygen concentration. The preparation procedure described here is expected to enable the preparation of a micro-size oxygen sensor in principle. Thickness and gas permeability of the oxygen-transport-limiting layer is easily controlled by changing plasma conditions. This permits to optimize the sensor performance.

References

1. I. Bergman, *Nature*, **218**, 266 (1968).
2. S. Kuwata, N. Miura, and N. Yamazoe, *Chem. Lett.*, **1988**, 1197 (1988).
3. N. Yamazoe, J. Hisamoto, N. Miura, and S. Kuwata, *Sens. Actuators*, **12**, 415 (1987).
4. D. P. Lucero, *Anal. Chem.*, **41**, 613, (1969).
5. K. Katakura, A. Noma, Z. Ogumi, and Z. Takehara, *Chem. Lett.*, **1990**, 1291 (1990).
6. Z. Ogumi, Z. Takehara, and S. Yoshizawa, *J. Electrochem. Soc.*, **131**, 769 (1984).
7. J. V. Dobson and M. J. Taylor, *Electrochim. Acta.*, **31**, 231 (1986).
8. I. Terada, T. Kajiyama, and T. Haraguchi, *Nippon Kagaku Kaishi*, **1985**, 1889 (1985).
9. Z. Ogumi, N. Yoshida, Z. Takehara, and S. Yoshizawa, *Denki Kagaku*, **52**, 503 (1984).
10. I. Bergman, *Analyst*, **110**, 365 (1985).

Publication list

Part of this thesis have been or will be published on the following journals;

Chapter 1

Oxygen Permeation Through Perfluorinated Carboxylate Ion-Exchange Membranes.
M. Inaba, T. Kuroe, Z. Ogumi, Z. Takehara, K. Katakura, S. Ishikawa, and Y. Yamamoto,
Electrochimica Acta., **38**, 1727 (1993)

Chapter 2

Diffusion of Aniline Through Perfluorosulfonate Ion-Exchange Membranes.
Z. Ogumi, K. Toyama, Z. Takehara, K. Katakura, and S. Inuta,
J. Membrane Sci., **65**, 205 (1992).

Chapter 3

Electrotransportaion of Aniline Through a Perfluorosulfonate Ion-Exchange Membrane.
K. Katakura, M. Inaba, K. Toyama, Z. Ogumi, and Z. Takehara,
J. Electrochem. Soc., **141**, 1827 (1994).

Chapter 4

Microelectrode Simulation of Anode in Polymer Electrolyte Membrane Fuel Cells.
K. Katakura, M. Inaba, K. Inatomi, J. T. Hinatsu, Z. Ogumi, and Z. Takehara,
J. Electroanal. Chem., submitted for publication.

Chapter 5

An Oxygen Sensor Composed of Tightly Stacked Membrane/Electrolyte/Electrode.
K. Katakura, A. Noma, Z. Ogumi, and Z. Takehara,
Chemistry Letters, 1291 (1990).

Chapter 6

Preparation of An Oxygen Sensor Composed of Tightly Stacked Membrane/Electrolyte/Electrode.
K. Katakura, A. Noma, Z. Ogumi, and Z. Takehara,
Denki Kagaku, **58**, 1184 (1990).